Cells Deploy a Two-Pronged Quality Control Strategy to Degrade Misfolded Proinsulin Mutants

By

Corey Nathaniel Cunningham

A dissertation submitted in partial fulfillment
of the requirements for the degree of
Doctor of Philosophy
(Cellular and Molecular Biology)
in the University of Michigan
2019

Doctoral Committee:

Professor Billy Tsai, Chair
Professor Peter Arvan
Associate Professor Diane Fingar
Professor Robert S. Fuller
Professor Jiandie Lin

Corey Nathaniel Cunningham

cncunnin@umich.edu

ORCiD: 0000-0002-1755-4881

ACKNOWLEDGEMENTS

This thesis would not be possible without the guidance of my mentor, Dr. Billy Tsai. His enthusiasm and overwhelming support throughout my graduate school career is invaluable. I will always be indebted to him and the team of scientists he assembled over the years. I would also like to extend a special thanks to my thesis committee: Drs. Peter Arvan, Diane Fingar, Robert Fuller, and Jiandie Lin, for their insight and thought-provoking discussions during my committee meetings.

The work presented in this thesis would not be without the support of each member of the Tsai Lab. Working daily with all of you has been a dream. You all helped create an amazingly collaborative, fun, and exciting environment over the last five years. I would like to especially thank my mentor Dr. Kaiyu He and our laboratory manager Jeffrey Williams for working on the MIDY project with me.

I would also like to extend my thanks to my amazing family, friends, and my fiancée, Bethany. Your amazing support over my graduate career has been tremendous and I cannot thank each of you enough. A special thanks to my parents for putting up with my constant scientific phone calls during the months prior to my preliminary exam. I would also like to extend gratitude to all the musicians I have had the pleasure of jamming with every weekend since my second year in graduate school: Drs. Robert Fuller, Anthony Antonellis, Peter Larson, Kevin Bohannon, and Brian Magnuson.

Sincerest thanks to my undergraduate mentors Drs. Karen Resendes and Joshua Corrette-Bennett who guided me when I was a young, training scientist. Karen, thank you for always pushing me in your laboratory and always accepting my twenty-page lab reports. You helped me foster so many ideas and my interest in graduate school and scientific discovery. Josh, thank you for always being tough on me and motivating me to continue to work hard throughout undergrad. An extended thanks to my mentor at St. Jude Children's Research Hospital, Dr. Jie Zheng, who allowed a 19-year-old training scientist the freedom to explore 2D and 3D protein NMR.

Finally, figures in this thesis were performed by Kaiyu He, Nandini Mackinam, Anoop Arunagiri, and Jeffrey Williams. Kaiyu He is credited or assisted in performing the following experiments: Figures 2-3A-G, Figure 2-4, Figure 2-S1A/B/D, Figure 2-S2, Figure 3-1, Figure 3-4C, Figure 3-5B-C, Figure 3-6E-G. Nandini Mackinam is credited in performing the experiment published in Figure 2-3H and Figure 2-S3. Anoop Arunagiri assisted in isolating the *Akita* and C57B/6 islets used in Figure 3-6G. Jeffrey Williams is credited or assisted in performing: Figure 4-1B and 4-1D, Figure 4-3A-B, Figure 4-4B, and Supplemental Figures 4-S2-S3. Your help in creating this thesis will never go unnoticed and I am grateful to each of you!

TABLE OF CONTENTS

LIST OF FIGURES

ABSTRACT

There are over 30 missense mutations found in the human insulin gene responsible for a newly-characterized diabetic syndrome called Mutant *INS*-gene-induced Diabetes of Youth (MIDY). In MIDY, mutations in the insulin gene lead to toxic misfolding of mutant proinsulin in the endoplasmic reticulum (ER). Importantly, MIDY proinsulin mutants bind to and sequester wild-type (WT) proinsulin via mixed disulfide bonds in the ER, resulting in decreased insulin maturation and secretion. These mixed disulfide-bonded WT-mutant complexes oligomerize into high molecular weight (HMW) species, eventually forming toxic insoluble aggregates that lead to β-cell death. To alleviate the disease, we posit that the efficient degradation of the MIDY mutant proinsulins should allow WT proinsulin to properly fold in the ER and mature into insulin poised for secretion.

In this thesis, we uncover two ER-dependent protein quality control pathways that are used to eliminate the classic MIDY mutant proinsulin *Akita*. We first reveal that *Akita* is degraded via the ER-associated degradation (ERAD) pathway. In this pathway, the ER-resident chaperone Grp170 acts to prevent aggregation of the *Akita* HMW complex, while the PDI redox enzyme reduces the HMW species to generate ERAD-competent smaller oligomers of *Akita*. These smaller *Akita* oligomers in turn translocate across the ER membrane via the Hrd1-Sel1L membrane proteins and are extracted into the cytosol by the p97 ATPase. Upon reaching the cytosol, *Akita* is delivered to the proteasome for destruction. Strikingly, we found that enhancing Grp170-dependent ERAD degradation

of *Akita* led to restoration of WT insulin secretion. In a second and distinct protein quality control pathway, we discovered that the *Akita* aggregates (that are formed despite the action of Grp170) are in fact removed by a RTN3-dependent ER-coupled autophagy (ER-phagy) pathway. Importantly, RTN3-dependent clearance of aggregated *Akita* also stimulates WT insulin secretion.

In sum, my thesis unveils a two-pronged quality control strategy – ERAD and ER-phagy – that are strategically deployed against a mutant proinsulin molecule. Our results raise the possibility that enhancing the activities of key components within the ERAD and ER-phagy pathways that stimulate degradation of mutant proinsulins and concomitantly promote WT insulin secretion may provide a rational therapeutic approach to combat MIDY.

CHAPTER 1: Introduction

Approximately one-third of the human proteome enters the endoplasmic reticulum (ER) to fold and traffic to their proper spatial positions along the secretory pathway or to be secreted out of the cell (Braakman and Hebert, 2013). The extracellular environment is more oxidizing than the cytosolic milieu, so eukaryotic cells need internal compartments to prepare proteins for a life outside of the cell. The rich oxidative environment of the ER makes it ideal for polypeptide biosynthesis and folding. During protein biosynthesis, ribosome-nascent chains destined to the ER recruit the signal recognition particle (SRP) to the signal sequence on the nascent chain (Chartron et al., 2016; Connolly and Gilmore, 1989). This binding slows translation until the ribosome is selectively docked at the SRP receptor of the ER, where release of the SRP recommences polypeptide synthesis into the ER in a process known as cotranslational translocation (Rapoport, 2007). Distinct from cotranslational translocation, a subset of nascent polypeptide chains are targeted to the ER via a process known as posttranslational translocation. In this case, fully synthesized proteins do not require SRP. Instead, cytosolic chaperones guide the new polypeptides to the ER membrane translocation complex where the chaperones release the polypeptide chains, enabling their translocation through the Sec61 translocon (Plath and Rapoport, 2000). Soluble proteins cross the Sec61 translocon via a ratcheting mechanism in which iterative cycles of binding to Binding Immunoglobulin Protein (BiP) drive forward translocation (Matlack et al., 1999).

Removal of the signal sequence by signal peptidase untethers the polypeptide from the ER membrane, thereby releasing the polypeptide within the ER lumen (Figure 1-1).

In the ER lumen, the polypeptide engages chaperones of the heat shock protein (HSP) families, lectins, and oxidoreductases, such as the protein disulfide isomerase (PDI) family; these chaperones assist the polypeptide chain to obtain its tertiary and quaternary native structures (Braakman and Hebert, 2013) (Figure 1-1). To support folding, the polypeptide chain is often subjected to multiple posttranslational modifications, including glycosylation, disulfide bond oxidation, as well as *cis-trans* prolyl isomerization (Ellgaard et al., 2016). Upon proper folding, the polypeptide chain is no longer associated with ER resident quality control proteins and is ready to exit the ER and be transported to the *cis* Golgi apparatus via COPII-coated vesicles (Barlowe et al., 1994). Eventual transport of the folded polypeptide chain out of the *trans* Golgi network enables it to traffic further to the cell surface or to the endo-lysosomal membranous system where it can reside and function.

While many aspects of protein folding in the ER have been elucidated, it remains unclear how the cell deploys quality control mechanisms to determine the fate of improperly folded polypeptides. The research presented in this thesis focuses on how pancreatic β-cells handle a terminally misfolded insulin precursor protein as a model to understand these quality control processes, and to further clarify the underlying causes of a severe form of diabetes. The following introductory sub-sections highlight our

current understanding of protein quality control mechanisms that exist to maintain cellular proteostasis.

Unfolded Protein Response

Protein misfolding is the etiology of many human diseases including but not limited to Parkinson's Disease (PD), Huntington's Disease (HD), Alzheimer's Disease (AD), and some forms of cancer and diabetes. In this collection of maladies, mutant or misfolded disease-causing proteins accumulate and often aggregate, leading to severe cellular stress (Bates, 2003; Irvine et al., 2008). In AD, amyloid β-peptide aggregates outside of neurons leading to toxic plaque formation (Tanzi and Bertram, 2005), while a phenotype of PD involves α-synuclein molecules aggregating in Lewy Bodies, which are cytoplasmic inclusions that hinder proper neuron homeostasis (Spillantini et al., 1997). In HD, polyglutamine repeats in the huntingtin protein results in severe aggregation (Bates, 2003; Scherzinger et al., 1997). Collectively, these diseases represent models of protein-misfolding diseases which are significant human health concerns.

Interestingly, a majority of the aforementioned protein aggregates are cytosolic or extracellular in nature. Rarely are protein aggregates found within the ER of specific cells (Vincenz-Donnelly et al., 2018). As indicated, the ER has a rich chaperone and oxidative environment which laboriously assists polypeptides to achieve their native structure. However, even within this environment, proteins can misfold (Wang and Kaufman, 2016) (Figure 1-1). Some proteins misfold in the ER due to genetic mutations (see below), or because they possess highly hydrophobic, disordered regions or

complex tertiary structures. Regardless of the cause, the ER must respond to misfolded protein accumulation before these proteins ultimately cause ER stress or aggregate into toxic misfolded species (Wang and Kaufman, 2016) (Figure 1-1).

In this context, the ER has developed a homeostatic quality control pathway called the unfolded protein response (UPR) which is designed to respond to the accumulation of misfolded proteins. Originally coined by Mary-Jane Gething and Joseph Sambrook, UPR regulates and minimizes ER stress by controlling the levels of ER chaperone and protein at the transcriptional and translational levels (Gething and Sambrook, 1992; Kozutsumi et al., 1988). UPR is divided into three major arms: ATF6, PERK, and IRE1.

The ATF6 arm of the UPR is a relatively defined pathway. While the mechanism by which ATF6 senses misfolded ER proteins remains elusive, the downstream and transcriptional activation of this transmembrane protein is more clearly understood. Upon sensing the accumulation of misfolded ER proteins, the ER-resident ATF6 migrates to the Golgi, where two site-specific proteases cleave ATF6 to generate a cytosolic fragment of ATF6 (Haze et al., 1999; Ye et al., 2000). This fragment translocates to the nucleus where its acts as a transcriptional activator of genes encoding HSPs, PDIs, and additional ER chaperones (Walter and Ron, 2011). Hence, this arm of UPR enhances the folding capacity of the ER in order to alleviate accumulation and potential aggregation of misfolded proteins.

Conversely, the PERK arm of UPR lessens protein folding load, thereby alleviating ER stress. After sensing the accumulation of misfolded ER proteins, the PERK transmembrane serine/threonine kinase undergoes dimerization and autophosphorylation. This initiates a signaling cascade leading to the phosphorylation of eIF2α, the latter of which directly downregulates protein influx by inhibiting protein translation (Harding et al., 2000).

In the IRE1 arm of the UPR, inactive IRE1 is initially bound by BiP. BiP dissociates from IRE1 due to buildup of misfolded ER proteins. Oligomerization and phosphorylation activate IRE1's endonuclease activity, which cleaves mRNAs to translationally repress the biosynthesis of new proteins (Korennykh et al., 2009). IRE1 also splices the Xbp1 mRNA which generates an active Xbp1 transcription factor that upregulates the expression of numerous ER chaperones (Yanagitani et al., 2011).

In the context of this thesis, many UPR-upregulated genes are components of a major quality control pathway called ER-associated degradation (ERAD) (Travers et al., 2000) (Figure 1-1,1-2; see below). This pathway is one of two known mechanisms by which the ER removes misfolded ER substrates for degradation.

ERAD and ER-phagy Dependent Protein Quality Control

ERAD is the major ER quality control pathway that disposes misfolded ER luminal and ER membrane proteins for 26S proteasome degradation in the cytosol. This is executed using a process known as retrotranslocation whereby ERAD components move

misfolded proteins to the cytosol (Werner et al., 1996) (Figure 1-2). ERAD is an intricate system of concerted chaperones and enzymes that recognizes misfolded clients, retrotranslocates them through an ER membrane channel, poly-ubiquinates the misfolded clients for their extraction, and delivers them to the proteasome for degradation. ERAD is categorized into three groups, depending on the nature of the misfolded client: ERAD-L represents a pathway that disposes a soluble or membrane protein in which the recognized substrate begins in the lumen, ERAD-M represents a pathway that degrades a membrane substrate containing a lesion within the transmembrane domain, and ERAD-C represents a pathway that disposes a membrane substrate with a lesion in the cytosolic domain (Ruggiano et al., 2014). For the research presented in this thesis, ERAD-L will be the focus.

For misfolded ER luminal proteins to undergo ERAD, the client must be first recognized by ERAD luminal components. These components include, but are not limited to, Hsp70s and their co-chaperones, Hsp90s, Hsp40s, and ER oxidoreductases. One example of these chaperones is the ER-resident Hsp70 chaperone BiP. BiP harbors a substrate binding domain (SBD) which recognizes short unfolded amino acid sequences, and a nucleotide binding domain (NBD). Through ATP hydrolysis stimulated by an Hsp40 harboring a J-domain, BiP-ADP interacts with a substrate via its SBD. The SBD of BiP is relatively nonspecific (Marcinowski et al., 2011; Pobre et al., 2019; Yang et al., 2017) allowing BiP to have a multitude of diverse substrates. Apo-BiP targets a substrate to membrane-bound ERAD components before BiP is released from the

substrate via the action of one of two ER-resident nucleotide exchange factors (NEF) Sil1 or Grp170 (Behnke et al., 2015; Inoue and Tsai, 2015; Weitzmann et al., 2006).

In addition to acting as a NEF of BiP, Grp170 can also function as a chaperone. In fact, it has a higher propensity than BiP to bind to and sequester terminally misfolded substrates that are destined for ERAD (Behnke and Hendershot, 2014). In concert with ERdj4 and ERdj5, Grp170 recognizes misfolded protein sequences that are buried in properly folded clients (Behnke et al., 2016) (Figure 1-2). When a client is misfolded, these three co-chaperones, along with BiP and other chaperones, delivers it directly to ERAD (Figure 1-2).

In addition to the HSPs, ER oxidoreductases are necessary for clients that contain disulfide bonds (Figure 1-2). ER oxidoreductases, such as the aforementioned PDI family, use conserved Cys-X-X-Cys motifs to reduce, oxidize, or isomerize cysteines involved in disulfide bonds (Hatahet and Ruddock, 2009; Tu et al., 2000). This family of over 20 ER oxidoreductases are responsible for reducing disulfide bonds for clients to be funneled through the retrotranslocon, the ERAD membrane channel (see below). An example of client reduction was shown by the ERdj5-mediated reduction of mutant low-density lipoprotein receptors (LDLR), a required step for LDLR retrotranslocation and degradation (Oka et al., 2013). Together with HSPs, these chaperones and enzymes coordinately recognize and prepare ERAD clients for dislocation through the ER membrane.

After misfolded proteins have been recognized as substrates destined for retrotranslocation, they are delivered to ER membrane ERAD components, specifically an E3 ubiquitin ligase and its adaptors. Hrd1, an E3 ubiquitin ligase and its adaptor Sel1L, are members of the canonical ERAD pathway (Figure 1-2). Hrd1 is a multi-pass transmembrane E3 ubiquitin ligase featuring a RING finger domain on its cytosolic tail (Schoebel et al., 2017). Importantly, Hrd1 was demonstrated to be the retrotranslocon, the channel by which misfolded clients are retrotranslocated through the ER membrane from the ER lumen into the cytosol (Baldridge and Rapoport, 2016). Its major adaptor protein Sel1L is single-pass type I transmembrane protein with a large N-terminal luminal domain containing nine Sel1-like repeats (SLRs), tetratricopeptide repeats which mediate protein-protein interactions (Mueller et al., 2006; Ye et al., 2004). Delivery of reduced clients to Sel1L via luminal chaperones mediates client transition to the Hrd1 retrotranslocon. Once lysine residues are exposed on the cytosolic surface of the retrotranslocon, Hrd1's RING domain poly-ubiquitinates the clients prior to their extraction into the cytosol (Stein et al., 2014) (Figure 1-2).

Cytosolic extraction of the polyubiquitinated client requires an AAA+ ATPase called p97/VCP and its co-factors Npl4 and Ufd1 (Bodnar et al., 2018; Ye et al., 2001) (Figure 1-2). In order to extract polyubiquitinated clients to the cytosol, p97 uses ATP hydrolysis at each of its Walker A and Walker B domains to generate sufficient force to eject the client into the cytosol (Meyer et al., 2012). Interestingly, misfolded clients cannot be extracted from the ER (or proteoliposomes) in the absence of Npl4 and Ufd1,

demonstrating a critical need for these components for proper extraction and delivery to the proteasome.

If misfolded proteins are incompetent to undergo ERAD because they form large aggregates, the ER can deploy another major degradative pathway called ER-coupled autophagy (or ER-phagy). Autophagy is a catabolic process in which the cell recycles damaged organelles or portions of organelles for homeostatic maintenance. In the case of a damaged organelle, autophagic initiation factors (i.e. Atg proteins, Beclin1, LC3/GABARAP) create a phagophore, which is an isolated membrane that begins to encapsulate the organelle (Parzych and Klionsky, 2014). The phagophore matures through an intricate expansion process to surround the target organelle and seals to become an autophagosome. This autophagosome fuses with the lysosome to allow for lysosomal breakdown and degradation of the internal organelle and its constituents.

One of the earliest pieces of evidence of ER-phagy was the observation of ER-derived cisternae within autophagosomes after ER stress-induction (Bernales et al., 2006). Prior to this finding, a model ER-resident HDEL substrate was discovered in the vacuole under starvation conditions, suggesting that segments of the ER are degraded via autophagy (Hamasaki et al., 2005). Together, these results introduced two new exciting concepts: the existence of an ER-specific autophagy pathway (Figure 1-3), and a strong relationship between the UPR and autophagy.

A key question in ER-phagy is how accumulation of large aggregates in the ER “signals” to the cytosolic macroautophagy machinery to fragment specific ER segments. One hypothesis is that ER transmembrane receptors, acting as ER-phagy receptors, must transmit this signal (Figure 1-3). These receptors would directly link the buildup of large aggregates in the ER to the core cytosolic macroautophagic machinery. To date, four ER-phagy receptors have been identified, namely FAM134B, Sec62, Cell Cycle Progression Gene 1 (CCPG1), and Reticulon3 (RTN3) (Figure 1-3). Each of these receptors contain at least one LC3-interacting region (LIR), a crucial motif that enables the receptors to connect to the core macroautophagic machinery (Birgisdottir et al., 2013) (Figure 1-3).

Perhaps the most-well studied of these receptors is FAM134B (homologous to Atg40 in yeast). FAM134B is an integral membrane protein, containing a N-terminal cytosolic tail, a reticulon-homology domain (RHD), and a C-terminal cytosolic tail containing one LIR (Figure 1-3). Localized to ER sheets, FAM134B was the first mammalian ER-phagy receptor to be identified that assist in the turnover of ER segments to the lysosome for degradation (Khaminets et al., 2015; Mochida et al., 2015). Moreover, recent studies have identified specific cargos for FAM134B-dependent ER-phagy (Forrester et al., 2019; Schultz et al., 2018).

Relevant to this thesis is the ER-phagy receptor RTN3. Reticulons are wedge-like sculptors of the ER, creating a complex and dynamic network of tubular ER branches emanating from ER sheets. Each reticulon harbors an RHD region with varying lengths of N- and C-terminal cytoplasmic tails. Moreover, reticulons gene products are subject

to differential splicing, generating smaller isomers (Yang and Strittmatter, 2007). For example, RTN4 has 3 splice variants, with RTN4A being full length and 4B and 4C having shorter N-terminal tails (Yang and Strittmatter, 2007). The expression of RTN4A is almost exclusively neural while RTN4B is found in most tissues (Oertle and Schwab, 2003; Ramo et al., 2016). While reticulons have been studied for years, only recently was RTN3's role in ER-phagy discovered.

Analogous to FAM134B, RTN3 is an integral membrane protein, extending only as far as the cytosolic-facing leaflet of ER membrane. This receptor contains six LIR domains on its N-terminal cytosolic tail. Although RTN3-mediated ER-phagy has been shown to promote ER tubule turnover during starvation conditions (Grumati et al., 2017), no known cargos of RTN3-mediated ER-phagy have yet been reported.

Because many diseases result from protein misfolding, cells must deploy ER protein selective degradative mechanisms, including ERAD and ER-phagy, in order to maintain proper homeostasis. A key gap in our knowledge is how specific misfolded substrates are recognized by these pathways and efficiently degraded. The research presented in Chapters 2-4 focuses on how the ERAD and ER-phagy protein quality control pathways are deployed in response to misfolding of a mutant proinsulin molecule that causes a newly identified form of diabetes called Mutant *INS*-gene-induced Diabetes of Youth (MIDY).

Mutant *INS*-gene-induced Diabetes of Youth (MIDY)

Insulin is a peptide hormone secreted from pancreatic β-cells to regulate blood glucose levels. Similar to other peptide hormones, insulin is synthesized as an inactive precursor. Preproinsulin harbors a N-terminal signal sequence, followed by a B chain, a connecting C-peptide, and an A chain. Preproinsulin is co-translationally translocated into the ER where signal peptidase cleaves the signal sequence resulting in formation of proinsulin (Chan et al., 1976; Steiner et al., 1967). Proinsulin then undergoes multiple rounds of oxidative folding in which three conserved disulfide bonds are formed.

The first disulfide bond formed is between the cysteine at the 19th residue on the B chain (named B19) and the cysteine at the 20th position on the A chain (A20), thereby generating the B19-A20 disulfide bond (Haataja et al., 2016; Hua et al., 2006; Yan et al., 2003). Once this is generated, two additional disulfide bonds will form between cysteine B7 and cysteine A7 (called the B7-A7 disulfide bond) and a final intrachain A6-A11 disulfide bond. Upon proper folding, non-covalent proinsulin dimers exit the ER via COPII-coated vesicles, followed by transport through the Golgi apparatus where proinsulin is packaged into immature secretory granules. Here prohormone convertase PC1/3 and PC2 excise proinsulin's C-peptide. The resulting bioactive insulin, with its B and A chains connected via the B7-A7 and B19-A20 disulfide bonds, is poised for secretion.

Mutant *INS*-gene-induced Diabetes of Youth (MIDY) is an autosomal dominant diabetes mellitus (DM) characterized by early age of onset, severe hyperglycemia, and β-cell death (Liu et al., 2010a; Stoy et al., 2007; Weiss, 2009, 2013). As the name suggests,

MIDY is caused by mutations in the *INS* gene. Over the past decade, ~30 MIDY mutations have been identified. These missense mutations do not map to a specific region of the proinsulin molecule. Instead, they tend to be found in conserved hydrophobic residues or at the cysteines themselves (Liu et al., 2010b).

MIDY mutations result in proinsulin misfolding in the ER (Figure 1-4). When this occurs, proinsulin fails to exit the ER. As a result, its maturation through the secretory pathway does not occur and the β-cell fails to make sufficient insulin. Despite this, the failed maturation of these mutant proinsulins is not the direct cause of insulin deficiency. Instead, mutant proinsulin binds to and interferes with ER exit of WT proinsulin. A majority of MIDY mutant proinsulins form mixed disulfide-linked complexes with coexpressed WT proinsulin in the ER leading to decreased WT insulin secretion (Liu et al., 2010a). Surprisingly, this toxic gain of function effect on bystander WT occurs even in MIDY mutants where the missense mutation does not feature a cysteine addition or subtraction. For instance, the L(B11)P and G(B23)V mutants decrease total mature insulin while also engaging WT in disulfide-linked complexes (Liu et al., 2010a). In the case of the G(B23)V MIDY mutant, its inability to interchain disulfide bond between the B and A chains ultimately leads to availability of the free thiols to engage in mixed disulfide bonds with coexpressed WT proinsulin (Liu et al., 2010a; 2010b). Thus, while not directly adding or subtracting out a cysteine residue, some MIDY proinsulin mutants are unable to properly fold resulting in free reactive thiols that readily engage coexpressed folding WT proinsulin (Figure 1-4).

Based on this insight, MIDY can conceptually be managed by two approaches. The first is to promote efficient WT proinsulin folding such that it can "escape" from the MIDY proinsulin mutant by rapidly exiting the ER. The second is to selectively degrade the MIDY proinsulin mutant. In this scenario, efficient removal of MIDY proinsulin mutant from the ER would allow bystander WT proinsulin to fold properly and exit the ER, producing mature bioactive insulin that would alleviate the disease phenotype. My thesis is motivated by the second conceptual approach.

Prior to my work, the underlying ER quality control mechanisms that degrade MIDY proinsulin mutants were not fully understood. Although previous studies implicated UPR and several components of ERAD and autophagy as involved in removing mutant proinsulin (Allen et al., 2004; Bachar-Wikstrom et al., 2013; Gupta et al., 2010), mechanistic insights into how mutant proinsulins were triaged and degraded were lacking. In this thesis, I have focused on one model mutant proinsulin called *Akita*, a mutation in which the cysteine at the 7th position on the A chain is mutated to a tyrosine (Wang et al., 1999). The *Akita* proinsulin mutant fails to make the B7-A7 disulfide bond essential for proper folding in the ER. This results in the *Akita* mutant proinsulin forming massive disulfide-linked protein complexes with other *Akita* and WT proinsulin molecules, causing severe ER stress (Figure 1.4). Human patients and rodent models of *Akita*-mediated MIDY develop DM neonatally (human at <6 months of age; mice at 4 weeks of age). *Akita* males have extreme hyperglycemia, β-cell apoptosis, and often die around 12-14 weeks after birth (Izumi et al., 2003; Liu et al., 2007; Wang et al., 1999). For these reasons, *Akita* is an attractive misfolded model substrate for the MIDY

disease. The study of *Akita* should enable us to clarify the ER quality control mechanisms used to maintain cellular homeostasis in an effort to avoid or alleviate disease progression.

This thesis aims to address several major unknown questions: how is *Akita* mutant proinsulin degraded? What components of ER quality control triage and degrade the misfolded mutant proinsulin? Can modulating ER quality control mechanisms enhance *Akita* degradation to ultimately rescue WT insulin secretion deficiencies in the disease? Chapter 2 of this thesis uncovers how *Akita* mutant proinsulin is recognized by an ER oxidoreductase called protein disulfide isomerase (PDI). My analyses revealed that PDI acts as a reductase, reducing *Akita* high molecular weight disulfide-bonded complexes to smaller oligomeric species that are competent to undergo ERAD. In this pathway, *Akita* retrotranslocates across the Hrd1 E3 ubiquitin ligase and is extracted into the cytosol by the p97 ATPase *en route* to the proteasome for degradation. In Chapter 3, I begin to dissect the role of the ER luminal chaperone Grp170 in triaging *Akita*. I found that overexpression of Grp170 enhances *Akita* degradation, thereby restoring WT insulin secretion – this finding provided a proof-in-principle strategy to alleviate the MIDY disease. In Chapter 4, I further clarify Grp170's molecular function by revealing that it acts to prevent aggregation of *Akita*. Strikingly, my results demonstrate that if *Akita* continues to aggregate despite the presence of Grp170, the ER-phagy receptor RTN3 can help to dispose of these aggregates via the ER-phagy pathway. This, to our knowledge, is the identification of the first substrate for RTN3-dependent ER-phagy.

In summary, the collective findings presented in my thesis elucidate how a specific misfolded ER substrate - *Akita* mutant proinsulin - is recognized, triaged, and degraded by coordinated ER quality control mechanisms. I envision that insights from this work can provide a framework for a rational approach to alleviate the MIDY disease.

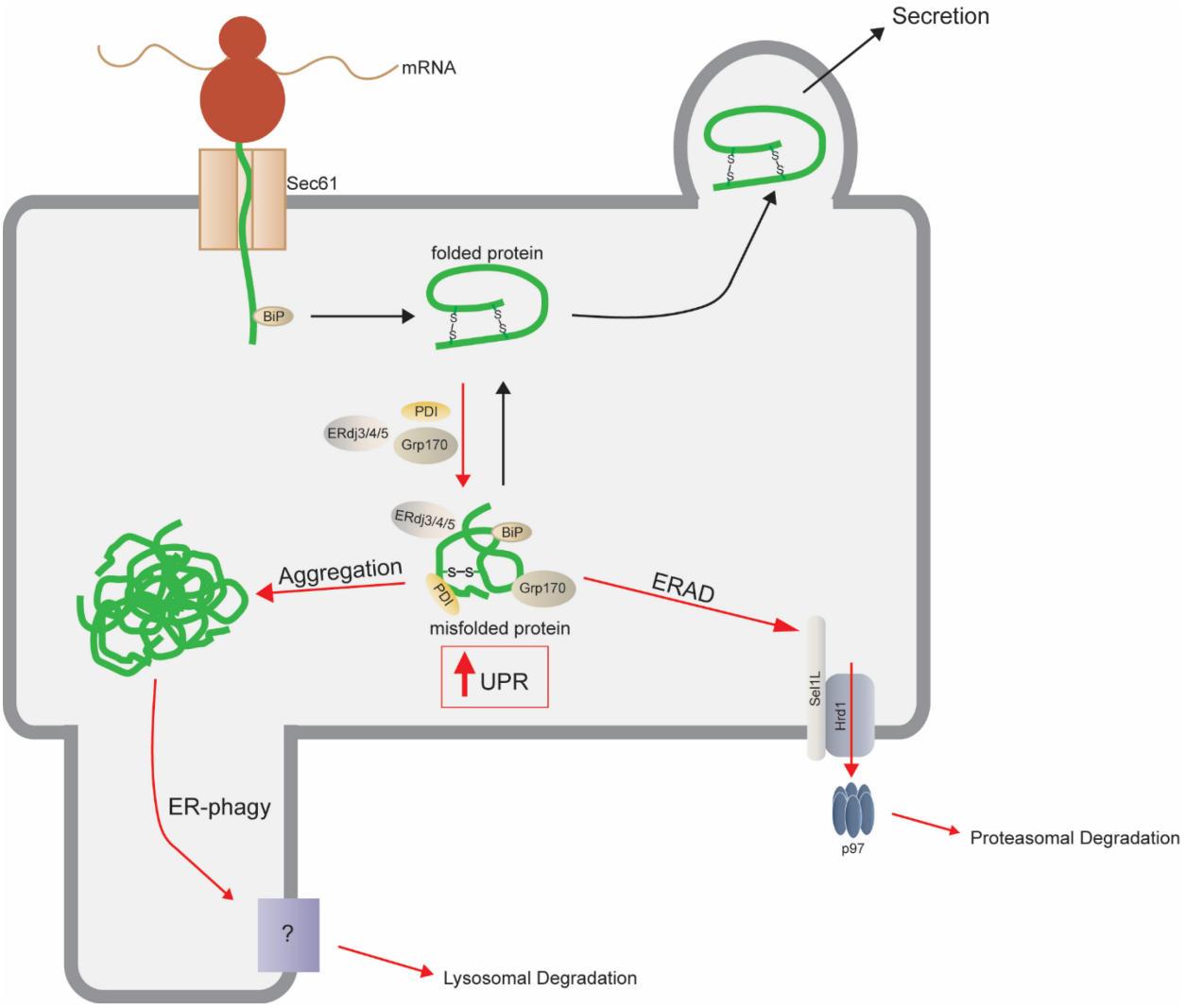

Figure 1-1. Protein folding and misfolding in the Endoplasmic Reticulum. Newly synthesized polypeptides enter the endoplasmic reticulum (ER) by translocation through the Sec61 channel via a ratcheting mechanism performed by the Hsp70 chaperone BiP. In the ER, multiple rounds of oxidative folding will assist the polypeptide fold into its native, functional structure. If problems arise, other chaperones (i.e. PDI oxidoreductases, Hsp40s, Hsp70s, Hsp90s) will attempt to refold the misfolded substrate. When correctly refolded, the polypeptide can exit the ER for anterograde transport through the endomembrane system. Proteins that fail to reach a correct conformational state can be degraded via the ERAD pathway (cytosolic proteasomal degradation) or ER-phagy (lysosomal degradation) if aggregation occurs. Misfolded protein accumulation will activate the Unfolded Protein Response (UPR), which directly upregulates ERAD and ER-phagy components to assist in removal of these misfolded substrates.

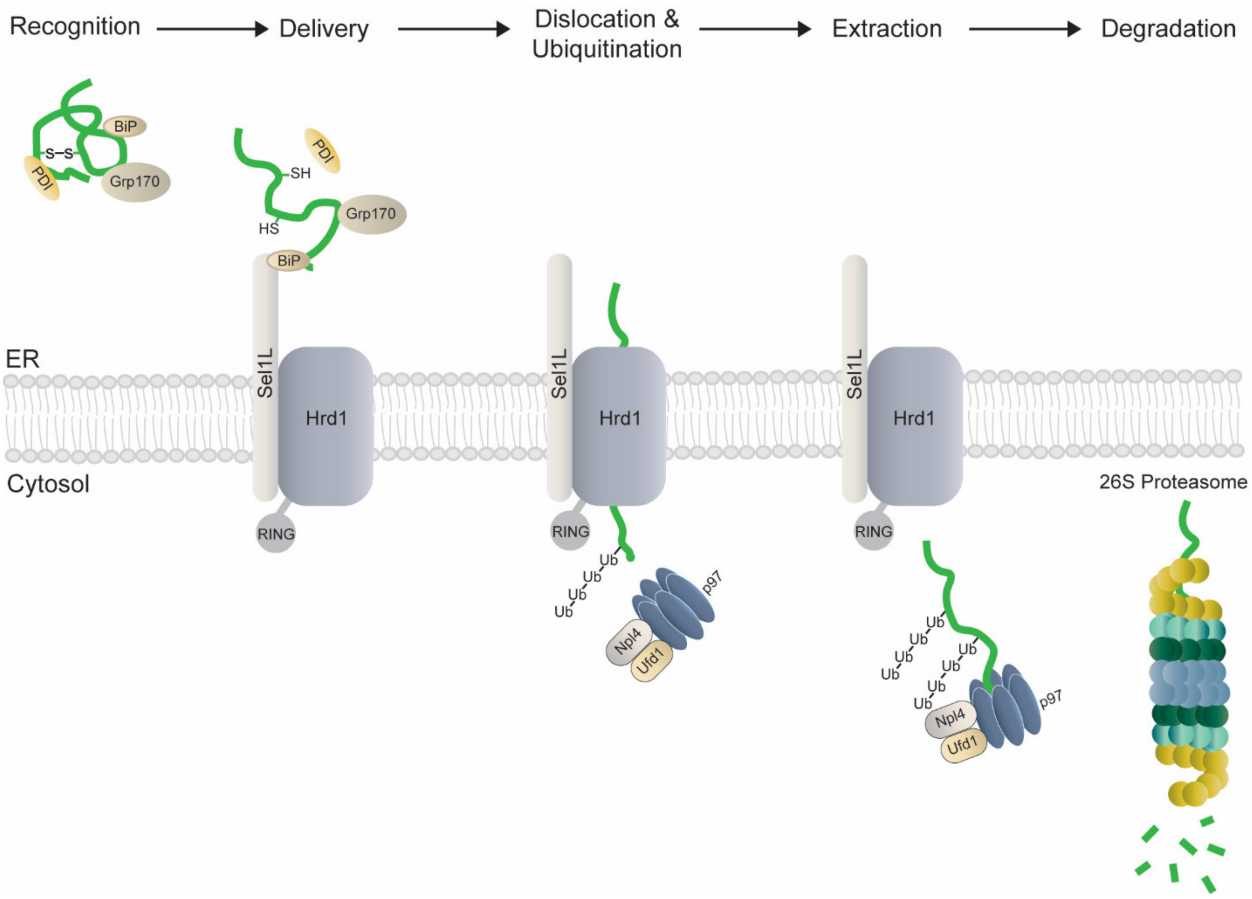

Figure 1-2. Canonical Endoplasmic Reticulum-associated degradation (ERAD-L) pathway. Misfolded ER-luminal clients will be selectively recognized and triaged by ER-resident chaperones. Substrates that contain disulfide bonds will be reduced by ER oxidoreductases, preparing the substrate for delivery to the ERAD ER-membrane channel. Here, the substrate will be passed to Sel1L, the major adaptor for Hrd1, the E3 ubiquitin ligase and retrotranslocon. Once chaperones dissociate from the substrate, the substrate will be dislocated through the Hrd1 channel. Once exposed on the cytosolic surface of the ER, Hrd1 polyubiquitinates the substrate through its RING domain. Extraction from Hrd1 involves the AAA+ ATPase, p97, and its co-factors Npl4 and Ufd1. p97 will then deliver the polyubiquitinated substrate to the 26S proteasome for degradation.

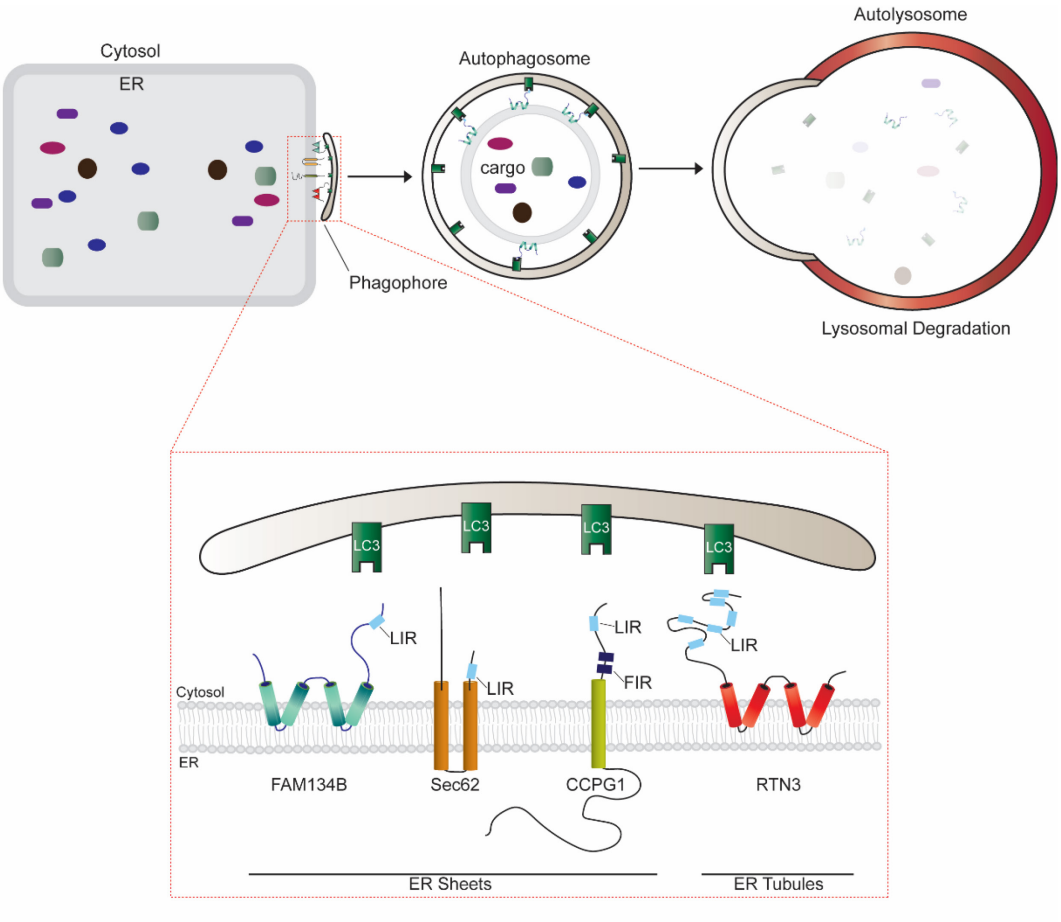

Figure 1-3. ER-phagy pathway and structural analysis of the ER-phagy ER-receptors. ER luminal and membrane misfolded clients unable to undergo ERAD can be degraded by ER-phagy. ER-phagy begins with signaling from one of four ER-phagy ER-receptors: ER sheet localized FAM134B, Sec62, and CCPG1, and ER tubule localized RTN3. These receptors directly link to LC3-II, the lipidated LC3, initiating phagophore recruitment and engulfment of a segment of ER membrane and lumen. The phagophore expands and closes off forming an autophagosome which then fuses downstream with the lysosome. Internal proteins and lipids will be degraded in the lysosome for nutrient recycling and to restore homeostasis.

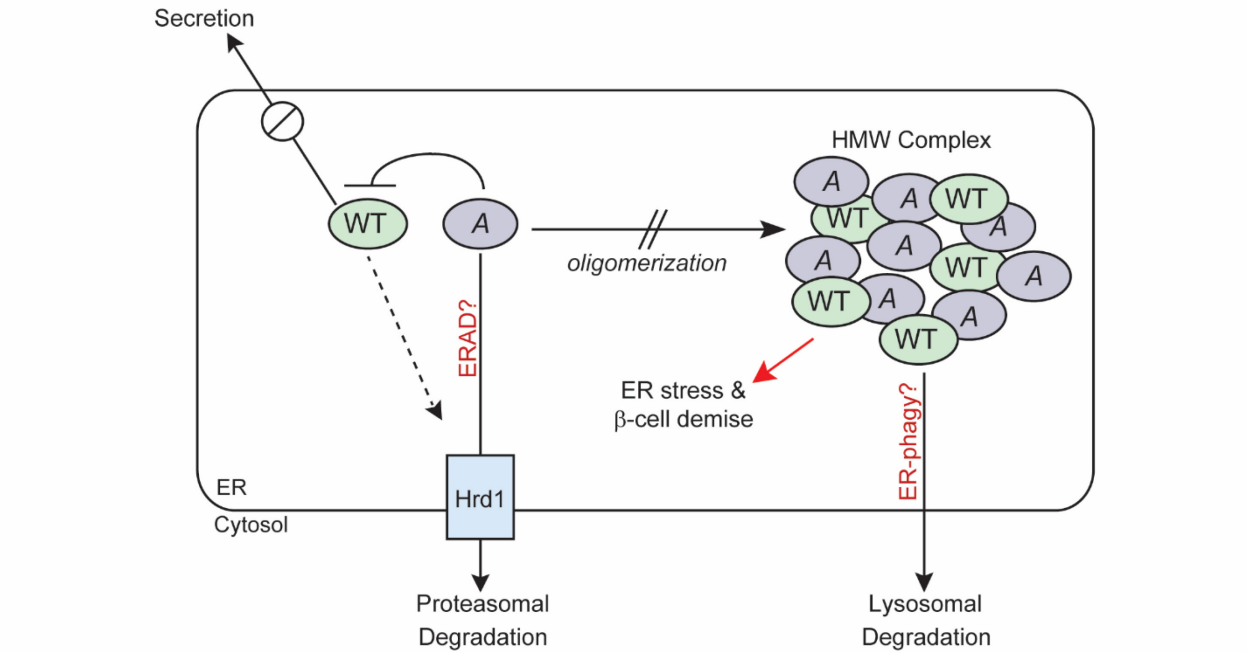

Figure 1-4. Pathogenesis of the *Akita* proinsulin mutant in Mutant *INS*-gene-induced Diabetes of Youth. *Akita* (*A* in purple) mutant proinsulin binds to WT proinsulin (WT in green) via mixed disulfides, sequestering it within the ER. As a result, WT proinsulin cannot mature and secrete as insulin. Misregulation of blood glucose levels signals back to pancreatic b-cells to upregulate the insulin gene. However, this exacerbates the problem as more *Akita* and WT proinsulin enter the ER, oligomerize into high molecular weight complexes which induce severe ER stress and β-cell demise. To counteract this toxic gain of function effect from *Akita* proinsulin, pancreatic β-cells may use ERAD, ER-phagy, or other ER protein quality control mechanisms to degrade the misfolded *Akita*.

REFERENCES

Allen, J.R., Nguyen, L.X., Sargent, K.E., Lipson, K.L., Hackett, A., and Urano, F. (2004). High ER stress in beta-cells stimulates intracellular degradation of misfolded insulin. Biochem Biophys Res Commun *324*, 166-170.

Bachar-Wikstrom, E., Wikstrom, J.D., Ariav, Y., Tirosh, B., Kaiser, N., Cerasi, E., and Leibowitz, G. (2013). Stimulation of autophagy improves endoplasmic reticulum stress-induced diabetes. Diabetes *62*, 1227-1237.

Baldridge, R.D., and Rapoport, T.A. (2016). Autoubiquitination of the Hrd1 Ligase Triggers Protein Retrotranslocation in ERAD. Cell *166*, 394-407.

Barlowe, C., Orci, L., Yeung, T., Hosobuchi, M., Hamamoto, S., Salama, N., Rexach, M.F., Ravazzola, M., Amherdt, M., and Schekman, R. (1994). COPII: a membrane coat formed by Sec proteins that drive vesicle budding from the endoplasmic reticulum. Cell *77*, 895-907.

Bates, G. (2003). Huntingtin aggregation and toxicity in Huntington's disease. Lancet *361*, 1642-1644.

Behnke, J., Feige, M.J., and Hendershot, L.M. (2015). BiP and its nucleotide exchange factors Grp170 and Sil1: mechanisms of action and biological functions. J Mol Biol *427*, 1589-1608.

Behnke, J., and Hendershot, L.M. (2014). The large Hsp70 Grp170 binds to unfolded protein substrates in vivo with a regulation distinct from conventional Hsp70s. J Biol Chem *289*, 2899-2907.

Behnke, J., Mann, M.J., Scruggs, F.L., Feige, M.J., and Hendershot, L.M. (2016). Members of the Hsp70 Family Recognize Distinct Types of Sequences to Execute ER Quality Control. Mol Cell *63*, 739-752.

Bernales, S., McDonald, K.L., and Walter, P. (2006). Autophagy counterbalances endoplasmic reticulum expansion during the unfolded protein response. PLoS Biol *4*, e423.

Birgisdottir, A.B., Lamark, T., and Johansen, T. (2013). The LIR motif - crucial for selective autophagy. J Cell Sci *126*, 3237-3247.

Bodnar, N.O., Kim, K.H., Ji, Z., Wales, T.E., Svetlov, V., Nudler, E., Engen, J.R., Walz, T., and Rapoport, T.A. (2018). Structure of the Cdc48 ATPase with its ubiquitin-binding cofactor Ufd1-Npl4. Nat Struct Mol Biol *25*, 616-622.

Braakman, I., and Hebert, D.N. (2013). Protein folding in the endoplasmic reticulum. Cold Spring Harb Perspect Biol *5*, a013201.

Chan, S.J., Keim, P., and Steiner, D.F. (1976). Cell-free synthesis of rat preproinsulins: characterization and partial amino acid sequence determination. Proc Natl Acad Sci U S A *73*, 1964-1968.

Chartron, J.W., Hunt, K.C., and Frydman, J. (2016). Cotranslational signal-independent SRP preloading during membrane targeting. Nature *536*, 224-228.

Connolly, T., and Gilmore, R. (1989). The signal recognition particle receptor mediates the GTP-dependent displacement of SRP from the signal sequence of the nascent polypeptide. Cell *57*, 599-610.

Ellgaard, L., McCaul, N., Chatsisvili, A., and Braakman, I. (2016). Co- and Post-Translational Protein Folding in the ER. Traffic *17*, 615-638.

Forrester, A., De Leonibus, C., Grumati, P., Fasana, E., Piemontese, M., Staiano, L., Fregno, I., Raimondi, A., Marazza, A., Bruno, G.*, et al.* (2019). A selective ER-phagy exerts procollagen quality control via a Calnexin-FAM134B complex. EMBO J *38*.

Gething, M.J., and Sambrook, J. (1992). Protein folding in the cell. Nature *355*, 33-45.

Grumati, P., Morozzi, G., Holper, S., Mari, M., Harwardt, M.I., Yan, R., Muller, S., Reggiori, F., Heilemann, M., and Dikic, I. (2017). Full length RTN3 regulates turnover of tubular endoplasmic reticulum via selective autophagy. Elife *6*.

Gupta, S., McGrath, B., and Cavener, D.R. (2010). PERK (EIF2AK3) regulates proinsulin trafficking and quality control in the secretory pathway. Diabetes *59*, 1937-1947.

Haataja, L., Manickam, N., Soliman, A., Tsai, B., Liu, M., and Arvan, P. (2016). Disulfide Mispairing During Proinsulin Folding in the Endoplasmic Reticulum. Diabetes *65*, 1050-1060.

Hamasaki, M., Noda, T., Baba, M., and Ohsumi, Y. (2005). Starvation triggers the delivery of the endoplasmic reticulum to the vacuole via autophagy in yeast. Traffic *6*, 56-65.

Harding, H.P., Zhang, Y., Bertolotti, A., Zeng, H., and Ron, D. (2000). Perk is essential for translational regulation and cell survival during the unfolded protein response. Mol Cell *5*, 897-904.

Hatahet, F., and Ruddock, L.W. (2009). Protein disulfide isomerase: a critical evaluation of its function in disulfide bond formation. Antioxid Redox Signal *11*, 2807-2850.

Haze, K., Yoshida, H., Yanagi, H., Yura, T., and Mori, K. (1999). Mammalian transcription factor ATF6 is synthesized as a transmembrane protein and activated by proteolysis in response to endoplasmic reticulum stress. Mol Biol Cell *10*, 3787-3799.

Hua, Q.X., Mayer, J.P., Jia, W., Zhang, J., and Weiss, M.A. (2006). The folding nucleus of the insulin superfamily: a flexible peptide model foreshadows the native state. J Biol Chem *281*, 28131-28142.

Inoue, T., and Tsai, B. (2015). A nucleotide exchange factor promotes endoplasmic reticulum-to-cytosol membrane penetration of the nonenveloped virus simian virus 40. J Virol *89*, 4069-4079.

Irvine, G.B., El-Agnaf, O.M., Shankar, G.M., and Walsh, D.M. (2008). Protein aggregation in the brain: the molecular basis for Alzheimer's and Parkinson's diseases. Mol Med *14*, 451-464.

Izumi, T., Yokota-Hashimoto, H., Zhao, S., Wang, J., Halban, P.A., and Takeuchi, T. (2003). Dominant negative pathogenesis by mutant proinsulin in the Akita diabetic mouse. Diabetes *52*, 409-416.

Khaminets, A., Heinrich, T., Mari, M., Grumati, P., Huebner, A.K., Akutsu, M., Liebmann, L., Stolz, A., Nietzsche, S., Koch, N.*, et al.* (2015). Regulation of endoplasmic reticulum turnover by selective autophagy. Nature *522*, 354-358.

Korennykh, A.V., Egea, P.F., Korostelev, A.A., Finer-Moore, J., Zhang, C., Shokat, K.M., Stroud, R.M., and Walter, P. (2009). The unfolded protein response signals through high-order assembly of Ire1. Nature *457*, 687-693.

Kozutsumi, Y., Segal, M., Normington, K., Gething, M.J., and Sambrook, J. (1988). The presence of malfolded proteins in the endoplasmic reticulum signals the induction of glucose-regulated proteins. Nature *332*, 462-464.

Liu, M., Haataja, L., Wright, J., Wickramasinghe, N.P., Hua, Q.X., Phillips, N.F., Barbetti, F., Weiss, M.A., and Arvan, P. (2010a). Mutant INS-gene induced diabetes of youth: proinsulin cysteine residues impose dominant-negative inhibition on wild-type proinsulin transport. PLoS One *5*, e13333.

Liu, M., Hodish, I., Haataja, L., Lara-Lemus, R., Rajpal, G., Wright, J., and Arvan, P. (2010b). Proinsulin misfolding and diabetes: mutant INS gene-induced diabetes of youth. Trends Endocrinol Metab *21*, 652-659.

Liu, M., Hodish, I., Rhodes, C.J., and Arvan, P. (2007). Proinsulin maturation, misfolding, and proteotoxicity. Proc Natl Acad Sci U S A *104*, 15841-15846.

Marcinowski, M., Holler, M., Feige, M.J., Baerend, D., Lamb, D.C., and Buchner, J. (2011). Substrate discrimination of the chaperone BiP by autonomous and cochaperone-regulated conformational transitions. Nat Struct Mol Biol *18*, 150-158.

Matlack, K.E., Misselwitz, B., Plath, K., and Rapoport, T.A. (1999). BiP acts as a molecular ratchet during posttranslational transport of prepro-alpha factor across the ER membrane. Cell *97*, 553-564.

Meyer, H., Bug, M., and Bremer, S. (2012). Emerging functions of the VCP/p97 AAA-ATPase in the ubiquitin system. Nat Cell Biol *14*, 117-123.

Mochida, K., Oikawa, Y., Kimura, Y., Kirisako, H., Hirano, H., Ohsumi, Y., and Nakatogawa, H. (2015). Receptor-mediated selective autophagy degrades the endoplasmic reticulum and the nucleus. Nature *522*, 359-362.

Mueller, B., Lilley, B.N., and Ploegh, H.L. (2006). SEL1L, the homologue of yeast Hrd3p, is involved in protein dislocation from the mammalian ER. J Cell Biol *175*, 261-270.

Oertle, T., and Schwab, M.E. (2003). Nogo and its paRTNers. Trends Cell Biol *13*, 187-194.

Oka, O.B., Pringle, M.A., Schopp, I.M., Braakman, I., and Bulleid, N.J. (2013). ERdj5 is the ER reductase that catalyzes the removal of non-native disulfides and correct folding of the LDL receptor. Mol Cell *50*, 793-804.

Parzych, K.R., and Klionsky, D.J. (2014). An overview of autophagy: morphology, mechanism, and regulation. Antioxid Redox Signal *20*, 460-473.

Plath, K., and Rapoport, T.A. (2000). Spontaneous release of cytosolic proteins from posttranslational substrates before their transport into the endoplasmic reticulum. J Cell Biol *151*, 167-178.

Pobre, K.F.R., Poet, G.J., and Hendershot, L.M. (2019). The endoplasmic reticulum (ER) chaperone BiP is a master regulator of ER functions: Getting by with a little help from ERdj friends. J Biol Chem *294*, 2098-2108.

Ramo, O., Kumar, D., Gucciardo, E., Joensuu, M., Saarekas, M., Vihinen, H., Belevich, I., Smolander, O.P., Qian, K., Auvinen, P.*, et al.* (2016). NOGO-A/RTN4A and NOGO-B/RTN4B are simultaneously expressed in epithelial, fibroblast and neuronal cells and maintain ER morphology. Sci Rep *6*, 35969.

Rapoport, T.A. (2007). Protein translocation across the eukaryotic endoplasmic reticulum and bacterial plasma membranes. Nature *450*, 663-669.

Ruggiano, A., Foresti, O., and Carvalho, P. (2014). Quality control: ER-associated degradation: protein quality control and beyond. J Cell Biol *204*, 869-879.

Scherzinger, E., Lurz, R., Turmaine, M., Mangiarini, L., Hollenbach, B., Hasenbank, R., Bates, G.P., Davies, S.W., Lehrach, H., and Wanker, E.E. (1997). Huntingtin-encoded

polyglutamine expansions form amyloid-like protein aggregates in vitro and in vivo. Cell *90*, 549-558.

Schoebel, S., Mi, W., Stein, A., Ovchinnikov, S., Pavlovicz, R., DiMaio, F., Baker, D., Chambers, M.G., Su, H., Li, D.*, et al.* (2017). Cryo-EM structure of the protein-conducting ERAD channel Hrd1 in complex with Hrd3. Nature *548*, 352-355.

Schultz, M.L., Krus, K.L., Kaushik, S., Dang, D., Chopra, R., Qi, L., Shakkottai, V.G., Cuervo, A.M., and Lieberman, A.P. (2018). Coordinate regulation of mutant NPC1 degradation by selective ER autophagy and MARCH6-dependent ERAD. Nat Commun *9*, 3671.

Spillantini, M.G., Schmidt, M.L., Lee, V.M., Trojanowski, J.Q., Jakes, R., and Goedert, M. (1997). Alpha-synuclein in Lewy bodies. Nature *388*, 839-840.

Stein, A., Ruggiano, A., Carvalho, P., and Rapoport, T.A. (2014). Key steps in ERAD of luminal ER proteins reconstituted with purified components. Cell *158*, 1375-1388.

Steiner, D.F., Cunningham, D., Spigelman, L., and Aten, B. (1967). Insulin biosynthesis: evidence for a precursor. Science *157*, 697-700.

Stoy, J., Edghill, E.L., Flanagan, S.E., Ye, H., Paz, V.P., Pluzhnikov, A., Below, J.E., Hayes, M.G., Cox, N.J., Lipkind, G.M.*, et al.* (2007). Insulin gene mutations as a cause of permanent neonatal diabetes. Proc Natl Acad Sci U S A *104*, 15040-15044.

Tanzi, R.E., and Bertram, L. (2005). Twenty years of the Alzheimer's disease amyloid hypothesis: a genetic perspective. Cell *120*, 545-555.

Travers, K.J., Patil, C.K., Wodicka, L., Lockhart, D.J., Weissman, J.S., and Walter, P. (2000). Functional and genomic analyses reveal an essential coordination between the unfolded protein response and ER-associated degradation. Cell *101*, 249-258.

Tu, B.P., Ho-Schleyer, S.C., Travers, K.J., and Weissman, J.S. (2000). Biochemical basis of oxidative protein folding in the endoplasmic reticulum. Science *290*, 1571-1574.

Vincenz-Donnelly, L., Holthusen, H., Korner, R., Hansen, E.C., Presto, J., Johansson, J., Sawarkar, R., Hartl, F.U., and Hipp, M.S. (2018). High capacity of the endoplasmic reticulum to prevent secretion and aggregation of amyloidogenic proteins. EMBO J *37*, 337-350.

Walter, P., and Ron, D. (2011). The unfolded protein response: from stress pathway to homeostatic regulation. Science *334*, 1081-1086.

Wang, J., Takeuchi, T., Tanaka, S., Kubo, S.K., Kayo, T., Lu, D., Takata, K., Koizumi, A., and Izumi, T. (1999). A mutation in the insulin 2 gene induces diabetes with severe pancreatic beta-cell dysfunction in the Mody mouse. J Clin Invest *103*, 27-37.

Wang, M., and Kaufman, R.J. (2016). Protein misfolding in the endoplasmic reticulum as a conduit to human disease. Nature *529*, 326-335.

Weiss, M.A. (2009). Proinsulin and the genetics of diabetes mellitus. J Biol Chem *284*, 19159-19163.

Weiss, M.A. (2013). Diabetes mellitus due to the toxic misfolding of proinsulin variants. FEBS Lett *587*, 1942-1950.

Weitzmann, A., Volkmer, J., and Zimmermann, R. (2006). The nucleotide exchange factor activity of Grp170 may explain the non-lethal phenotype of loss of Sil1 function in man and mouse. FEBS Lett *580*, 5237-5240.

Werner, E.D., Brodsky, J.L., and McCracken, A.A. (1996). Proteasome-dependent endoplasmic reticulum-associated protein degradation: an unconventional route to a familiar fate. Proc Natl Acad Sci U S A *93*, 13797-13801.

Yan, H., Guo, Z.Y., Gong, X.W., Xi, D., and Feng, Y.M. (2003). A peptide model of insulin folding intermediate with one disulfide. Protein Sci *12*, 768-775.

Yanagitani, K., Kimata, Y., Kadokura, H., and Kohno, K. (2011). Translational pausing ensures membrane targeting and cytoplasmic splicing of XBP1u mRNA. Science *331*, 586-589.

Yang, J., Zong, Y., Su, J., Li, H., Zhu, H., Columbus, L., Zhou, L., and Liu, Q. (2017). Conformation transitions of the polypeptide-binding pocket support an active substrate release from Hsp70s. Nat Commun *8*, 1201.

Yang, Y.S., and Strittmatter, S.M. (2007). The reticulons: a family of proteins with diverse functions. Genome Biol *8*, 234.

Ye, J., Rawson, R.B., Komuro, R., Chen, X., Dave, U.P., Prywes, R., Brown, M.S., and Goldstein, J.L. (2000). ER stress induces cleavage of membrane-bound ATF6 by the same proteases that process SREBPs. Mol Cell *6*, 1355-1364.

Ye, Y., Meyer, H.H., and Rapoport, T.A. (2001). The AAA ATPase Cdc48/p97 and its partners transport proteins from the ER into the cytosol. Nature *414*, 652-656.

Ye, Y., Shibata, Y., Yun, C., Ron, D., and Rapoport, T.A. (2004). A membrane protein complex mediates retro-translocation from the ER lumen into the cytosol. Nature *429*, 841-847.

CHAPTER 2: PDI Reductase Acts on *Akita* Mutant Proinsulin to Initiate Retrotranslocation Along the Hrd1/Sel1L-p97 Axis

He K, Cunningham CN, Manickam N, Liu M, Arvan P, Tsai B. PDI reductase acts on Akita mutant proinsulin to initiate retrotranslocation along the Hrd1/Sel1L-p97 axis. *Mol Biol Cell*. 2015;26(19):3413-23.

INTRODUCTION

Insulin biosynthesis is initiated when preproinsulin is translocated into the endoplasmic reticulum (ER) (Steiner et al., 1967) and its signal sequence is cleaved to generate proinsulin. Oxidative folding of proinsulin ensues (Liu et al., 2012), characterized by formation of three highly conserved disulfide bonds (denoted as B7-A7, B19-A20, and A6-A11). Properly folded proinsulin then exits the ER, is transported to the Golgi, and is delivered to secretory granules, where pro–hormone convertases excise the C-peptide, with B and A chains of mature insulin remaining attached via B7-A7 and B19-A20 interchain disulfide bonds.

Recently a subset of human insulin gene mutations has been discovered to cause an autosomal-dominant syndrome that we call mutant *INS* gene–induced diabetes of youth (MIDY; (Liu et al., 2010a; Stoy et al., 2007; Weiss, 2013)): insulin-deficient diabetes

without islet autoantibodies. MIDY is a protein-misfolding disease, and most MIDY proinsulin mutants misfold within the ER, causing permanent neonatal or later-onset diabetes, depending upon the particular mutation. Among these, the most-studied MIDY mutant is *Akita* proinsulin: substitution at the A7 cysteine causes severe early-onset diabetes in both humans and *Akita* mice.

MIDY mutants fail to be transported from the ER to the Golgi complex. Moreover, MIDY mutants impair wild-type (WT) proinsulin exit from the ER, thereby limiting WT insulin production, provoking increased blood glucose excursions, and stimulating expression of even more proinsulin (both mutant and WT), which remains entrapped within the ER (Liu et al., 2007; Weiss, 2013). This triggers ER stress that may ultimately result in β-cell death.

Eliminating buildup of mutant proinsulin in the ER might restore β-cell function and survival. This possibility motivates us to investigate cellular mechanisms of degradation of misfolded proinsulin. One such mechanism is the ER-associated degradation (ERAD) pathway (Smith et al., 2011; Tsai et al., 2002). In ERAD, a misfolded ER substrate must first be identified by ER lumenal components and then delivered across (retrotranslocated) to the cytosolic side of the ER membrane for ubiquitination, with the assistance of ERAD membrane components (Carvalho et al., 2010; Stein et al., 2014). Finally, the ubiquitinated substrate is extracted from the ER membrane into the cytosol for delivery to proteasomes for degradation (Ye et al., 2001).

There is reason to suspect that MIDY mutants may use the ERAD pathway (Allen et al., 2004; Hartley et al., 2010; Tiwari et al., 2013), although how misfolded proinsulin in the ER lumen is recognized and primed for retrotranslocation remains unknown. Here we establish that canonical ERAD membrane components, including the E3 ubiquitin ligase Hrd1, its membrane-binding partner Sel1L, and cytosolic p97, help to conduct *Akita* proinsulin from the ER lumen to the cytosol. Strikingly, we find that protein disulfide isomerase (PDI), a profolding enzyme known to drive oxidation of disulfide bonds (Benham, 2012; Hatahet and Ruddock, 2009), instead exhibits a novel interaction with misfolded proinsulin to exert a prodegradative role that includes reducing proinsulin disulfide bonds. Our findings provide a framework for rational therapeutic approaches to preventing and treating diabetes provoked by proinsulin misfolding.

MATERIALS AND METHODS

Reagents

Antibodies used were as follows: rabbit anti-Myc (Immunology Consultants Laboratories, Portland, OR); mouse anti-VCP (p97), anti-PDI (RL90), and anti-ERp57 (Abcam, Cambridge, MA); rabbit anti-Hrd1 (Proteintech, Chicago, IL); rabbit anti-Hsp90 (H-114; Santa Cruz Biotechnology, Santa Cruz, CA); mouse anti-ubiquitin (Invitrogen, Carlsbad, CA); rabbit anti-FLAG, anti-Sel1L, and mouse and rabbit horseradish peroxidase (HRP) secondary antibodies (Sigma-Aldrich, St. Louis, MO); rabbit anti-Myc (9E10) for immunoprecipitation (IP; K. Verhey, University of Michigan, Ann Arbor, MI). Chemicals were from Sigma-Aldrich except when noted otherwise. Phenylmethylsulfonyl fluoride (PMSF) was from Acros Organics; DMEM, RPM1 1640 medium, and other cell culture reagents were from Life Technologies (Carlsbad, CA). An expression plasmid encoding Myc-epitope–tagged human C(A7)Y *Akita* mutant proinsulin (*Akita*-Myc) was previously described (Liu et al., 2010b). A second expression plasmid encoding Myc-tagged human C(A7)Y proinsulin was constructed in which all five remaining Cys residues were mutated to Ser residues; this kind of construct, previously referred to as proinsulin-DelCys (Liu et al., 2010a), is also known here as ΔCys-Myc. Six related expression plasmids encoding Myc-tagged human proinsulin were constructed in which five Cys residues were mutated to Ser; each construct retains only one Cys residue, and they are referred to as Keep B7, Keep B19, Keep A6, Keep A7, Keep A11, and Keep A20, respectively. Purification of His-tagged PDI from bacteria was as previously described (Forster et al., 2009). Human PDI trap mutants were gifts from T. Rapoport (Harvard University, Cambridge, MA). The INS-1 832/13 β-

cell line was a generous gift from Christopher Newgard (University of Texas Southwestern, Dallas, TX).

Cell culture, plasmid transfection, cycloheximide chase, immunoprecipitation, and immunoblotting

Rat INS-1 832/13 or human HEK 293T cells were cultured at 37°C in a humid incubator (5% CO_2). Cells were seeded on six-well plates 1 d before transfection of 1–3 μg of plasmid DNA using home-made polyethylenimine (PEI) or Lipofectamine 2000 (Invitrogen). At 4 h posttransfection, cells were treated with cycloheximide (100 μg/ml) and chased for 0, 2, 4, and 6 h. In experiments using ΔCys-Myc or single-Cys Keep mutants, cells were treated with MG132 (10 μM) for 3 h before cell lysis. Cells were harvested in phosphate-buffered saline (PBS) containing 10 mM *N*-ethylmaleimide (NEM). For IP, cells were lysed in 400 μl of RIPA buffer (Tris-HCl, pH 7.5, 150 mM NaCl, 1% NP-40, 1% sodium dexoycholate, 0.1% SDS) supplemented with 10 mM NEM and 1 mM PMSF; in Figure 3H, the modified RIPA buffer contained 0.25% SDS. Cells were incubated on ice for 10 min and centrifuged, and the resulting whole-cell extract (WCE) was incubated with antibody (1:200) at 4°C for 24 h, followed by 2 h of incubation with precleared protein A/G-agarose beads at 4°C. Beads were washed three times and boiled in SDS sample buffer with or without 100 mM DTT. For immunoblot analyses, cells were lysed in 100 μl of RIPA buffer to generate WCE, which was boiled in SDS sample buffer with 100 mM DTT. Then samples were resolved on 8–15% SDS–PAGE gels, transferred to nitrocellulose, and blotted with specific primary

and HRP-conjugated secondary (1:2000) antibodies according to manufacturer's protocols (Sigma-Aldrich).

siRNA knockdown of Hrd1, Sel1L, and PDI

siRNA was transfected into cells using RNAiMAX (Invitrogen), and cells were chased and harvested 48–72 h posttreatment. The sequences of the siRNAs are as follows: Dharmacon human Hrd1, 5′-GGAGACUGCCACUACAGUUGUUU-3′, at 10 nM for 48-h knockdown; Dharmacon human Sel1L, 5′-GAAACAAACAUUCGAGAUAUU-3′, at 25 nM for 48-h knockdown; and human PDI, 5′-CAACUUUGAAGGGGAGGUCTT-3′, and rat PDI, 5′-GCGCAUACUUGAGUUCUUUTT-3′, at 75 nM for 72-h knockdown.

siRNA-resistant PDI construct

siRNA-resistant WT PDI was generated with KOD Hot Start DNA polymerase (EMD Chemicals, Billerica, MA) from mouse WT PDI according to the manufacturer's protocol. The sequences of forward and reverse primers are as follows: forward, 5′-GCAGCTAGCCCCCATTTGGGACAAGCTCGGCGAAACCTACAAGGATCATGAGAATATC-3′; and reverse, 5′-GATATTCTCATGATCCTTGTAGGTTTCGCCGAGCTTGTCCCAAATGGGGGCTAGCTGC-3′. The mutated siRNA-resistant PDI construct was confirmed by sequencing. A 2-μg amount of siRNA-resistant PDI plasmid was transfected into HEK 293T cells with PEI 24 h posttransfection of the PDI siRNA.

Sucrose cushion sedimentation

Cells transfected with scrambled or PDI siRNA were lysed in RIPA buffer to generate a WCE as described. WCE was centrifuged at 50,000 rpm at 4°C for 20 min using a TLA

100 rotor (Beckman, Brea, CA). Half of the resulting supernatant (50 µl) was treated or not with DTT (100 mM) for 30 min on ice, layered over an equal volume of a 20% sucrose solution, and centrifuged at 75,000 rpm at 4°C for 30 min using the same rotor. Top (50 µl) and bottom (50 µl) fractions were separated and subjected to immunoblot analyses.

In vitro PDI reduction assay

PDI was expressed in *Escherichia coli* strain BL21-Pro and purified as previously described (Forster et al., 2009). Purified PDI was aliquoted and stored at −80°C. *Akita*-*Myc* was expressed in PDI-depleted HEK 293T cells for 24 h, followed by cell lysis (50 mM 4-(2-hydroxyethyl)-1-piperazineethanesulfonic acid [HEPES], 150 mM NaCl, 1% Triton X-100, 10 mM NEM, and 1 mM PMSF) and overnight immunoprecipitation as described. After three washes, *Akita*-Myc was eluted in 20 µl of a 0.5% SDS buffer at room temperature for 30 min, dialyzed, and diluted to 200 µl in a buffer containing 50 mM HEPES and 150 mM NaCl. Isolated *Akita*-Myc was incubated in the presence of 1 mM GSH and 1 mM GSSG with either PDI or PDI alkylated with 25 mM IAA, and the reaction was continued at 37°C for 30 min. Samples were separated on a nonreducing SDS–PAGE and subjected to immunoblot analysis.

RESULTS

The Hrd1-Sel1L complex promotes ERAD of *Akita* proinsulin

To determine whether *Akita* proinsulin is degraded by ERAD, we first evaluated whether Hrd1, the multitransmembrane E3 ubiquitin ligase that is also proposed to function as the retrotranslocon (Carvalho et al., 2010; Stein et al., 2014), controls the fate of transfected (Myc-tagged) *Akita* proinsulin. Using cycloheximide chase in 293T cells (and in β-cells; see later discussion), we found that Hrd1 knockdown markedly impaired degradation of *Akita* proinsulin (Figure 2-1A; quantified in Figure 2-1B). Of importance, depleting Hrd1 (or any other protein described in this study) did not trigger massive ER stress, as XBP1 remained largely unspliced under these conditions (Supplemental Figure 2-S1A). Our analyses also demonstrated that overexpressing enzymatically inactive, dominant-negative Hrd1-C291A (Bernardi et al., 2010) potently stabilized *Akita* proinsulin (Figure 2-1C, top). A smaller degree of inhibition of degradation of *Akita* proinsulin was also observed upon WT Hrd1-Myc overexpression (this is likely due to perturbation of the stoichiometric ratio of Hrd1 to its natural binding partners, in this way decreasing the efficiency of functional Hrd1-associated complexes). Overexpression of WT, mutant Hrd1, or any other construct in this study also did not provoke enhanced XBP1 splicing (Supplemental Figure 2-S1B). Together the results in Figure 2-1, A–C, indicate that Hrd1 participates in the degradation of *Akita* proinsulin.

Next we asked whether Sel1L also promotes ERAD of *Akita* proinsulin. Sel1L is a membrane protein that serves as a scaffold to engage ERAD lumenal components (Hosokawa et al., 2008; Mueller et al., 2008; Williams et al., 2013), interacts with Hrd1

(Mueller *et al.*, 2006), and recruits client substrates to Hrd1 (Bernasconi et al., 2010; Stanley et al., 2011). Using a similar cycloheximide-chase protocol, we found that Sel1L knockdown also impaired *Akita* ERAD (Figure 2-1D; quantified in Figure 2-1B), strongly implicating the Hrd1-Sel1L membrane complex in the degradation of *Akita* proinsulin.

Because *Akita* appears to use the classic ERAD pathway in which the Hrd1-Sel1L complex serves as the core membrane component, we asked whether expressing WT proinsulin might affect ERAD of *Akita*, as patients with MIDY harbor one WT copy of the proinsulin gene. Indeed, coexpressing superfolder green fluorescent protein–tagged WT proinsulin (SfGFP-WT proinsulin, which largely behaves as WT proinsulin; (Haataja et al., 2013) significantly impaired degradation of Myc-tagged *Akita* (Supplemental Figure 2-S1C, top). This result suggests that the established interaction between WT proinsulin and *Akita* (Liu et al., 2007) can functionally disrupt degradation of *Akita*, potentially exacerbating ER stress, which contributes to MIDY.

p97 facilitates *Akita* degradation

Because Hrd1 orients its catalytic E3 ligase domain on the cytosolic surface of the ER membrane, retrotranslocated substrates become available for ubiquitination, and the ubiquitinated substrates are then extracted into the cytosol—in most cases by the cytosolic p97 ATPase (Ye et al., 2001)—before being degraded by cytosolic proteasomes. To assess whether p97 participates in ERAD of *Akita* proinsulin, we overexpressed a histidine (His)-tagged WT or ATPase-defective dominant-negative version of p97 (QQ-p97). Whereas WT p97 was largely without effect, overexpression

of QQ p97-His markedly stabilized *Akita* proinsulin (Figure 2-2A; quantified in Figure 2-2B), implicating p97 in the extraction of *Akita* proinsulin from the ER membrane to the cytosol.

Because p97 binds to ubiquitinated substrates, blocking *Akita* proinsulin extraction into the cytosol should cause *Akita* proinsulin to accumulate as an ubiquitinated species. To test this, we cotransfected cells to express *Akita* proinsulin and QQ p97-His. When Myc-tagged *Akita* proinsulin was immunoprecipitated (Figure 2-2C, second from top), the polyubiquitinated species accumulated only in cells expressing QQ p97-His (Figure 2-2C, top). This finding is consistent with the idea that p97 extracts ubiquitinated *Akita* proinsulin from the ER membrane and supports that the classic Hrd1/Sel1L-p97 pathway promotes ERAD of *Akita* proinsulin.

PDI promotes *Akita* degradation

One major impediment to ERAD is the presence of disulfide bonds that hold the substrate in a plicated conformation believed to be incompatible with retrotranslocation. Because *Akita* proinsulin still harbors five cysteine residues in an aberrant disulfide configuration (Izumi et al., 2003; Liu et al., 2010a; Liu et al., 2007; Ye et al., 2001) that is unknown, enzymatic reduction of disulfide bonds is likely important for its retrotranslocation. The major ER-resident oxidoreductase is PDI, which is believed to promote oxidative folding of many newly synthesized secretory proteins (Benham, 2012; Hatahet and Ruddock, 2009). However, PDI does not appear to facilitate oxidative folding of proinsulin in the ER of pancreatic β-cells (Rajpal et al., 2012) and in fact has

been implicated in retrotranslocation of certain ERAD substrates and a bacterial toxin (Forster et al., 2006; Gillece et al., 1999). Indeed, we found that in cells in which PDI was knocked down for 3 d, *Akita* proinsulin was robustly stabilized (Figure 2-3A; quantified in Figure 2-3B). A similar effect on *Akita* degradation was observed when PDI was knocked down for only 2 d (Supplemental Figure 2-S1D). When a small interfering RNA (siRNA)–resistant PDI construct was expressed in PDI-knockdown cells, degradation of *Akita* proinsulin was largely restored (Figure 2-3C; quantified in Figure 2-3B). However, knockdown of ERp57 (Figure 2-3D) or ERdj5 (Figure 2-3E), ER-resident oxidoreductases (Appenzeller-Herzog and Ellgaard, 2008; Ushioda et al., 2008), did not significantly affect ERAD of *Akita* proinsulin (quantified in Figure 2-3B). These data strongly suggest that ERAD of *Akita* proinsulin is specifically targeted by PDI.

PDI can function as both an ER molecular chaperone and an ER oxidoreductase (Cai et al., 1994). To understand the predominant role of PDI in the ERAD of *Akita* proinsulin, we tested whether knockdown of PDI affected degradation of a proinsulin construct lacking all Cys residues (ΔCys-Myc; (Liu et al., 2010a), which is detected intracellularly in the presence, but not the absence, of MG132 treatment (Figure 2-3F). Of importance, silencing of PDI did not augment the steady-state level of ΔCys-Myc (Figure 2-3F), suggesting that the mechanism by which PDI facilitates retrotranslocation of *Akita* proinsulin likely involves interaction with one or more of its cysteine residues. A low level of a slower-migrating species (Figure 2-3F, asterisk) that appeared in the PDI-depleted cells may represent a different folded conformation of this artificial mutant proinsulin that persists even under SDS–PAGE, consistent with PDI being a chaperone

that unfolds ERAD substrates during retrotranslocation (Gillece et al., 1999). Of interest, treating cells with the reducing agent dithiothreitol (DTT) did not alter ΔCys-Myc's steady-state level but did for WT proinsulin-Myc (Figure 2-3G), suggesting that degradation of the cysteine-less proinsulin mutant is unaffected by changing the cellular redox state.

PDI interacts with, and acts as a reductase for, *Akita* proinsulin

To determine whether initiation of ERAD of *Akita* proinsulin involves a direct interaction with PDI, we exploited so-called PDI trap mutants, in which a CXXC thioredoxin motif (where C = cysteine and X = any amino acid) is mutated to CXXA. When functioning as a reductase, the first cysteine thiol of the CXXC motif attacks a disulfide bond in the substrate to form a mixed-disulfide intermediate that is rapidly broken by intradomain disulfide pairing with the second CXXC cysteine thiol. These steps reduce the substrate disulfide bond while internally oxidizing the thioredoxin motif. However, CXXA trap mutants can only cross-link with the substrate and cannot form the intradomain disulfide pair, thereby "trapping" mixed disulfide-bonded adducts between PDI and its substrates. Because PDI possesses two thioredoxin domains, we used two (FLAG-tagged) trap mutants: PDI C56A, to create the first CXXA, and PDI C400A, to create the second CXXA. When coexpressed with *Akita* proinsulin, we found that precipitation of either PDI trap mutant recovered disulfide-bonded adducts engaging both PDI and *Akita* under nonreducing conditions (Figure 2-4A, top). As a control, precipitating WT PDI did not recover any disulfide-bonded adduct with *Akita* (Supplemental Figure 2-S2A, compare lane 2 to lane 4). One of the main adducts recovered by precipitating PDI C56A had a

molecular mass of ~69 kDa (Figure 2-4A, asterisk) which corresponds precisely to the cumulative molecular masses of one PDI (59 kDa) plus one proinsulin (~10 kDa), strongly suggesting a direct disulfide bond rather than binding via intermediary proteins. Of interest, precipitation of PDI C400A recovered an adduct of ~79 kDa (Figure 2-4A, triple asterisks), likely representing one PDI molecule plus an *Akita* dimer. Other proinsulin-containing PDI adducts (Figure 2-4A, double and quadruple asterisks) were also recovered. By contrast, neither of two different ERp57 trap mutants nor three distinct ERp72 trap mutants captured *Akita* proinsulin (Supplemental Figure 2-S2B), strongly suggesting that PDI specifically engages *Akita* proinsulin.

We also found that the steady-state level of *Akita* proinsulin was higher in cells expressing PDI C56A than with other trap mutants (Supplemental Figure 2-S2B, fourth panel), suggesting that such trapping inhibits ERAD of *Akita* proinsulin. Indeed, cycloheximide-chase experiments confirmed that expression of PDI-C56A and PDI-C400A stabilized *Akita* proinsulin in comparison to expressing ERp57-C60A or P5 C58A (Supplemental Figure 2-S2C, top), where P5 represents yet another PDI family member. These analyses provide independent evidence that PDI specifically plays a functional role in targeting *Akita* proinsulin for ERAD.

Because *Akita* proinsulin lacks a cysteine at position A7, the Cys-B7 lacks its natural partner for disulfide bonding. Although this might render Cys-B7 especially available for cross-linking with PDI, proinsulin misfolding might involve a variety of disulfide mispairings, making other Cys residues more available for adduct formation with PDI.

To simplify our analysis, we constructed a family of proinsulin mutants each bearing only a single Cys residue. To our surprise, when coexpressed with the PDI-C56A trap mutant, two of the six single-Cys proinsulin mutants consistently coprecipitated to a greater degree with PDI: a proinsulin construct that harbors only the B19 Cys residue (Keep B19), and Keep A11 (Figure 2-3H; quantified in Supplemental Figure 2-S3A). However, even when Cys-B7 was the only available unpaired cysteine, the Keep B7 mutant did not preferentially interact with overexpressed PDI trap mutant (Figure 2-3H; quantified in Supplemental Figure 2-S3A). Similarly, when the various proinsulin mutants were precipitated (with anti-myc), Keep B7 consistently coprecipitated less PDI C56A-FLAG than did Keep B19 or Keep A11 (Supplemental Figure 2-S3B). (Curiously, Keep A20 was also able to coprecipitate PDI trap mutant more efficiently than others, suggesting that A20 is also a reactive cysteine, although association of Keep A20 with PDI trap might affect epitope exposure during immunoprecipitation with anti-FLAG.) Together these coprecipitation results support that even when freely available, the proinsulin B7 cysteine is disfavored from forming a disulfide bond with PDI; thus it is more likely that a complex pattern of intramolecular disulfide mispairing within *Akita* proinsulin accounts for the robust formation of *Akita* proinsulin adducts with PDI (Figure 2-4A).

We then examined the status of *Akita* in cells with PDI knockdown. When evaluated by nonreducing SDS–PAGE, *Akita* proinsulin in control cells formed high–molecular weight (MW) protein complexes and additionally migrated as a disulfide-bonded dimer and trimer (Figure 2-4B, top, lane 1). In PDI-knockdown cells (lane 2), the dimer and trimer

disappeared and likely entered the high-MW complex. The *Akita* monomer was revealed when the samples were subjected to reducing SDS–PAGE, with the *Akita* level being higher in PDI-depleted cells (Figure 2-4B, second from top, lanes 1 and 2). Addition of the proteasome inhibitor MG132 did not restore loss of the *Akita* dimer or trimer observed by nonreducing SDS–PAGE in PDI-depleted cells (Figure 2-4B, top, compare lanes 4 and 3), although the steady-state level of low-MW *Akita* did increase in the MG132-treated sample as expected (Figure 2-4B, top, compare lane 3 with lane 1). Whereas incubation with the autophagy inhibitor LY294002 (Blommaart et al., 1997) did enhance the steady-state level of *Akita* in control cells (Supplemental Figure 2-S4, compare lane 3 to lane 1), this inhibitor clearly did not restore the loss of *Akita* dimer or trimer in PDI-knockdown cells (Supplemental Figure 2-S4, top, compare lanes 4 and 3). These results suggest that autophagy is unlikely to be responsible for the disappearance of *Akita* dimer or trimer when PDI is depleted, although this process may contribute to quality control of *Akita* in control cells. Thus the data are consistent with the idea that disappearance of dimeric and trimeric *Akita* in PDI-depleted cells reflects a loss of proinsulin reductase activity rather than ERAD or ER-dependent autophagy of dimeric and trimeric *Akita* proinsulin, suggesting that enzymatically active PDI helps to limit *Akita* proinsulin from becoming engaged in high-MW disulfide-linked complexes.

As yet another independent approach, we layered cell extracts expressing *Akita* proinsulin over a 20% sucrose cushion and centrifuged, generating bottom and top fractions. The top fraction harbors lower-MW species, likely dimeric and monomeric species of *Akita* proinsulin (Figure 2-4C, top, lane 1), whereas the bottom fraction

(Figure 2-4C, top, lane 2) contains *Akita* proinsulin predominantly in high-MW complexes whose sizes are heterogeneous and appear to be larger than ~55 kDa. In control cells, a small portion of *Akita* proinsulin was recovered in the top fraction, with most detected at bottom (Figure 2-4C, top, lanes 1 and 2) whereas in PDI-knockdown cells, *Akita* proinsulin in the top fraction was eliminated (lanes 3 and 4). Of importance, when DTT was added to cell extracts before fractionation, even the PDI-knockdown cells yielded recovery of *Akita* proinsulin in the top fraction (Figure 2-4C, second from top), mimicking the effect of PDI. In PDI-depleted cells, the combined level of *Akita* in top plus bottom fractions of DTT-treated samples is similar to the *Akita* level found in the bottom fraction only in non–DTT-treated samples (Figure 2-4C, compare second from top and top, lanes 3 and 4). As expected, DTT reduced *Akita* in cell extracts derived from PDI-depleted cells, generating *Akita* monomer and dimer (Supplemental Figure 2-S5). However, a significant fraction of *Akita* proinsulin remained in high-MW complexes even after reduction by DTT (Figure 2-4C, bottom, lane 4), presumably due to noncovalent associations with each other or with other cellular proteins. This is consistent with a report suggesting that *Akita* engages in both covalent and noncovalent interactions to remain in the high-MW complexes (Yoshinaga et al., 2005). Our data thus strongly suggest that the inability to partition to the top fraction after PDI knockdown is due to a lack of reducing power for *Akita* proinsulin in the ER, supporting the notion that PDI acts as a reductase for *Akita* proinsulin. To assess whether PDI can reduce *Akita* in vitro, we used a modified protocol from the cell-based assay. *Akita* was first isolated from PDI-depleted cells by immunoprecipitation, followed by elution of the bound material using SDS and then dialysis to remove the detergent. Isolated *Akita* was

subsequently incubated with bacterially purified PDI (Figure 2-4D, lane 1) or, as a negative control, PDI alkylated with iodoacetamide (IAA; IAA-PDI), which should not reduce substrates, because its active cysteines are blocked. When this experiment was performed under a condition that mimics the ER redox environment (1 mM reduced glutathione [GSH] and 1 mM oxidized glutathione [GSSG]; Hwang *et al.*, 1992), PDI but not IAA-PDI induced formation of *Akita* dimer and trimer (Figure 2-4D, lanes 2 and 3; the dimer and trimer levels are quantified in the bottom graph), indicating that PDI uses its catalytic cysteines to reduce *Akita*. Note that *Akita* migrated slightly differently in this experiment (Figure 2-4D) compared with the cell-based assay (Figure 2-4B), possibly due to the harsh conditions used to isolate *Akita* in the in vitro assay. Nonetheless, these findings support the idea that PDI directly reduces *Akita* present in high-MW disulfide-bonded complexes to generate lower-MW species.

We previously reported that a subset of PDI localizes to the lumenal side of the Hrd1 membrane complex (Bernardi et al., 2010), which may allow this subset of PDI molecules to reduce ERAD substrates more efficiently. To test this, we examined the extent to which PDI trap mutants can capture *Akita* proinsulin when Hrd1 expression is silenced. Indeed, upon Hrd1 knockdown, the trapping of *Akita* proinsulin by PDI-C56A and PDI-C400A declined (Figure 2-4E, top). Thus Hrd1 availability enhances the efficiency of PDI in engaging *Akita* to reduce proinsulin disulfide bonds before retrotranslocation.

PDI, Hrd1, and p97 promote ERAD of *Akita* in pancreatic β-cells

We next explored the roles of PDI, Hrd1, and p97 in the ERAD of *Akita* proinsulin in the INS-1 832/13 pancreatic β-cell line. Similar to results observed in 293T cells (Supplemental Figure 2-S2C), expressing the PDI trap mutants in β-cells slowed degradation of *Akita* proinsulin compared with controls (GFP-FLAG, Figure 2-5A, top; the *Akita* band intensity is quantified in the graph at right). In addition, in INS-1 832/13 cells, *Akita* proinsulin was robustly stabilized by dominant-negative Hrd1-C291A but more modestly by WT Hrd1 (Figure 2-5B, top; the *Akita* band intensity is quantified in the graph at right). Finally, expressing QQ p97 potently inhibited *Akita* degradation (Figure 2-5C, top; the *Akita* band intensity is quantified in the graph at right). Together these findings indicate that, as in 293T cells, the role of the PDI-Hrd1-p97 axis in the ERAD of *Akita* proinsulin is indeed maintained within the context of pancreatic β-cells.

DISCUSSION

We propose the following model for cellular disposal of *Akita* mutant proinsulin (Figure 2-6): disulfide bonds engaged by *Akita* proinsulin, including intermolecular disulfide bonds, are reduced by PDI (step 1), whereupon *Akita* proinsulin retrotranslocates across the ER membrane via the Hrd1/Sel1L membrane complex (indeed, Hrd1 availability enhances PDI engagement of *Akita* proinsulin; step 2). Consistent with the known enzymatic activity of Hrd1, *Akita* proinsulin becomes polyubiquitinated upon arrival at the cytosolic side of the ER membrane (step 3) before extraction into the cytosol by p97, delivering *Akita* proinsulin to cytosolic proteasomes (step 4).

Degradation of *Akita* proinsulin engages key elements of the classic ERAD pathway Classic ERAD involves the Hrd1-Sel1L membrane complex and the cytosolic p97 ATPase (Smith et al., 2011; Tsai et al., 2002). The core component is the six-transmembrane-spanning Hrd1 (Kikkert et al., 2004), which associates with numerous adaptor proteins. Hrd1 is believed to serve, first, as the physical conduit for transfer of client substrates from the ER lumen to the cytosol (Carvalho et al., 2010; Stein et al., 2014) and, second, as the major E3 ligase that ubiquitinates ERAD substrates upon arrival at the cytosolic face of the ER membrane (Claessen et al., 2012). Using cycloheximide chase in conjunction with selective siRNA-mediated knockdown of Hrd1, we find that inhibiting Hrd1 function robustly blocks the degradation of *Akita* proinsulin, increasing its steady-state level (Figure 2-1, A and B). We also find that overexpression of enzymatically inactive Hrd1 (or, to a much lesser extent, WT Hrd1) similarly produces dominant-negative inhibition of *Akita* proinsulin degradation (Figure 2-1C). The

dominant effects of recombinant Hrd1 are believed to arise by competing for natural Hrd1 binding partners, thereby impairing the proper stoichiometry and function of Hrd1-associated protein complexes. Although the results of our WT Hrd1 overexpression experiments differ slightly from those reported previously (Allen et al., 2004), our conclusions are entirely concordant with the idea that the Hrd1 E3 ligase is involved in ERAD of *Akita* proinsulin, ubiquitinating the substrate when it emerges on the cytosolic side of the ER membrane.

Moreover, our findings demonstrate that Sel1L, a membrane binding partner of Hrd1, also participates in ERAD of *Akita* proinsulin (Figure 2-1, B and D). Yet another Hrd1 interactor, Herp, was also reported to modestly increase the steady-state level of *Akita* proinsulin, suggesting that Herp may also be involved in ERAD of this substrate (Hartley et al., 2010). The findings with both Herp and Sel1L support our contention that Hrd1 and its interacting partners guide ER-to-cytosol retrotranslocation of misfolded proinsulin.

On presentation on the cytosolic side of the ER membrane, polyubiquitinated ERAD substrates encounter the cytosolic p97 ATPase, which (in conjunction with its binding partners, including Ufd1 and Npl4; (Woodman, 2003)) uses the energy of ATP hydrolysis to extract the substrate into the cytosol (Zhang and Ye, 2014). We found that overexpressing a catalytically inactive p97 dramatically blocked the degradation of *Akita* proinsulin (Figure 2-2, A and B), supported by a recent report that chemical inhibition of p97 modestly inhibits *Akita* proinsulin degradation in a manner generally

similar to that achieved by chemical inhibition of proteasomes (Zhang and Ye, 2014). The notion that p97 at the cytosolic face of the ER membrane facilitates the degradation of ubiquitinated *Akita* proinsulin is further demonstrated by the accumulation of polyubiquitinated *Akita* proinsulin in the presence of the dominant-negative p97 mutant (Figure 2-2C). Taken together, these findings strongly suggest that p97 mobilizes mutant proinsulin into the cytosol for delivery to proteasomes.

PDI's reductase activity primes *Akita* proinsulin for ERAD

A key and surprising finding of our study involves the role of PDI in initiating retrotranslocation of *Akita* proinsulin for ERAD. Such a conclusion is not unreasonable: whereas PDI does not serve as an oxidase for native proinsulin disulfide bond formation (Rajpal et al., 2012), disulfide isomerase activity may be used to help break nonnative disulfide bonds. Moreover, the development of nonremediable misfolding may "tag" *Akita* proinsulin as a potential ERAD substrate. PDI can operate as a chaperone, facilitating the unfolding of substrates targeted for ERAD before their retrotranslocation (Schelhaas et al., 2007; Tsai et al., 2001), but it is likely that, once selected for ERAD, nonnative (and probably even remaining native) proinsulin disulfide bonds must be reduced so that the unfolded substrate can thread through the retrotranslocon.

In the context of genetic mutation of one of the six evolutionarily conserved proinsulin cysteine residues, the development of nonremediable proinsulin misfolding is guaranteed. An unpaired proinsulin cysteine residue may have the opportunity to attack other cysteines within the same proinsulin molecule or other proteins present in the ER (including other copies of proinsulin, ER oxidoreductases, or others). PDI appears to

preferentially interact with the Cys-B19, Cys-A11, and even Cys-A20 of proinsulin (Figure 2-3H and Supplemental Figure S3), but Cys-B7 (the normal disulfide bonding partner of Cys-A7) is not a preferential site of adduct formation with PDI.

Thus, *Akita* proinsulin is likely to be involved in a more complex pattern of disulfide mispairing that leads to the generation of PDI adducts. Consistent with this, intermolecular disulfide bonds are observed for *Akita* proinsulin, including both nonnative disulfide-linked proinsulin dimers and trimers and disulfide bonds with other proteins in high- MW complexes (Izumi et al., 2003; Liu et al., 2010b; Liu et al., 2007)Figure 2-4), and knockdown of PDI causes loss of the dimers and trimers (Figure 2-4B) while specifically blocking ERAD of *Akita* proinsulin (Figure 2-3).

Several new and novel observations support the idea that the role of PDI in the ERAD of *Akita* proinsulin is as a reductase. First, trap mutants that can mimic initial PDI reductase activity capture *Akita* proinsulin in disulfide-linked adducts, including adducts that correspond to a direct 1:1 interaction between PDI and *Akita* proinsulin (Figure 2-4A). Second, expression of these same PDI trap mutants inhibits degradation of *Akita* proinsulin (Supplemental Figure 2-S2C). Third, PDI knockdown causes simple disulfide-bonded *Akita* dimers to be lost (Figure 2-4B) and to fractionate with high-MW complexes, whereas addition of a chemical reductant mimics the effect of PDI (Figure 2-4C), strongly suggesting that lack of PDI results in a lack of reducing power for *Akita* proinsulin in the ER. Fourth, purified PDI is capable of reducing *Akita* proinsulin in the high-MW complexes to generate *Akita* dimers and trimers (Figure 2-4D). Thus our

collective findings argue strongly that PDI acts as a reductase to initiate retrotranslocation of *Akita* proinsulin. Because many MIDY mutations involve a loss or gain of a cysteine that promotes formation of nonnative disulfide bonds (Liu et al., 2010b), the reductase activity of PDI is also likely to promote ERAD of other MIDY mutants. Indeed, the role of PDI in ERAD is far more widespread than for proinsulin alone. We note that the classic components of ERAD, including Sel1L, Hrd1, and p97, are conserved down to yeast; indeed, it is well established that the yeast Sel1L homologue (Hrd3p) recruits lumenal factors for ERAD of substrates that also engage yeast Hrd1 (Denic et al., 2006). With this in mind, we note that even in this simple eukaryote, the redox activity of PDI has been shown to be important for ERAD of the mutant CPY* (Grubb et al., 2012). Thus it is not surprising that our results for ERAD of *Akita* proinsulin in heterologous HEK 293T cells are also obtained in pancreatic β-cells (Figure 2-5), as ERAD uses common, ancient, essential pathways.

The pathogenesis of MIDY is attributed to the inability of WT proinsulin to exit the ER, which is a critical step for normal insulin production (Liu et al., 2010b; Weiss, 2013). Because MIDY proinsulin entraps WT proinsulin in the ER, the less abundant the misfolded proinsulin, the less is the risk of diabetes (Hodish et al., 2011). In principle, restoration of WT proinsulin exit from the ER, resulting in more WT insulin production, should be possible if efficient disposal of misfolded proinsulin can be achieved. Although there is still much to be learned about the degradation of misfolded proinsulin in the ER, exploiting ERAD may serve as a crucial platform for the development of

future therapeutic approaches to combat diabetes caused by ER stress–induced β-cell failure linked to misfolded proinsulin within the ER.

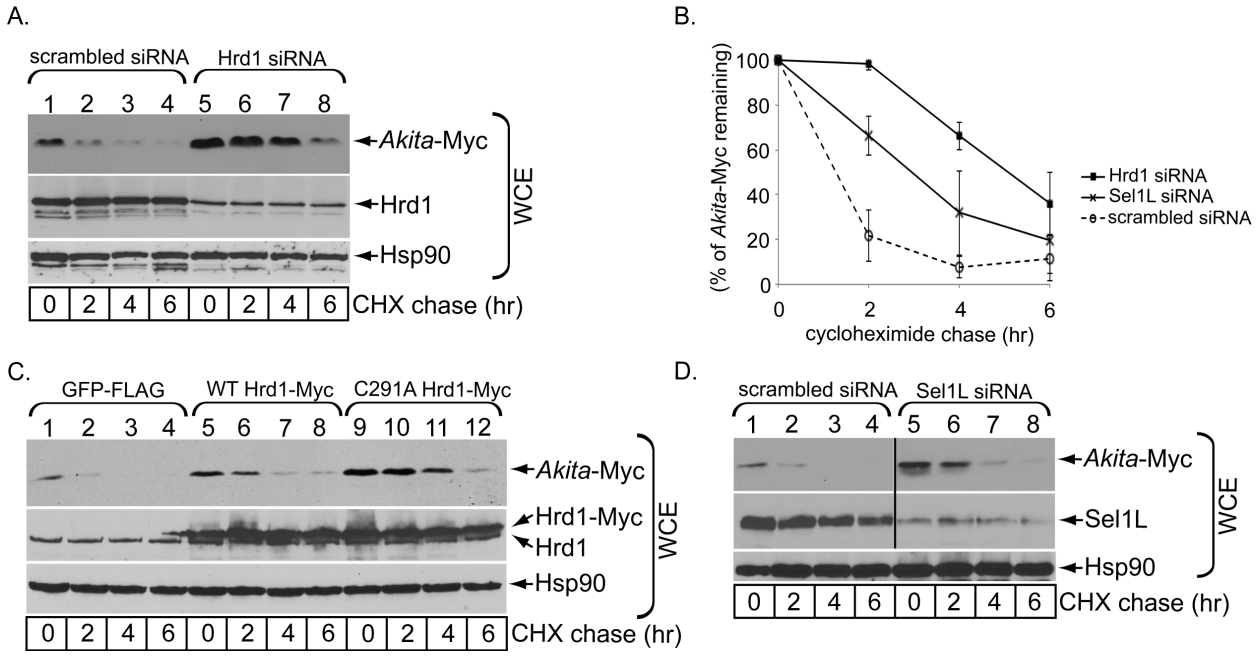

Figure 2-1. The Hrd1-Sel1L complex promotes ERAD of *Akita*. (A) 293T cells expressing *Akita*-Myc were transfected with a scrambled or Hrd1-specific siRNA. Cells were then treated with cycloheximide for the indicated time and harvested, and the resulting WCE was analyzed by using the indicated antibodies. (B) The *Akita* band intensity in A and D was quantified with ImageJ (National Institutes of Health, Bethesda, MD). Data represent mean ± SD of at least three independent experiments. (C) As in A, except that cells were transfected with GFP-FLAG, WT Hrd1-Myc, or C291A Hrd1-Myc construct. (D) As in A, except cells were transfected with a siRNA against Sel1L. The black vertical line indicates that an intervening lane from the same immunoblot has been spliced out.

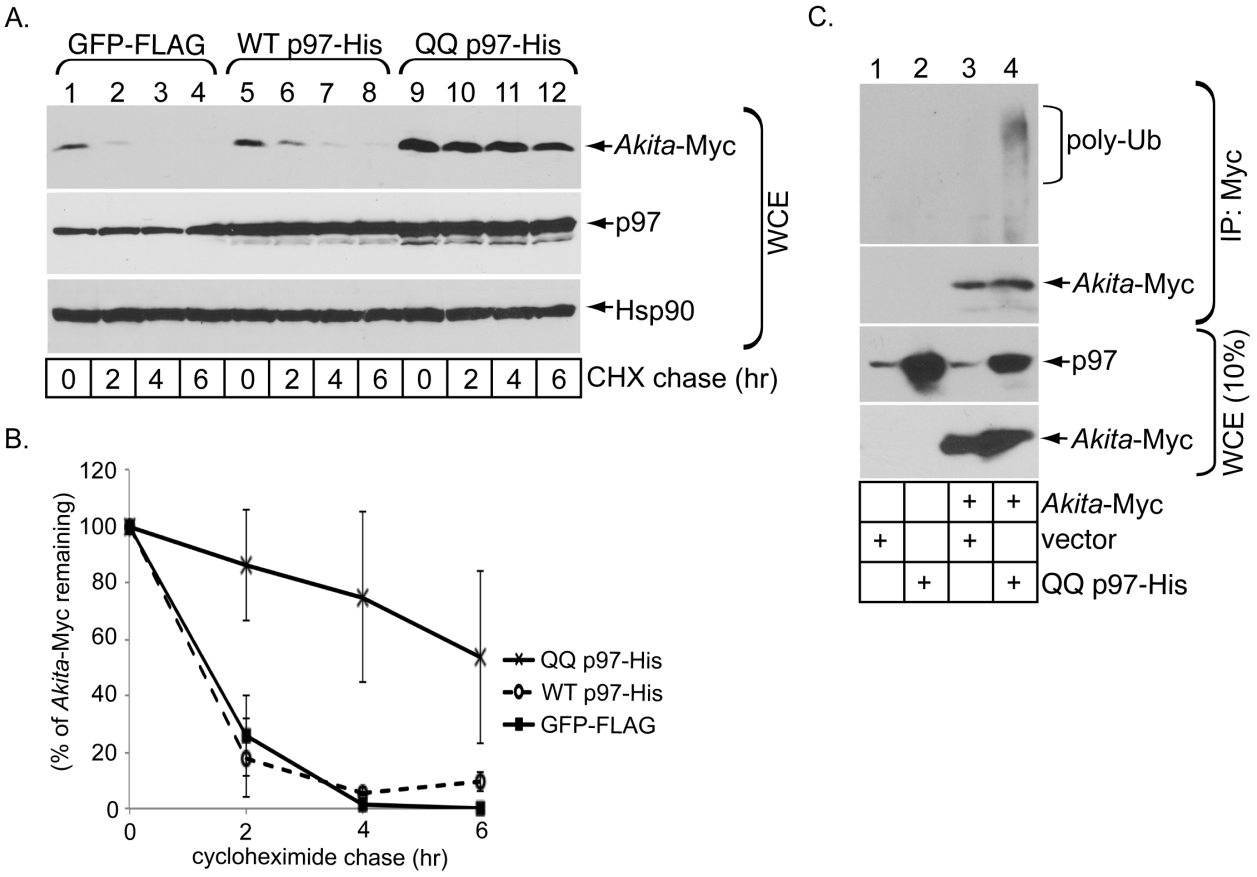

Figure 2-2. p97 facilitates *Akita* degradation. (A) As in Figure 2-1C, except that 293T cells were transfected with WT p97-His or QQ p97-His. (B) As in Figure 2-1B, except that the *Akita* band intensity in A is quantified. (C) 293T cells expressing *Akita*-Myc or not were transfected with an empty vector or QQ p97-His as indicated. Cells were lysed in a RIPA buffer and *Akita* immunoprecipitated from the resulting WCE using a Myc antibody. The precipitated material was subjected to SDS–PAGE and immunoblotted with the indicated antibodies. The WCE was also immunoblotted.

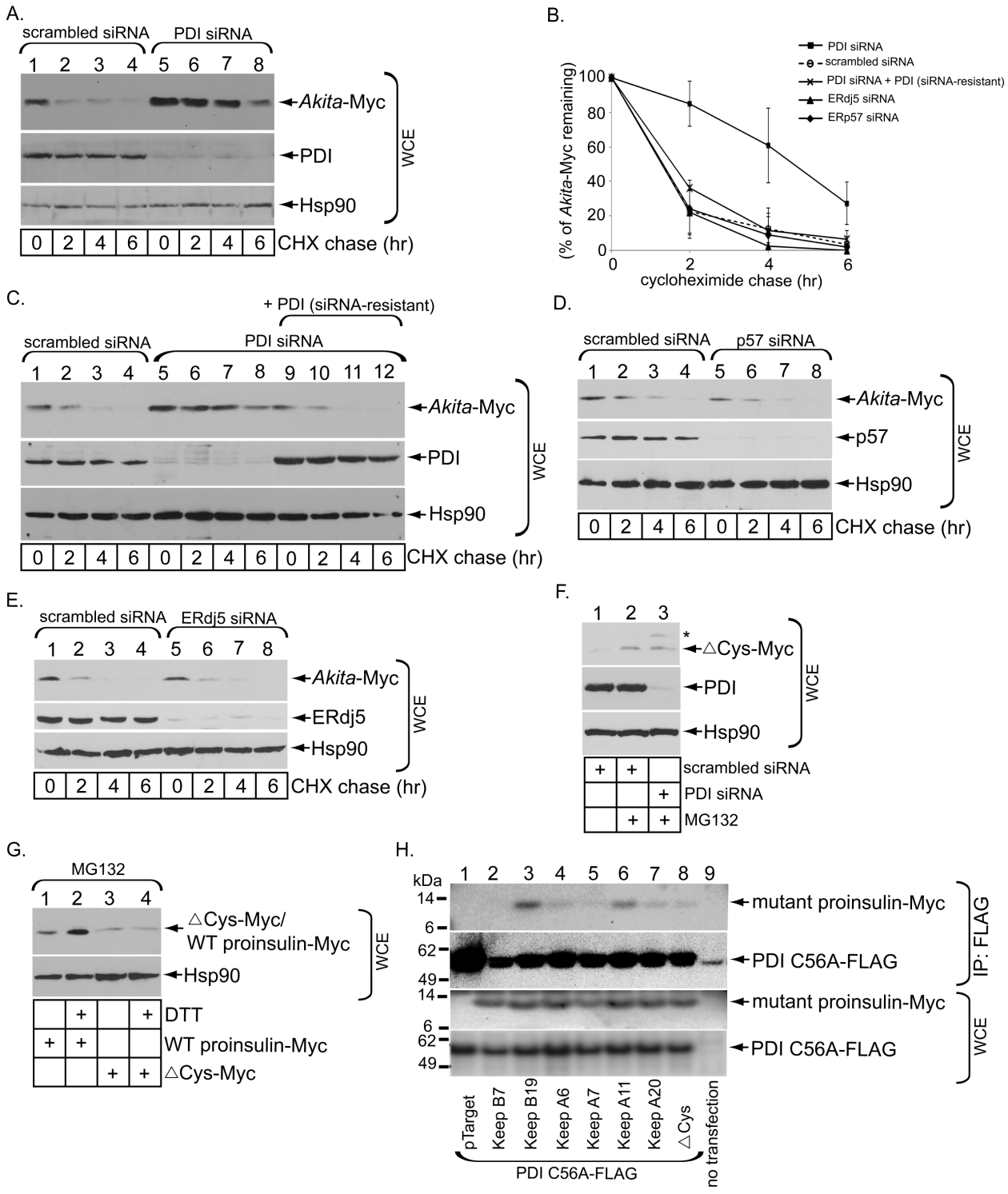

Figure 2-3. PDI exerts a key role in regulating *Akita* degradation. (A) As in Figure 2-1A, except that 293T cells were transfected with a PDI-specific siRNA for 3 d. (B) As in Figure 2-1C, except that the *Akita* band intensity in A and C–E are quantified. (C) As in A, except where indicated cells transfected with a PDI-specific siRNA for 3 d were cotransfected with a PDI construct resistant to the PDI-specific siRNA. (D) As in A,

except hat cells were transfected with an ERp57-specific siRNA. (E) As in A, except that cells were transfected with an ERdj5-specific siRNA. (F) 293T cells expressing either a control or PDI-specific siRNA were cotransfected with ΔCys-Myc and treated or not with MG132 as indicated. (G) Cells expressing WT proinsulin-Myc or ΔCys-Myc were treated with DTT (10 μM) in the presence of MG132 and the WCE analyzed as in F. (H) 293T cells expressing the indicated Myc-tagged mutant proinsulins were cotransfected with PDI C56A-FLAG. The cells were lysed and immunoprecipitated with M2 FLAG antibody-conjugated beads, analyzed by reducing SDS–PAGE, and immunoblotted using the appropriate antibodies. The WCE was also directly immunoblotted with anti-Myc or anti-FLAG antibodies. pTarget was the plasmid used as a control for the mutant proinsulin constructs.

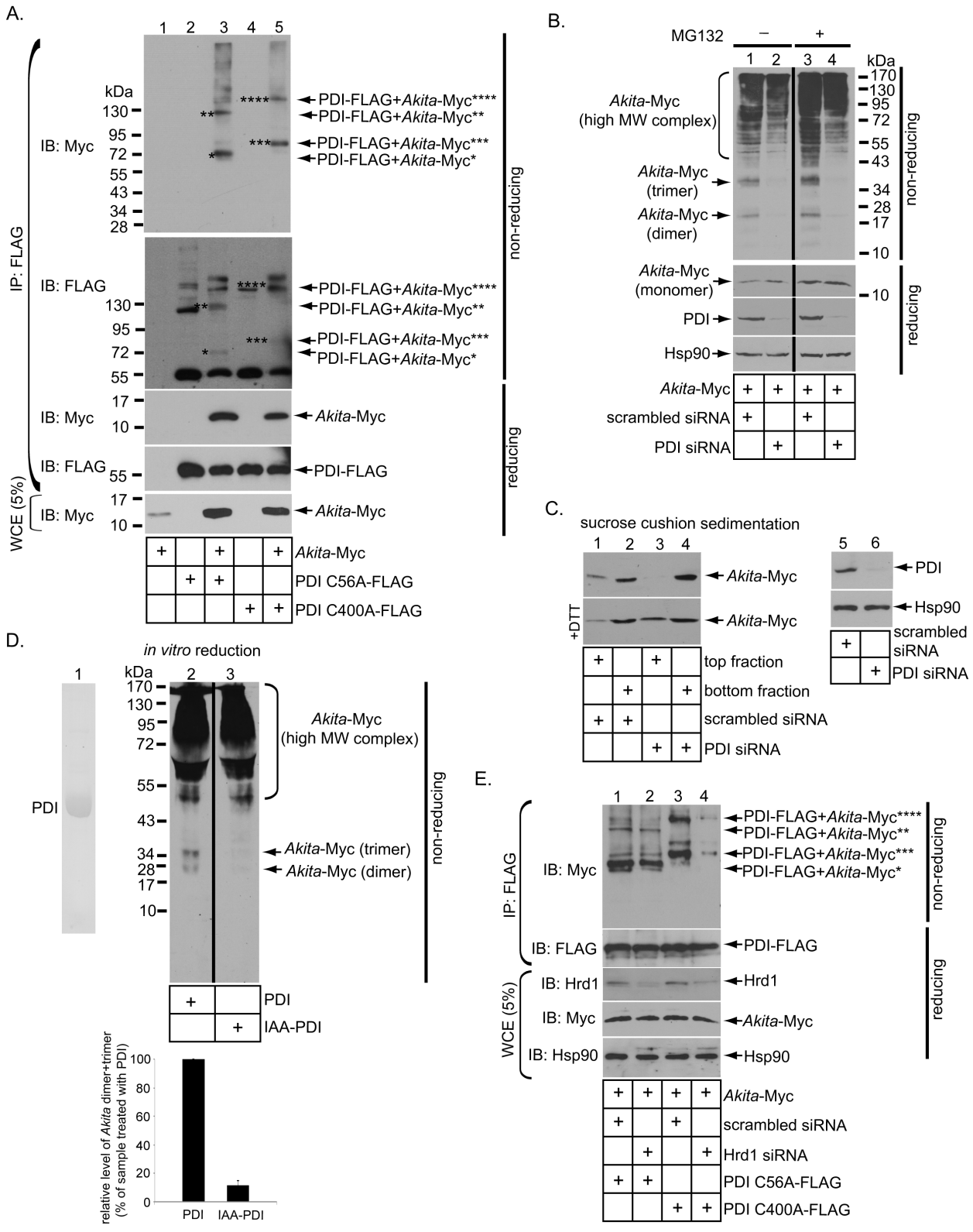

Figure 2-4. PDI acts as a reductase against *Akita*. (A) 293T cells expressing *Akita* were transfected with or without PDI C56A-FLAG or PDI C400A-FLAG. Tagged PDI proteins were immunoprecipitated from the resulting WCE using a

FLAG antibody. The precipitated material was subjected to nonreducing or reducing SDS–PAGE as indicated and immunoblotted using the appropriate antibodies. The WCE was also immunoblotted with a Myc antibody. (B) 293T cells expressing *Akita* and transfected with either a scrambled or PDI-specific siRNA were treated with or without MG132. The resulting WCE was subjected to nonreducing or reducing SDS–PAGE as indicated and immunoblotted using the indicated antibodies. The black vertical line indicates that an intervening lane from the same immunoblot has been spliced out. (C) Lanes 1–4, WCE in B was treated with or without DTT, layered over a 20% sucrose cushion, and centrifuged. The top and bottom fractions were separated and subjected to SDS–PAGE, followed by immunoblotting using a Myc antibody. Lanes 5 and 6, WCE was subjected to SDS–PAGE, followed by immunoblotting using the indicated antibodies. (D) His-tagged PDI purified from bacteria is shown in the Coomassie gel. Immunoprecipitated *Akita*-Myc from PDI-knockdown cells was incubated with PDI or IAA-modified PDI in the presence of 1 mM GSH and 1 mM GSSG, and the samples were subjected to nonreducing SDS–PAGE, followed by immunoblotting with a Myc antibody. Bottom graph, the intensity level of *Akita* dimer and trimer was quantified by ImageJ. Data represent the mean ± SD of three independent experiments. The black vertical line indicates that an intervening lane from the same immunoblot has been spliced out. (E) Cells expressing *Akita* transfected with a scrambled or Hrd1-specific siRNA were cotransfected with either PDI C56A-FLAG or PDI C400A-FLAG. The ability of tagged PDI protein to interact with *Akita* was analyzed as in A.

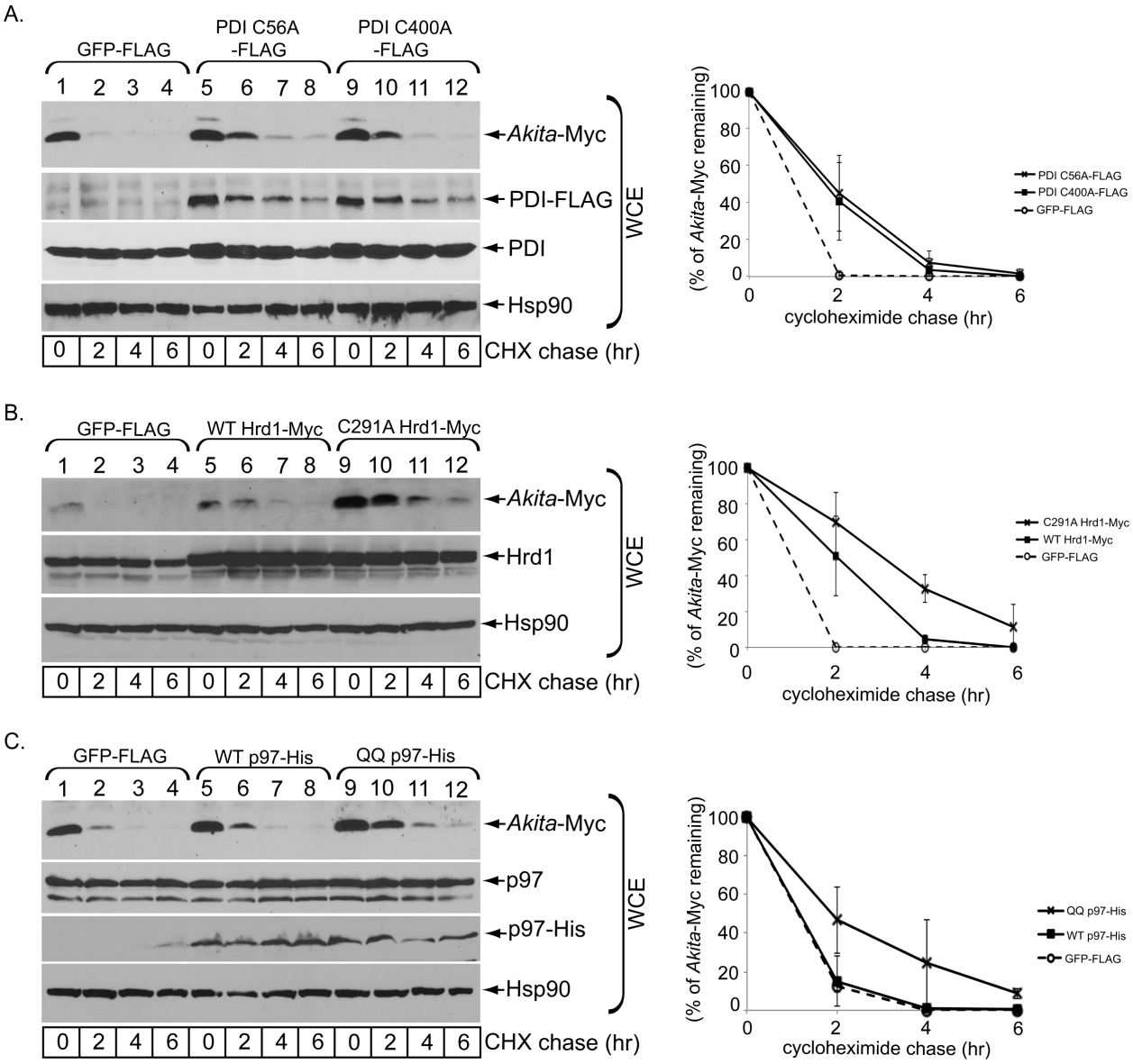

Figure 2-5. PDI, Hrd1, and p97 promote ERAD of *Akita* in pancreatic β-cells. (A) As in Supplemental Figure 2-S2C, except that rat pancreatic INS-1 832/13 β-cells were used and GFP-FLAG was expressed instead of ERp57 C60A-FLAG. The *Akita* band intensity is quantified as in Figure 2-1B. (B) As in Figure 2-1C, except that the experiment was performed in INS-1 832/13 β-cells and GFP-FLAG was transfected instead of vector. The *Akita* band intensity is quantified as in Figure 2-1B. (C) As in Figure 2-2A, except that the experiment was performed in INS-1 832/13 β-cells and GFP-FLAG was transfected instead of vector. The *Akita* band intensity is quantified as in Figure 2-1B.

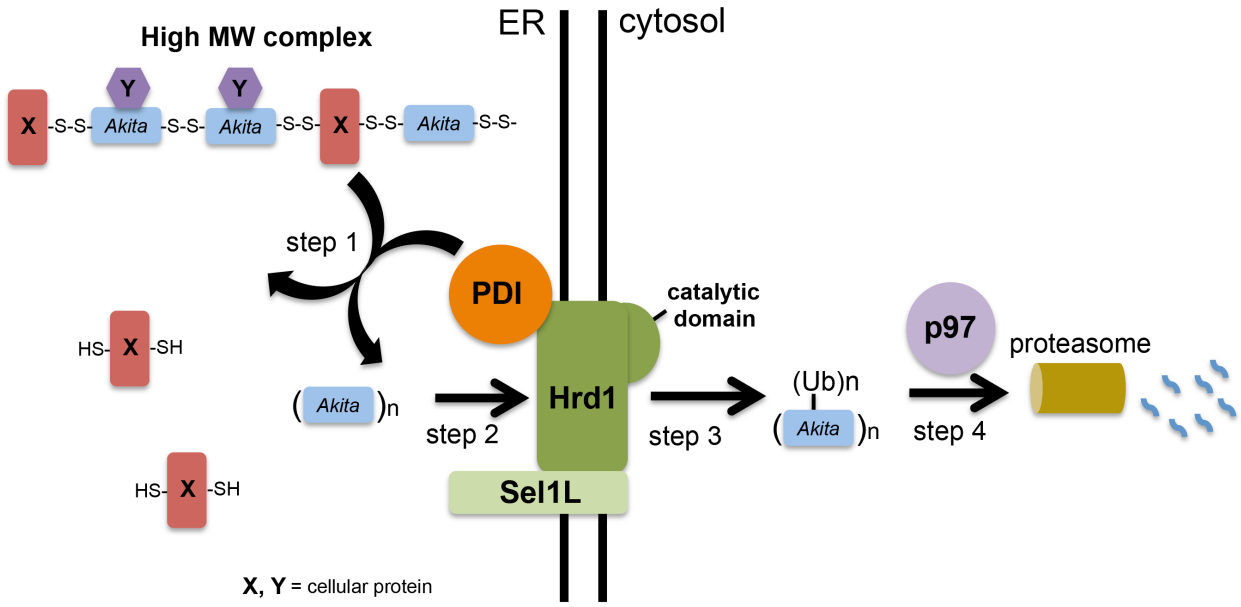

Figure 2-6. Model depicting ERAD of *Akita*. To dispose of *Akita* via the ERAD pathway, PDI reduces the disulfide bonds in this mutant proinsulin to initiate its retrotranslocation into the cytosol (step 1). The precise pairing of disulfide bonds in *Akita* proinsulin is not known. In the second step, *Akita* retrotranslocates across the ER membrane by using the Hrd1/Sel1L membrane complex (step 2). Once it is presented to the cytosol, *Akita* becomes polyubiquitinated using Hrd1's catalytic activity (step 3). In the final step, p97 propels polyubiquitinated *Akita* into the cytosol, targeting it to the proteasome for degradation (step 4).

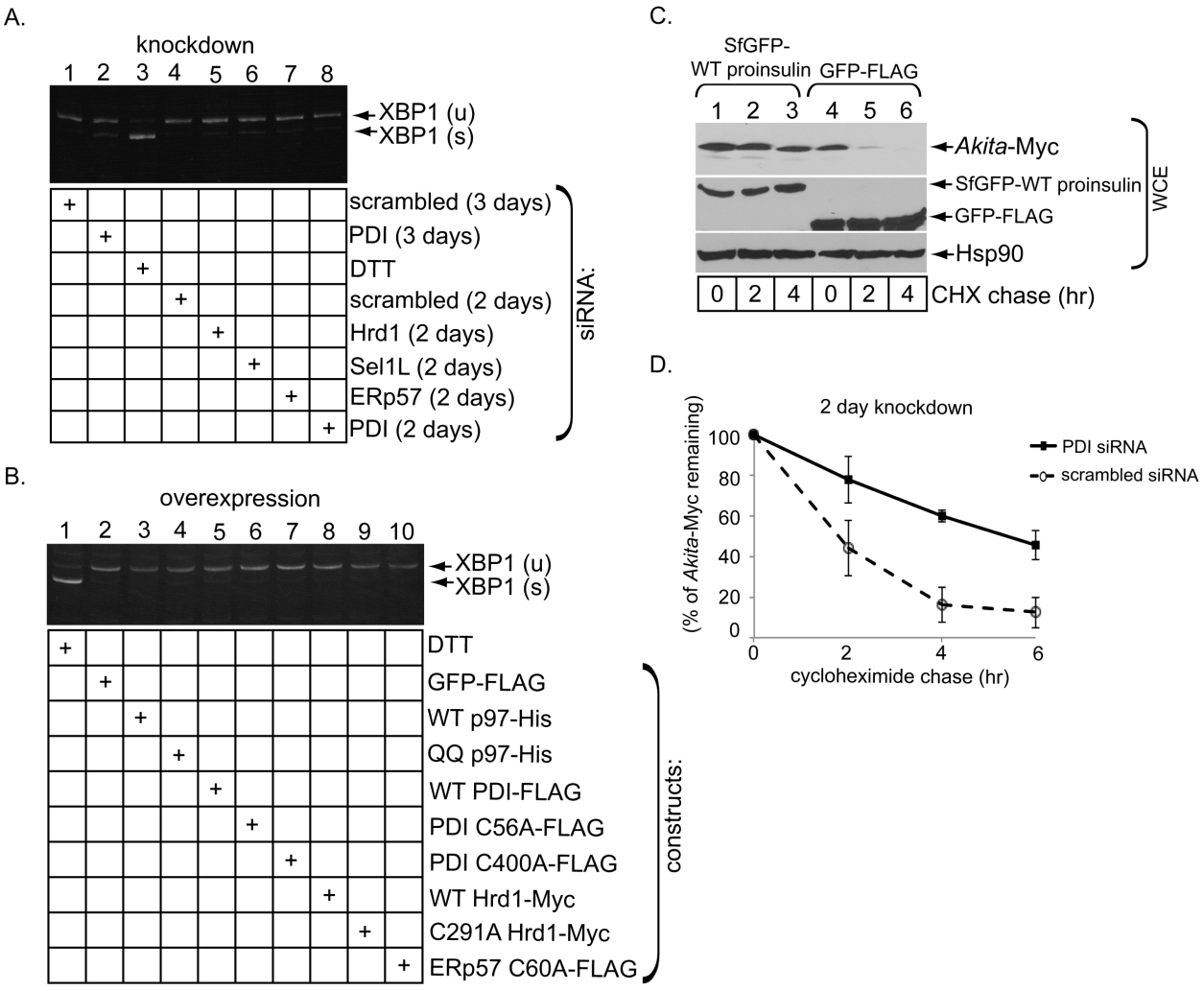

Figure 2-S1. Additional characterization under different knockdown and overexpression conditions. A. Induction of XBP1 splicing was analyzed in cells transfected with the indicated siRNA for the indicated number of days. DTT-treated cells were used as a positive control. B. As in A, except cells were transfected with the indicated construct. C. As in Figure 2-1C, except cells were transfected with either SfGFP-WT proinsulin or GFPFLAG. D. *Akita* degradation was analyzed as in Figure 2-3A, except cells were transfected with the PDI specific siRNA for only 2 days.

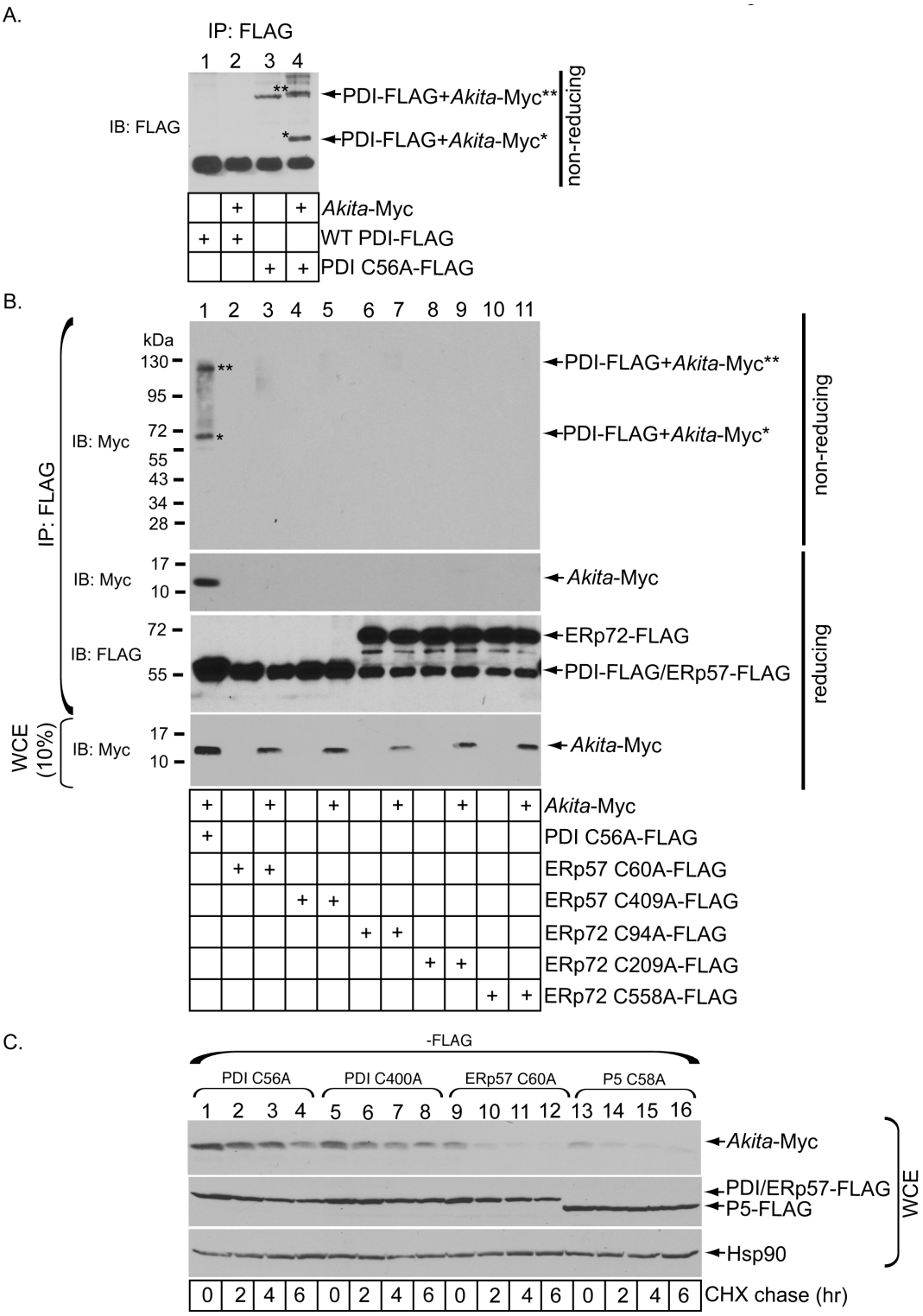

Figure 2-S2. PDI trap mutants selectively capture *Akita* and block its degradation. A. As in 2-4A, expect WT PDI-FLAG was used. B. As in 2-4A, except the indicated ERp57 or ERp72 trap mutant constructs were used. C. As in 2-2A, except the indicated PDI, ERp57, or p5 trap mutant constructs was used.

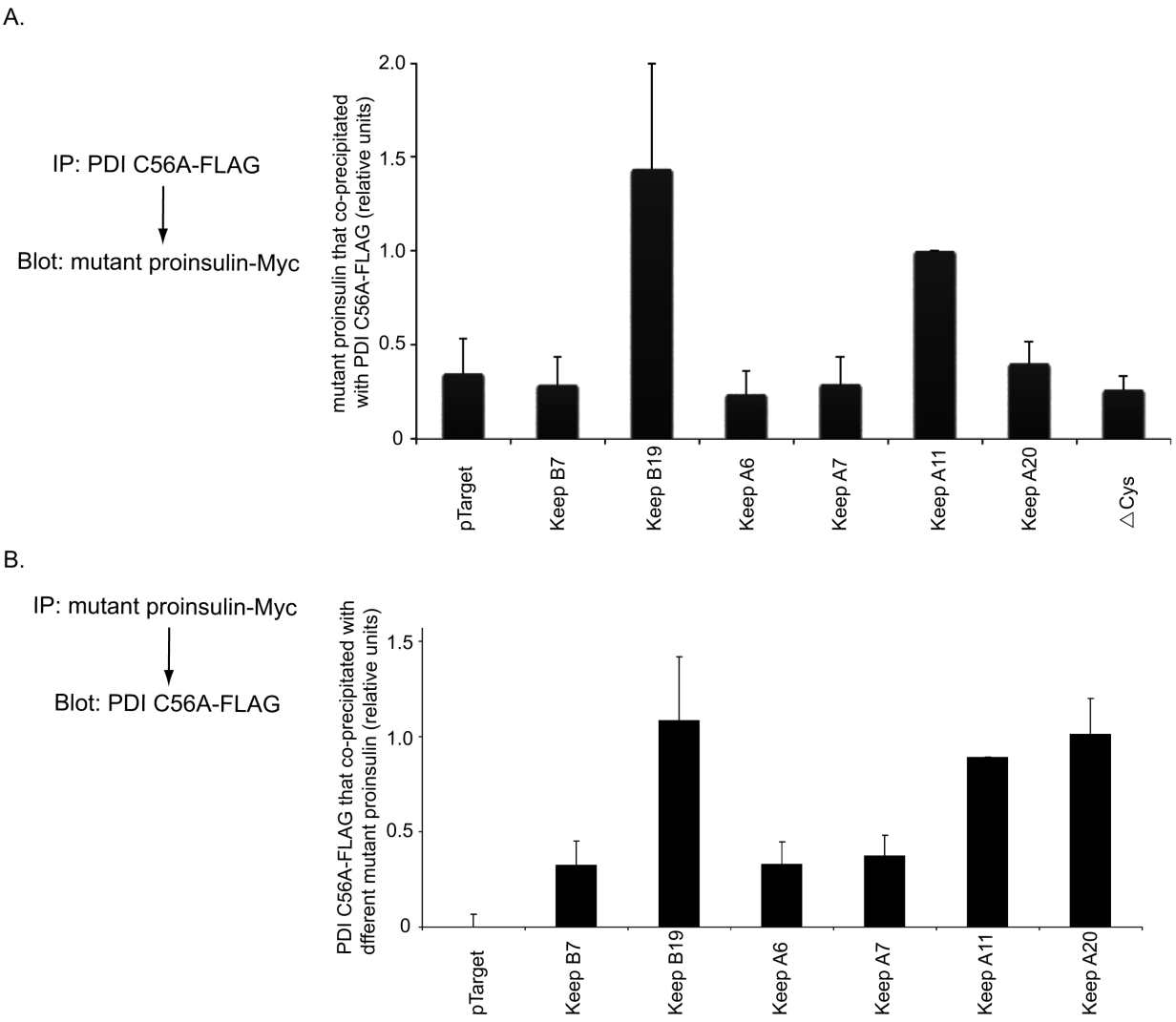

Figure 2-S3. The B7 cysteine residue in *Akita* does not preferentially form a disulfide bond with PDI. A. The level of mutant proinsulin-Myc in 2-3H was quantified using ImageJ (NIH). B. 293T cells expressing the indicated Myc-tagged mutant proinsulin were co-transfected with PDI C56A-FLAG. The cells were lysed and immunoprecipitated with anti-Myc (9E10) antibody, analyzed by reducing SDS-PAGE, and immunoblotted using the appropriate antibodies. The level of PDI C56A-FLAG was quantified using ImageJ (NIH).

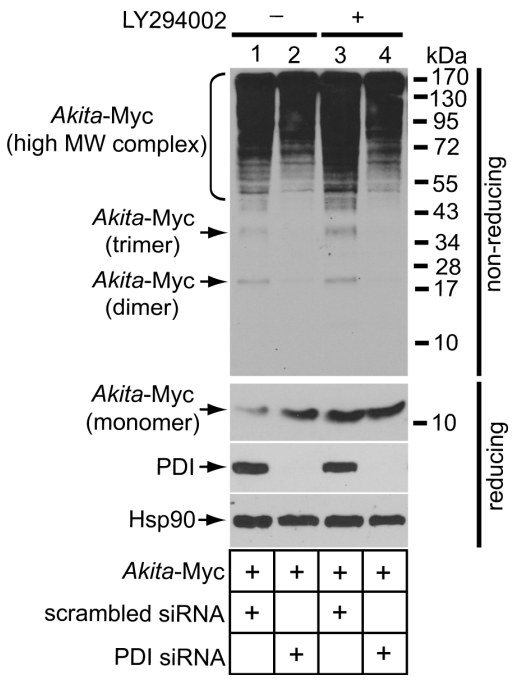

Figure 2-S4. Autophagy inhibition does not prevent loss of *Akita* dimer and trimer in PDI-depleted cells. As in Figure 2-4B, except cells were treated with 20 μM of the autophagy inhibitor LY294002 for 2 h instead of MG132.

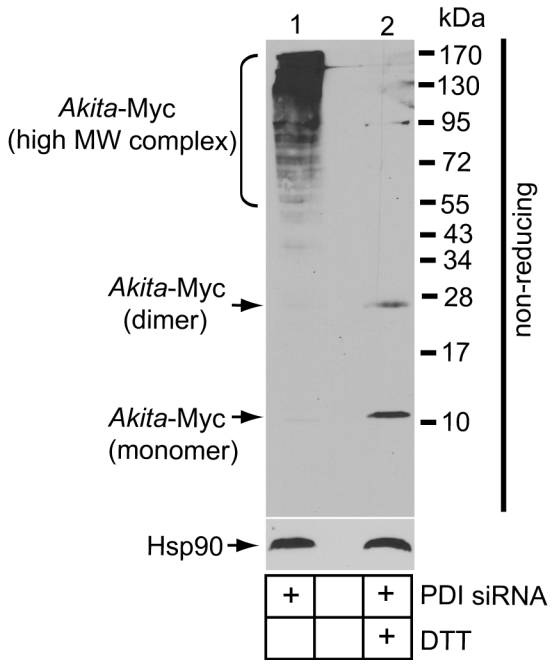

Figure 2-S5. DTT reduces *Akita*. A cell extract derived from PDI-depleted cells was treated with or without DTT, and analyzed by non-reducing SDS-PAGE.

REFERENCES

Allen, J.R., Nguyen, L.X., Sargent, K.E., Lipson, K.L., Hackett, A., and Urano, F. (2004). High ER stress in beta-cells stimulates intracellular degradation of misfolded insulin. Biochem Biophys Res Commun *324*, 166-170.

Appenzeller-Herzog, C., and Ellgaard, L. (2008). The human PDI family: versatility packed into a single fold. Biochim Biophys Acta *1783*, 535-548.

Benham, A.M. (2012). The protein disulfide isomerase family: key players in health and disease. Antioxid Redox Signal *16*, 781-789.

Bernardi, K.M., Williams, J.M., Kikkert, M., van Voorden, S., Wiertz, E.J., Ye, Y., and Tsai, B. (2010). The E3 ubiquitin ligases Hrd1 and gp78 bind to and promote cholera toxin retro-translocation. Mol Biol Cell *21*, 140-151.

Bernasconi, R., Galli, C., Calanca, V., Nakajima, T., and Molinari, M. (2010). Stringent requirement for HRD1, SEL1L, and OS-9/XTP3-B for disposal of ERAD-LS substrates. J Cell Biol *188*, 223-235.

Blommaart, E.F., Krause, U., Schellens, J.P., Vreeling-Sindelarova, H., and Meijer, A.J. (1997). The phosphatidylinositol 3-kinase inhibitors wortmannin and LY294002 inhibit autophagy in isolated rat hepatocytes. Eur J Biochem *243*, 240-246.

Cai, H., Wang, C.C., and Tsou, C.L. (1994). Chaperone-like activity of protein disulfide isomerase in the refolding of a protein with no disulfide bonds. J Biol Chem *269*, 24550-24552.

Carvalho, P., Stanley, A.M., and Rapoport, T.A. (2010). Retrotranslocation of a misfolded luminal ER protein by the ubiquitin-ligase Hrd1p. Cell *143*, 579-591.

Claessen, J.H., Kundrat, L., and Ploegh, H.L. (2012). Protein quality control in the ER: balancing the ubiquitin checkbook. Trends Cell Biol *22*, 22-32.

Denic, V., Quan, E.M., and Weissman, J.S. (2006). A luminal surveillance complex that selects misfolded glycoproteins for ER-associated degradation. Cell *126*, 349-359.

Forster, M.L., Mahn, J.J., and Tsai, B. (2009). Generating an unfoldase from thioredoxin-like domains. J Biol Chem *284*, 13045-13056.

Forster, M.L., Sivick, K., Park, Y.N., Arvan, P., Lencer, W.I., and Tsai, B. (2006). Protein disulfide isomerase-like proteins play opposing roles during retrotranslocation. J Cell Biol *173*, 853-859.

Gillece, P., Luz, J.M., Lennarz, W.J., de La Cruz, F.J., and Romisch, K. (1999). Export of a cysteine-free misfolded secretory protein from the endoplasmic reticulum for

degradation requires interaction with protein disulfide isomerase. J Cell Biol *147*, 1443-1456.

Grubb, S., Guo, L., Fisher, E.A., and Brodsky, J.L. (2012). Protein disulfide isomerases contribute differentially to the endoplasmic reticulum-associated degradation of apolipoprotein B and other substrates. Mol Biol Cell *23*, 520-532.

Haataja, L., Snapp, E., Wright, J., Liu, M., Hardy, A.B., Wheeler, M.B., Markwardt, M.L., Rizzo, M., and Arvan, P. (2013). Proinsulin intermolecular interactions during secretory trafficking in pancreatic beta cells. J Biol Chem *288*, 1896-1906.

Hartley, T., Siva, M., Lai, E., Teodoro, T., Zhang, L., and Volchuk, A. (2010). Endoplasmic reticulum stress response in an INS-1 pancreatic beta-cell line with inducible expression of a folding-deficient proinsulin. BMC Cell Biol *11*, 59.

Hatahet, F., and Ruddock, L.W. (2009). Protein disulfide isomerase: a critical evaluation of its function in disulfide bond formation. Antioxid Redox Signal *11*, 2807-2850.

Hodish, I., Absood, A., Liu, L., Liu, M., Haataja, L., Larkin, D., Al-Khafaji, A., Zaki, A., and Arvan, P. (2011). In vivo misfolding of proinsulin below the threshold of frank diabetes. Diabetes *60*, 2092-2101.

Hosokawa, N., Wada, I., Nagasawa, K., Moriyama, T., Okawa, K., and Nagata, K. (2008). Human XTP3-B forms an endoplasmic reticulum quality control scaffold with the HRD1-SEL1L ubiquitin ligase complex and BiP. J Biol Chem *283*, 20914-20924.

Izumi, T., Yokota-Hashimoto, H., Zhao, S., Wang, J., Halban, P.A., and Takeuchi, T. (2003). Dominant negative pathogenesis by mutant proinsulin in the Akita diabetic mouse. Diabetes *52*, 409-416.

Kikkert, M., Doolman, R., Dai, M., Avner, R., Hassink, G., van Voorden, S., Thanedar, S., Roitelman, J., Chau, V., and Wiertz, E. (2004). Human HRD1 is an E3 ubiquitin ligase involved in degradation of proteins from the endoplasmic reticulum. J Biol Chem *279*, 3525-3534.

Liu, M., Haataja, L., Wright, J., Wickramasinghe, N.P., Hua, Q.X., Phillips, N.F., Barbetti, F., Weiss, M.A., and Arvan, P. (2010a). Mutant INS-gene induced diabetes of youth: proinsulin cysteine residues impose dominant-negative inhibition on wild-type proinsulin transport. PLoS One *5*, e13333.

Liu, M., Hodish, I., Haataja, L., Lara-Lemus, R., Rajpal, G., Wright, J., and Arvan, P. (2010b). Proinsulin misfolding and diabetes: mutant INS gene-induced diabetes of youth. Trends Endocrinol Metab *21*, 652-659.

Liu, M., Hodish, I., Rhodes, C.J., and Arvan, P. (2007). Proinsulin maturation, misfolding, and proteotoxicity. Proc Natl Acad Sci U S A *104*, 15841-15846.

Liu, M., Lara-Lemus, R., Shan, S.O., Wright, J., Haataja, L., Barbetti, F., Guo, H., Larkin, D., and Arvan, P. (2012). Impaired cleavage of preproinsulin signal peptide linked to autosomal-dominant diabetes. Diabetes *61*, 828-837.

Mueller, B., Klemm, E.J., Spooner, E., Claessen, J.H., and Ploegh, H.L. (2008). SEL1L nucleates a protein complex required for dislocation of misfolded glycoproteins. Proc Natl Acad Sci U S A *105*, 12325-12330.

Rajpal, G., Schuiki, I., Liu, M., Volchuk, A., and Arvan, P. (2012). Action of protein disulfide isomerase on proinsulin exit from endoplasmic reticulum of pancreatic beta-cells. J Biol Chem *287*, 43-47.

Schelhaas, M., Malmstrom, J., Pelkmans, L., Haugstetter, J., Ellgaard, L., Grunewald, K., and Helenius, A. (2007). Simian Virus 40 depends on ER protein folding and quality control factors for entry into host cells. Cell *131*, 516-529.

Smith, M.H., Ploegh, H.L., and Weissman, J.S. (2011). Road to ruin: targeting proteins for degradation in the endoplasmic reticulum. Science *334*, 1086-1090.

Stanley, A.M., Carvalho, P., and Rapoport, T. (2011). Recognition of an ERAD-L substrate analyzed by site-specific in vivo photocrosslinking. FEBS Lett *585*, 1281-1286.

Stein, A., Ruggiano, A., Carvalho, P., and Rapoport, T.A. (2014). Key steps in ERAD of luminal ER proteins reconstituted with purified components. Cell *158*, 1375-1388.

Steiner, D.F., Cunningham, D., Spigelman, L., and Aten, B. (1967). Insulin biosynthesis: evidence for a precursor. Science *157*, 697-700.

Stoy, J., Edghill, E.L., Flanagan, S.E., Ye, H., Paz, V.P., Pluzhnikov, A., Below, J.E., Hayes, M.G., Cox, N.J., Lipkind, G.M.*, et al.* (2007). Insulin gene mutations as a cause of permanent neonatal diabetes. Proc Natl Acad Sci U S A *104*, 15040-15044.

Tiwari, A., Schuiki, I., Zhang, L., Allister, E.M., Wheeler, M.B., and Volchuk, A. (2013). SDF2L1 interacts with the ER-associated degradation machinery and retards the degradation of mutant proinsulin in pancreatic beta-cells. J Cell Sci *126*, 1962-1968.

Tsai, B., Rodighiero, C., Lencer, W.I., and Rapoport, T.A. (2001). Protein disulfide isomerase acts as a redox-dependent chaperone to unfold cholera toxin. Cell *104*, 937-948.

Tsai, B., Ye, Y., and Rapoport, T.A. (2002). Retro-translocation of proteins from the endoplasmic reticulum into the cytosol. Nat Rev Mol Cell Biol *3*, 246-255.

Ushioda, R., Hoseki, J., Araki, K., Jansen, G., Thomas, D.Y., and Nagata, K. (2008). ERdj5 is required as a disulfide reductase for degradation of misfolded proteins in the ER. Science *321*, 569-572.

Weiss, M.A. (2013). Diabetes mellitus due to the toxic misfolding of proinsulin variants. FEBS Lett *587*, 1942-1950.

Williams, J.M., Inoue, T., Banks, L., and Tsai, B. (2013). The ERdj5-Sel1L complex facilitates cholera toxin retrotranslocation. Mol Biol Cell *24*, 785-795.

Woodman, P.G. (2003). p97, a protein coping with multiple identities. J Cell Sci *116*, 4283-4290.

Ye, Y., Meyer, H.H., and Rapoport, T.A. (2001). The AAA ATPase Cdc48/p97 and its partners transport proteins from the ER into the cytosol. Nature *414*, 652-656.

Yoshinaga, T., Nakatome, K., Nozaki, J., Naitoh, M., Hoseki, J., Kubota, H., Nagata, K., and Koizumi, A. (2005). Proinsulin lacking the A7-B7 disulfide bond, Ins2Akita, tends to aggregate due to the exposed hydrophobic surface. Biol Chem *386*, 1077-1085.

Zhang, T., and Ye, Y. (2014). The final moments of misfolded proteins en route to the proteasome. DNA Cell Biol *33*, 477-483.

CHAPTER 3: Chaperone-Driven Degradation of a Misfolded Proinsulin Mutant in Parallel with Restoration of Wild-Type Insulin Secretion

Diabetes 2017 Mar; 66(3): 741-753

INTRODUCTION

Insulin is a peptide hormone secreted by pancreatic β-cells that controls blood glucose levels (Hales, 1971). Insulin biosynthesis begins when the precursor preproinsulin is translocated into the endoplasmic reticulum (ER) (Steiner et al., 1967). This precursor harbors an N-terminal signal sequence, followed sequentially by the B chain, connecting C-peptide, and A chain. Upon translocation into the ER, the signal sequence is excised, forming proinsulin (Steiner et al., 1967). Folding of proinsulin to its native conformation in the ER is coordinated with the formation of three highly conserved disulfide bonds (B chain 7th residue to A chain 7th residue, called the B7-A7 disulfide bond, plus the B19-A20 and A6-A11 disulfide bonds). When properly folded and oxidized, proinsulin is transported from the ER via the Golgi complex to immature secretory granules. Upon proteolytic excision of the C-peptide in this organelle, the B and A chains remain attached via their two interchain disulfide bonds, representing bioactive insulin that is poised for secretion to the bloodstream via exocytosis of secretory granules

Recently over 29 missense mutations in the human insulin gene have been identified to cause an autosomal-dominant disease called mutant INS gene–induced diabetes of youth (MIDY) (Liu et al., 2010b; Liu et al., 2007; Stoy et al., 2007; Weiss, 2013). Whereas most MIDY proinsulin mutants are misfolded and cannot form bioactive insulin, the initial onset of clinical insulin deficiency appears to be driven by dominant interference with the folding of wild-type (WT) proinsulin, impairing its ER exit and thereby limiting the production and eventual secretion of bioactive insulin. A decrease in insulin secretion causes hyperglycemia, which may provoke β-cells to further upregulate proinsulin synthesis (including the products of both mutant and WT alleles). Concomitant with proinsulin misfolding is ER stress and diabetes with eventual β-cell demise.

The most-studied MIDY mutant is *Akita* proinsulin, in which mutation of the A7 cysteine to tyrosine, so-called C(A7)Y, leaves an unpaired cysteine partner at the B7 position (Wang et al., 1999). This unpaired cysteine can potentially form an intermolecular disulfide bond with another misfolded *Akita* molecule or with WT proinsulin, generating both disulfide-bonded and noncovalent high–molecular weight (MW) protein complexes that are likely to engage ER resident proteins such as molecular chaperones. As a result of entry into such complexes, efficient ER exit of WT proinsulin is prevented, leading to the disease (Liu et al., 2010b; Liu et al., 2007; Weiss, 2013). The extent of blockade of WT proinsulin is directly related to the relative abundance of the mutant proinsulin protein (Liu et al., 2007; Weiss, 2013). For this reason, we postulate that

selective disposal of *Akita* proinsulin might facilitate the folding and export of the WT counterpart, thereby enhancing insulin secretion.

Because approximately one-third of cellular proteins are synthesized in the ER, it is not surprising that this organelle harbors rigorous protein quality control processes. One such process is called ER-associated degradation (ERAD), in which misfolded ER clients are retrotranslocated to the cytosol, where they are degraded by proteasomes (Ruggiano et al., 2014; Smith et al., 2011; Tsai et al., 2002). Recently, our laboratory and others identified several components of the ERAD machinery that facilitate degradation of *Akita* proinsulin (Allen et al., 2004), including the ER membrane-bound E3 ubiquitin ligase Hrd1, its membrane-binding partner Sel1L, and the cytosolic AAA+ ATPase p97 (He et al., 2015). We also reported that the ER luminal protein disulfide isomerase (PDI) may participate in reducing disulfide bonds that can help to liberate *Akita* proinsulin from high-MW protein complexes, generating smaller dimeric/trimeric species that are competent for retrotranslocation (He et al., 2015); another PDI family member, PDIA6 (encoding the P5 protein), may also play a role in this process (Gorasia et al., 2016). Whether other ER luminal components can help to drive *Akita* proinsulin along the ERAD pathway, and whether enhanced degradation of *Akita* proinsulin degradation can impact WT proinsulin export, are unknown.

Here we demonstrate that the ER luminal chaperone Grp170, an atypical member of the Hsp70 superfamily (Behnke et al., 2015), promotes the degradation of *Akita* proinsulin.

We show that Grp170 shifts the balance of high-MW oligomers bearing *Akita* proinsulin toward smaller oligomeric species that are capable of undergoing ERAD. Importantly, whereas WT proinsulin is trapped alongside the mutant in these high-MW protein complexes, overexpressing Grp170 can liberate WT proinsulin, enhancing *Akita* degradation and increasing WT insulin secretion. Hence, the ability to improve insulin secretion by selectively triaging a MIDY mutant suggests a rational strategy to treat the disease by rectifying the underlying MIDY defect.

RESEARCH DESIGN AND METHODS

Antibodies

The antibodies used were as follows: rabbit anti-Myc (Immunology Consultants Laboratories); mouse anti-PDI and rabbit anti-Hsp90 (Santa Cruz Biotechnology); rabbit anti-FLAG, and mouse/rabbit horseradish peroxidase secondary antibodies (Sigma-Aldrich); rabbit anti-GFP (green fluorescent protein; Proteintech); rabbit anti-Orp150/Grp170 (Abcam); rabbit anti-Sil1 (GeneTex); and mouse anti-VCP/p97 (Thermo Scientific). Chemicals were from Sigma-Aldrich except when noted otherwise. Phenylmethylsulfonyl fluoride (PMSF) was from Acros Organics. DMEM, RPMI 1640 medium, and other cell culture reagents were from Life Technologies. Plasmids encoding Myc-epitope–tagged human C(A7)Y *Akita* mutant proinsulin (*Akita*-Myc), WT proinsulin-Myc, and WT proinsulin-superfolder GFP (sfGFP) were previously described (Haataja et al., 2013; Liu et al., 2010a). Human PDI trap mutant was a gift from T. Rapoport (Harvard University, Cambridge, MA). The INS-1 832/13 β-cell line was a gift from Christopher Newgard (University of Texas Southwestern Medical Center, Dallas, TX). Subtilase cytotoxin complex (SubAB) and mutant SubAA272B were expressed in recombinant Escherichia coli with a B-subunit COOH-terminal His6 tag and purified by Ni-NTA chromatography, as previously described (Paton et al., 2004).

Cell Culture, Plasmid Transfection, Cycloheximide Chase, Immunoprecipitation, and Immunoblotting

Rat INS-1 832/13, human HEK 293T cells, and their derivative cell line (Tet-induced Grp170 expression cell line) were cultured at 37°C. Cells were seeded 1 day before transfection of 0.25–2 μg of plasmid DNA using polyethylenimine or Lipofectamine 2000 (Invitrogen). Twenty-four hours after transfection, cells were treated with cycloheximide (100 μg/mL) and chased for 0, 2, 4, and 6 h. Cells were harvested in PBS containing 10 mmol/L N-ethylmaleimide (NEM). For immunoprecipitation (IP), cells were lysed in 400 μL of radioimmunoprecipitation assay (RIPA) buffer (Tris-HCl, pH 7.5, 150 mmol/L NaCl, 1% NP-40, 1% sodium deoxycholate, 0.1% SDS) supplemented with 10 mmol/L NEM and 1 mmol/L PMSF. Cells were incubated on ice for 10 min and centrifuged, and the resulting whole-cell extract (WCE) was incubated with antibody (1:200) at 4°C for 24 h, followed by 2 h of incubation with protein A/G-agarose beads at 4°C. Beads were washed and boiled in SDS sample buffer with or without 100 mmol/L dithiothreitol. For immunoblot analyses, cells were lysed in 100 μL of RIPA buffer to generate the WCE, which was boiled in SDS sample buffer with 100 mmol/L dithiothreitol. Samples were resolved on 8–15% SDS-PAGE, transferred to nitrocellulose, and immunoblotted with specific primary and secondary antibodies.

Small Interfering RNA Knockdown of Grp170, Sil1, and PDI

Small interfering RNA (siRNA) was transfected into cells using RNAi MAX (Invitrogen), and cells were chased and harvested 48–72 h after treatment. Sequences of the siRNAs are as follows:

PDI siRNA: (5′-CAACUUUGAAGGGGAGGUCTT-3′; Invitrogen),

Grp170 siRNA 1: (5′-GCUCAAUAAGGCCAAGUUUTddT-3′; Invitrogen),

Grp170 siRNA 2: (5′-GCCUUUAAAGUGAAGCCAUdTdT-3′; Invitrogen),

Grp170 siRNA 3: (5′-GCCUUUGAAGAACGACGAAdTdT-3′; Invitrogen),

Sil1 siRNA: (5′-GCUGAUCAACAAGUUCAAUdTdT-3′; Invitrogen).

Proinsulin Secretion Assay

A plasmid encoding WT proinsulin tagged with sfGFP in the C-peptide was transfected into Grp170-inducible and rat INS-1 832/13 β-cells using polyethylenimine and Lipofectamine 2000 (Invitrogen), respectively. For the inducible cell lines, 1 μg/mL tetracycline (Tet) was added at the time of transfection. Six hours after transfection, the medium was replaced with 500 μL fresh medium supplemented with Tet and incubated for 16 h. The medium was collected in a 1.7-mL tube with 6× SDS reducing sample buffer and boiled. Cells were also harvested in PBS, lysed in RIPA buffer, and denatured in reducing SDS sample buffer. These samples were analyzed by immunoblotting.

Sucrose Gradient Fractionation

To prepare the lysate, cells were harvested in 10 mL PBS supplemented with 10 mmol/L NEM and pelleted at 1,500g for 5 min. Cell pellets were lysed in RIPA buffer supplemented with 10 mmol/L NEM and 1 mmol/L PMSF and incubated on ice. After a first centrifugation at 16,000g for 10 min, the resulting supernatant was further cleared

by ultracentrifugation at 50,000 rpm (100,000g) for 20 min. The resulting supernatant was layered over a 10–50% discontinuous sucrose gradient and centrifuged using a Beckman SW50.1 rotor at 29,000 rpm for 24 h at 4°C. After centrifugation, tubes were removed and 50-µL fractions were collected.

RESULTS

Grp170 Knockdown Impairs Degradation of *Akita* Proinsulin With Depletion of Oligomeric Forms

Grp170 was recently identified as a novel ER luminal factor promoting ERAD of misfolded ER clients (Inoue and Tsai, 2016), as well as toxic agents that hijack the ERAD pathway to cause infection (Inoue and Tsai, 2015; Williams et al., 2015). We therefore tested whether this chaperone promotes the degradation of *Akita* proinsulin using a cycloheximide chase approach in HEK 293T cells transiently expressing *Akita*-Myc, where the tag is appended within the C-peptide domain. We found that Grp170 knockdown using two different siRNAs targeted against Grp170 (siRNA 1 and 2) (Fig. 3-1A, second panel) significantly impaired the degradation of *Akita*-Myc when compared with cells treated with the control siRNA (scrambled) (Fig. 1A, top panel [the intensity of the *Akita*-Myc band is quantified in Fig. 3-1B]). Because Grp170 can act as a nucleotide exchange factor (NEF) against the ER luminal BiP ATPase (Behnke et al., 2015), we asked whether the other ER-resident NEF called Sil1 also facilitates *Akita*-Myc degradation and found that it did not (Fig. 3-1C, top panel [quantified in Fig. 3-1B]). These results suggest Grp170 specifically promotes degradation of *Akita* proinsulin.

Using nonreducing SDS-PAGE, we previously reported that *Akita*-Myc forms high-MW protein complexes as well as smaller dimeric/trimeric oligomeric species (He et al., 2015). In cells with siRNA-mediated knockdown of Grp170, these smaller *Akita*-Myc oligomers were depleted when compared with the control (Fig. 3-2A, top panel;

quantified in graph). However, under reducing conditions, in cells with siRNA-mediated knockdown of Grp170, the total level of *Akita*-Myc was actually increased (Fig. 3-2A, bottom panel). One plausible explanation for these results is that in the absence of Grp170, smaller oligomeric species of *Akita* proinsulin may be further shifted into higher-MW protein complexes. To evaluate this possibility, extracts from control or Grp170-depleted cells expressing *Akita*-Myc were sedimented on a 10–50% discontinuous sucrose gradient. Individual fractions were collected and subjected to reducing SDS-PAGE followed by immunoblotting using an antibody against Myc. Whereas *Akita*-Myc distributed throughout the entire gradient under the control condition, in Grp170-depleted cells the mutant proinsulin accumulated in fractions corresponding to high-MW protein species (Fig. 3-2B, compare top and second panels; the *Akita*-Myc band intensity is quantified in the graph below). These results are consistent with the notion that when Grp170 is knocked down, smaller oligomeric species of *Akita* proinsulin are further shifted into high-MW protein complexes. Our findings support the hypothesis that Grp170 promotes degradation by shifting the balance of *Akita* proinsulin in favor of lower MW (smaller) species that are competent to undergo ERAD (He et al., 2015).

Overexpressing Grp170 Facilitates Degradation of *Akita* Proinsulin

To complement the loss-of-function (knockdown) approach, we used a gain-of-function (overexpression) strategy to further assess the role of Grp170 in the degradation of *Akita* proinsulin. We found that overexpressing Grp170-FLAG (Fig. 3-3A, second panel) stimulated the time-dependent disposal of *Akita*-Myc (Fig. 3-3A, top panel [quantified in

Fig. 3-3B]) but also lowered the steady-state level of *Akita* proinsulin even at the start of the experiment (Fig. 3-3A, top panel, zero time). The Grp170-induced degradation of *Akita* proinsulin is ERAD dependent because blocking ERAD by expressing the ATPase-defective p97 (QQ p97-His) (He et al., 2015; Ye et al., 2001) but not WT p97 prevented the overexpressed Grp170 from stimulating *Akita* degradation (Fig. 3-3C, top panel [*Akita*-Myc band intensity is quantified in Fig. 3-3B]). These data strongly suggest that Grp170 triggers *Akita* proinsulin degradation through the classic ERAD pathway.

To test the hypothesis that Grp170 promotes ERAD by shifting *Akita* proinsulin toward low-MW (smaller) species, we treated both control cells and cells overexpressing Grp170 with the proteasome inhibitor MG132 to block ERAD downstream in order to detect the oligomeric state of the accumulated *Akita*-Myc (omission of MG132 resulted in insufficient *Akita*-Myc accumulation to allow for such analysis; Fig. 3-3A, top panel). By sucrose gradient centrifugation, *Akita*-Myc in the control cell extract was found fairly evenly throughout the entire gradient (Fig. 3-3D, top panel and quantified below). Strikingly, in cells overexpressing Grp170, the distribution of *Akita*-Myc was shifted toward fractions 3–4, corresponding to low-MW (smaller) species (with an apparent decrease in fractions 6–8 corresponding to larger *Akita*-Myc oligomers) (Fig. 3-3D, bottom panel and quantified below). Thus, these gain-of-function studies also support the hypothesis that Grp170 facilitates ERAD of *Akita* proinsulin by favoring the generation of ERAD-competent low-MW (smaller) species.

Grp170 Promotes the Interaction of PDI With *Akita* Proinsulin

We envision that to promote an increase in ERAD-competent low-MW *Akita* proinsulin, Grp170 is likely to bind to the ERAD substrate. In cells expressing *Akita*-Myc and Grp170-FLAG (or a control protein [GFP-FLAG]), immunoprecipitating Grp170-FLAG but not GFP-FLAG coprecipitated *Akita*-Myc (Fig. 3-4A, top panel, compare lane 2 to 1). Endogenous BiP also coprecipitated with Grp170-FLAG but not GFP-FLAG (Fig. 3-4A, second panel). These findings are consistent with the established role of Grp170 as a NEF for BiP (Behnke et al., 2015). However, regardless of whether cells were intoxicated with the SubAB toxin that cleaves BiP or an inactive mutant SubAA272B that cannot degrade BiP (Fig. 3-4A, fifth panel, compare lane 3 to 2) (Paton et al., 2006), the Grp170-*Akita* proinsulin interaction persisted (Fig. 3-4A, top panel; quantified in graph), indicating that the Grp170-*Akita* proinsulin association is BiP independent.

Because PDI, an ER oxidoreductase, also interacts with *Akita* proinsulin (He et al., 2015), we examined the relationship between the respective PDI and Grp170 associations with *Akita*-Myc. We found that in cells coexpresssing Grp170-FLAG, knockdown of PDI caused *Akita* proinsulin association with Grp170 to be augmented (Fig. 3-4B, top panel, compare lane 3 to 2; quantified in graph). By contrast, in cells with knockdown of Grp170, the interaction of *Akita* proinsulin with a PDI “trap mutant” (that forms mixed disulfide adducts with *Akita* proinsulin) (He et al., 2015) diminished (Fig. 3-4C, top panel; quantified in graph). Thus, the efficiency of PDI interaction with *Akita* proinsulin appears to be promoted by the availability of Grp170, whereas the efficiency

of Grp170 interaction with *Akita* proinsulin is not promoted (and might even be competed) by the availability of PDI.

Grp170-Dependent Restoration of Small Oligomeric Forms Promotes ERAD of *Akita* Proinsulin Concomitant With ER Export of Coexpressed WT Proinsulin

Because WT and mutant proinsulins are coexpressed in the disease known as MIDY, we asked whether Grp170 displays preferential binding to either of these two proteins. In cells coexpressing Grp170-FLAG and either WT proinsulin-Myc or *Akita*-Myc (where the tag is incorporated within the C-peptide domain), precipitating equal amounts of Grp170-FLAG pulled down more *Akita* than WT proinsulin (Fig. 3-5A, top panel, compare lane 2 to 1). This preference is even more exaggerated when considering the lower abundance of *Akita* proinsulin levels in these cells (Fig. 3-5A, third panel, compare lane 2 to 1). Even when cells were treated with brefeldin A to block anterograde cargo exit from the ER (Klausner et al., 1992), the Grp170 interaction with ER-entrapped WT proinsulin was not enhanced (Fig. 3-5A, top panel, compare lane 3 to 1). Taken together, these results indicate that Grp170 intrinsically favors the misfolded *Akita* proinsulin over WT proinsulin.

Because Grp170 stimulates ERAD of *Akita* proinsulin (Fig. 3-3A and B), the preferential association of Grp170 with *Akita* proinsulin might allow WT proinsulin to escape from the ER en route to subsequent secretion. To test this, we used a 293T cell line with inducible expression of Grp170-FLAG (Inoue and Tsai, 2016). Conveniently, because

293T cells do not express prohormone convertases or secretory granules involved in the endoproteolytic conversion of proinsulin to insulin, proinsulin export from the ER of these cells can be monitored by the secretion of proinsulin itself. In these cells, transient expression of WT proinsulin-sfGFP (where sfGFP is incorporated within the C-peptide domain) was followed by induction of Grp170-FLAG via the addition of Tet. Tet addition did not affect WT proinsulin-sfGFP secretion (Fig. 3-5B, top panel [quantified in Fig. 3-5C]). As expected (Liu et al., 2010b; Liu et al., 2007), coexpression of *Akita*-Myc inhibited the secretion of WT proinsulin-sfGFP (Fig. 3-5B, top panel [quantified in Fig. 3-5C]). Strikingly, Grp170-FLAG induction in cells expressing *Akita*-Myc restored the secretory trafficking of WT proinsulin-sfGFP (Fig. 3-5B, top panel [quantified in Fig. 3-5C]). Overcoming this dominant-negative behavior of *Akita* proinsulin on WT proinsulin by Grp170 requires an intact ERAD pathway, as WT proinsulin rescue by Grp170 could no longer be observed in cells coexpressing QQ p97-His (Fig. 3-5D, lane 3). These findings strongly suggest that the rescue of WT proinsulin export by Grp170 requires active ERAD and is mediated in parallel with the selective degradation *Akita* proinsulin.

In the absence of WT proinsulin, *Akita* proinsulin can form high-MW protein complexes. In this condition, overexpressing Grp170 stimulates *Akita* proinsulin degradation by increasing the abundance of ERAD-competent low-MW (smaller) species (Fig. 3-3). When WT proinsulin is coexpressed with *Akita*, WT proinsulin becomes entrapped along with *Akita* proinsulin in the ER (He et al., 2015; Liu et al., 2010b). Thus, we hypothesize that increased activity of Grp170 should not only stimulate the degradation of *Akita* proinsulin, but WT proinsulin may also be disconnected from high-MW protein

complexes, enhancing the export of WT proinsulin from the ER. We used sucrose sedimentation analysis to evaluate changes in the oligomeric state of WT proinsulin upon coexpression with *Akita* proinsulin, along with the effect of induced expression of Grp170. When expressed by itself, WT proinsulin-sfGFP was found in fractions corresponding to low-MW oligomeric species (Fig. 3-5E, top panel; quantified in the graph below); induction of Grp170 did not affect its oligomeric state (Fig. 3-5E, second panel; quantified below). As expected, coexpressing *Akita*-Myc caused a pool of WT proinsulin-sfGFP to migrate into higher-MW fractions (Fig. 3-5E, third panel; quantified below). Importantly, upon Grp170 induction, a significant pool (≥25%) of WT proinsulin-sfGFP was shifted out of the higher MW fractions back to its original smaller oligomeric state (Fig. 3-5E, fourth panel; quantified below). These findings suggest that increased Grp170 activity helps to increase the abundance of low-MW forms of both *Akita* proinsulin and WT proinsulin, thereby facilitating ERAD of *Akita* proinsulin while concomitantly facilitating anterograde transport of WT proinsulin.

The Role of Grp170 in *Akita* Proinsulin Degradation and WT Proinsulin Secretion in β-Cells

Because the foregoing experiments were executed in a heterologous system, we asked whether these data could be recapitulated in the context of pancreatic β-cells. For this, we used INS1 832/13 (rat-derived) β-cells in which *Akita*-Myc is transiently expressed. Whereas depleting Grp170 decreased *Akita*-Myc degradation (Fig. 3-6A, top panel [quantified in Fig. 3-6B]), overexpressing Grp170-FLAG enhanced its degradation (Fig. 3-6C, top panel [quantified in Fig. 3-6D]).

To measure insulin secretion from β-cells, we expressed WT proinsulin-sfGFP and subsequently monitored the C-peptide-sfGFP released to the extracellular medium (using high-sensitivity immunoblotting with anti-GFP antibody). Because β-cells harbor prohormone convertases, the intervening C-peptide-sfGFP is excised from proinsulin, costored in secretory granules, and secreted in parallel with insulin (Haataja et al., 2013; Zhu et al., 2016). In these cells, we found that coexpressing *Akita*-Myc with WT proinsulin-sfGFP blocked secretion of the C-peptide-sfGFP, as anticipated (Fig. 3-6E, top panel [quantified in Fig. 3-6F]). Remarkably, additional expression of Grp170-FLAG decreased the intracellular abundance of *Akita*-Myc and restored C-peptide-sfGFP secretion (Fig. 3-6E, top panel [quantified in Fig. 3-6F]). Hence, in a more physiologically relevant cellular context, these findings confirm that enhancing Grp170 activity allows for facilitating the ERAD of *Akita* proinsulin while concomitantly facilitating anterograde transport of WT proinsulin with the production of insulin (and C-peptide-sfGFP), leading to enhanced insulin (and C-peptide-sfGFP) secretion.

As all “Grps” (glucose-regulated proteins) are induced during stress, we asked whether our overexpression system was comparable in Grp170 expression to *Akita* mouse islets. For this, we used different pharmacological and physiological conditions to examine the expression of Grp170. Interestingly, *Akita*-Myc expression in HEK 293T cells drives Grp170 protein expression to levels similar to *Akita* mouse islets (Fig. 3-6G, top panel, compare lanes 3 to 7), clearly indicating that Grp170 levels are upregulated by misfolded proinsulin entrapped in the ER. Importantly, overexpression of Grp170 in

HEK 293T cells enabled us to achieve protein levels that are slightly higher than the endogenous upregulation of Grp170 in *Akita* mouse islets (Fig. 3-6G, compare lanes 4 to 7). Indeed, it is this overexpression in 293T cells compared with the physiological ER stress response that drives the degradation of the *Akita* proinsulin mutant, supporting our central premise that it will require more than merely increasing Grp170 to ER stress levels in order to enhance degradation of the *Akita* proinsulin mutant in MIDY.

DISCUSSION

In this discussion, we address two main points developed by the current studies. First, we have identified a novel ER luminal component that promotes degradation of a misfolded proinsulin. Second, we highlight a principle that may be exploited to rectify the protein-misfolding problem underlying the disease known as MIDY.

Function of Grp170 in ERAD of *Akita* Proinsulin

First, on the basis of our studies conducted both in 293T cells and in a pancreatic β-cell line, we propose that the ER-resident chaperone Grp170 promotes ERAD of *Akita* proinsulin by shifting the balance of *Akita* proinsulin in favor of smaller oligomeric species that are competent to undergo ERAD (Fig. 3-6H). Grp170 may accomplish this feat by using two different potential mechanisms. In one mechanism, Grp170 binds to the smaller species of *Akita* proinsulin in the ER, preventing their further association in high-MW complexes; these smaller species are more efficiently targeted for destruction along the ERAD pathway. Indeed, a recent study (Behnke et al., 2016) suggests that Grp170 preferentially recognizes amino acids in clients that are predisposed to go on to aggregation. Whether Grp170 shields aggregation-prone residues within smaller species of *Akita* proinsulin remains to be tested. If this is the case, we speculate that the long COOH-terminal “holdase” domain of Grp170, which serves a role in substrate binding (Behnke et al., 2015; Behnke and Hendershot, 2014), may be responsible for interacting with these amino acids. Because Grp170 was shown to associate with the

core ERAD membrane machinery via binding directly to Sel1L (Inoue and Tsai, 2016), Grp170 can execute its function proximal to the retrotranslocation site. This scenario may potentially allow Grp170 to present smaller species of *Akita* proinsulin for ER-to-cytosol translocation, thereby enhancing the efficiency of ERAD.

In an alternative mechanism, Grp170 associates with high-MW aggregates of *Akita* proinsulin and dissociates small oligomeric species from their entrapment within the high-MW protein complexes by untangling the noncovalent forces that help to hold these complexes together. Because Grp170 is not a reductase, it cannot directly disrupt disulfide-bonded protein complexes such as those seen in Fig. 3-2. This suggests that Grp170 must operate coordinately with a bona fide ER reductase, such as PDI, to reduce aberrant intermolecular (and intramolecular) disulfide bonds (He et al., 2015). Indeed, not only are Grp170 and PDI found together in the same multiprotein complex (Meunier et al., 2002), but we also found that Grp170 availability promotes the association of PDI with *Akita* proinsulin. We consider it a reasonable possibility that Grp170-mediated disaggregation may expose disulfide bonds within the high-MW protein complexes, enabling PDI to more efficiently reduce these covalent bonds. Of note, the cytosolic counterpart of Grp170 is the Hsp110 chaperone family, including Hsp105 (Andreasson et al., 2010). In conjunction with a J-protein and Hsc70, Hsp105 has been shown to trigger disaggregation of aggregated protein complexes (Mattoo et al., 2013; Nillegoda et al., 2015; Rampelt et al., 2012; Shorter, 2011). Additionally, the Hsp105-Hsc70-J-protein triad can disassemble a large viral particle in vitro (Ravindran et al., 2015). These findings support the possibility that Grp170 may function in concert

with a J-protein and BiP (the Hsp70 family member of the ER) to disaggregate high-MW protein complexes of misfolded proinsulin. If so, the nucleotide exchange function of Grp170 for BiP might serve as a pivotal link that connects the actions of these two ER chaperones.

Restoring Insulin Secretion Concomitant with ERAD of Mutant Proinsulin

The second critical point revealed in this study is a strategy to rectify the block in insulin secretion that is fundamental to the pathogenesis of MIDY. Because all such patients are heterozygotes, WT proinsulin is coexpressed with mutant proinsulin in MIDY (Liu et al., 2010a; Stoy et al., 2007). Interestingly, our analyses demonstrated that Grp170 displays a higher affinity for *Akita* proinsulin compared with WT proinsulin, suggesting that the efficiency of association of this chaperone with proinsulin is linked to the misfolded state. Whereas the precise molecular feature that Grp170 recognizes within *Akita* proinsulin remains undefined, we note that when both WT and *Akita* proinsulin are coexpressed, imposing a block downstream in the ERAD pathway not only causes *Akita*-Myc to accumulate in cells, but the intracellular abundance of coexpressed WT proinsulin increases also (Fig. 3-5D). Moreover, coexpressed WT proinsulin associates much more with BiP in *Akita* pancreatic islets than it does in WT mouse islets (Liu et al., 2010a). Thus, WT proinsulin that is ordinarily recognized very little by Grp170 is likely to display new misfolded features that are more strongly recognized by Grp170 when WT proinsulin enters high-MW complexes containing *Akita* proinsulin.

With this in mind, we postulate that Grp170 engagement can have simultaneous beneficial effects on both *Akita* proinsulin and coexpressed WT proinsulin. Whereas small oligomeric species of *Akita* proinsulin (enriched by Grp170) are especially competent for ERAD, the enrichment of small oligomeric species of WT proinsulin offer an opportunity to fold successfully, followed by anterograde exit of WT proinsulin from the ER, allowing the formation of mature bioactive insulin that becomes available for secretion. Indeed, we found that in cells coexpressing *Akita* and WT proinsulins (where these two proteins are locked in the high-MW protein complexes), Grp170 induction liberated WT proinsulin from the high-MW complexes and restored insulin (C-peptide) secretion that was previously limited by the presence of *Akita* proinsulin. The dramatic effects of the overexpression of Grp170 in promoting insulin secretion suggest that the endogenous Grp170 level may be either insufficient to prevent *Akita* and WT proinsulins from entering the high-MW complexes or insufficiently abundant to effectively disaggregate high-MW species of misfolded proinsulin. In an in vivo transgenic mouse model, overexpressing Grp170 by 1.5-fold was unable to stimulate insulin secretion (Ozawa et al., 2005), suggesting that this is an insufficiently high level of Grp170 to overcome the misfolding block of proinsulin transport that leads to insulin secretion. Indeed, we now recognize that *Akita* mouse islets already have an ER stress–induced increase of Grp170 that is >1.5-fold and that still greater augmentation of Grp170 activity is required to rescue the WT proinsulin. As chemical compounds that act as allosteric regulators of the BiP/Hsp70 chaperones have been successfully developed (Li et al., 2013), it is conceivable that analogous compounds strongly stimulating Grp170

activity could also be generated. If so, the therapeutic benefit of such an agent in restoring insulin secretion should be explored.

Conclusion

This study not only identifies a new ER factor that triages a misfolded mutant proinsulin molecule for destruction, it also suggests a potential strategy for remedying the block in WT proinsulin transport that causes the insulin deficiency of MIDY. These findings may also have broad implications for other ER protein-misfolding diseases.

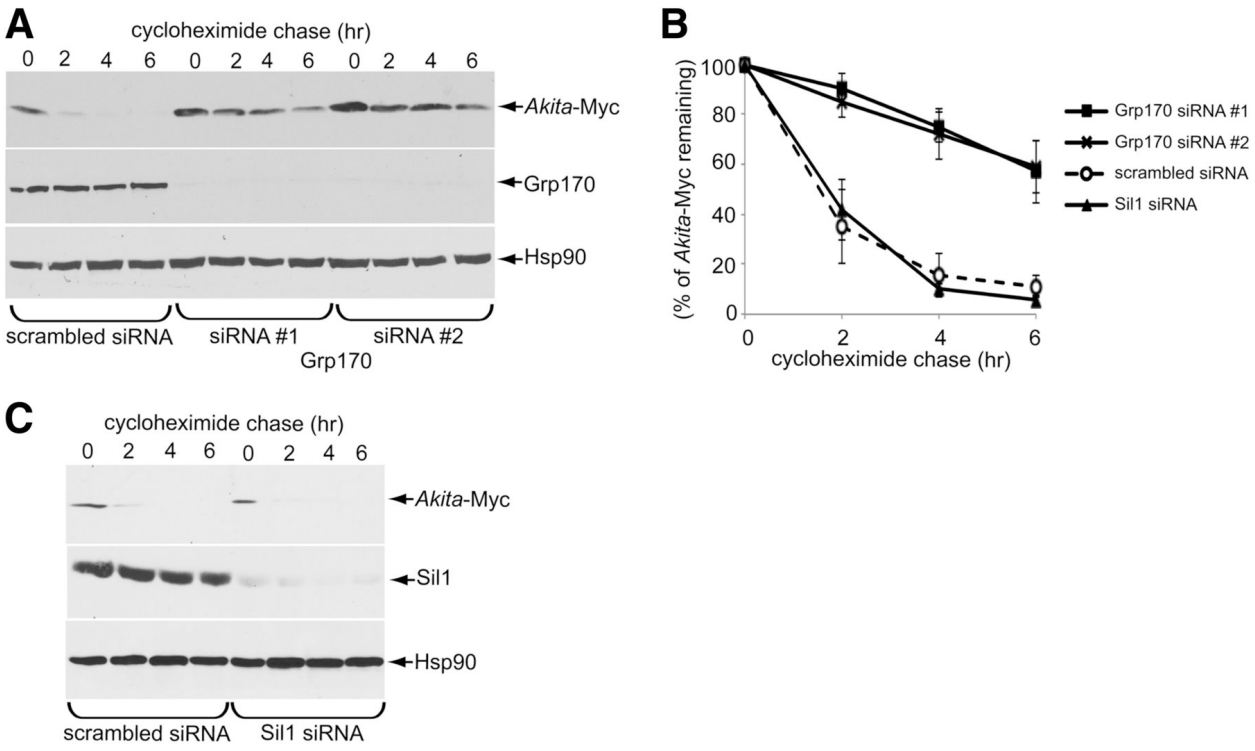

Figure 3-1. Grp170 knockdown impairs *Akita* degradation. *A*: 293T cells expressing *Akita*-Myc (1 µg) were transfected with scrambled or Grp170-specific siRNA. Cells were then treated with 100 µg/mL cycloheximide for the indicated time and harvested. The resulting WCE was analyzed by immunoblotting using the indicated antibodies. *B*: The *Akita*-Myc band intensity in *A* and *C* was quantified using ImageJ (National Institutes of Health). Data represent the mean ± SD of at least three independent experiments. *C*: As in *A*, except cells were transfected with Sil1 siRNA.

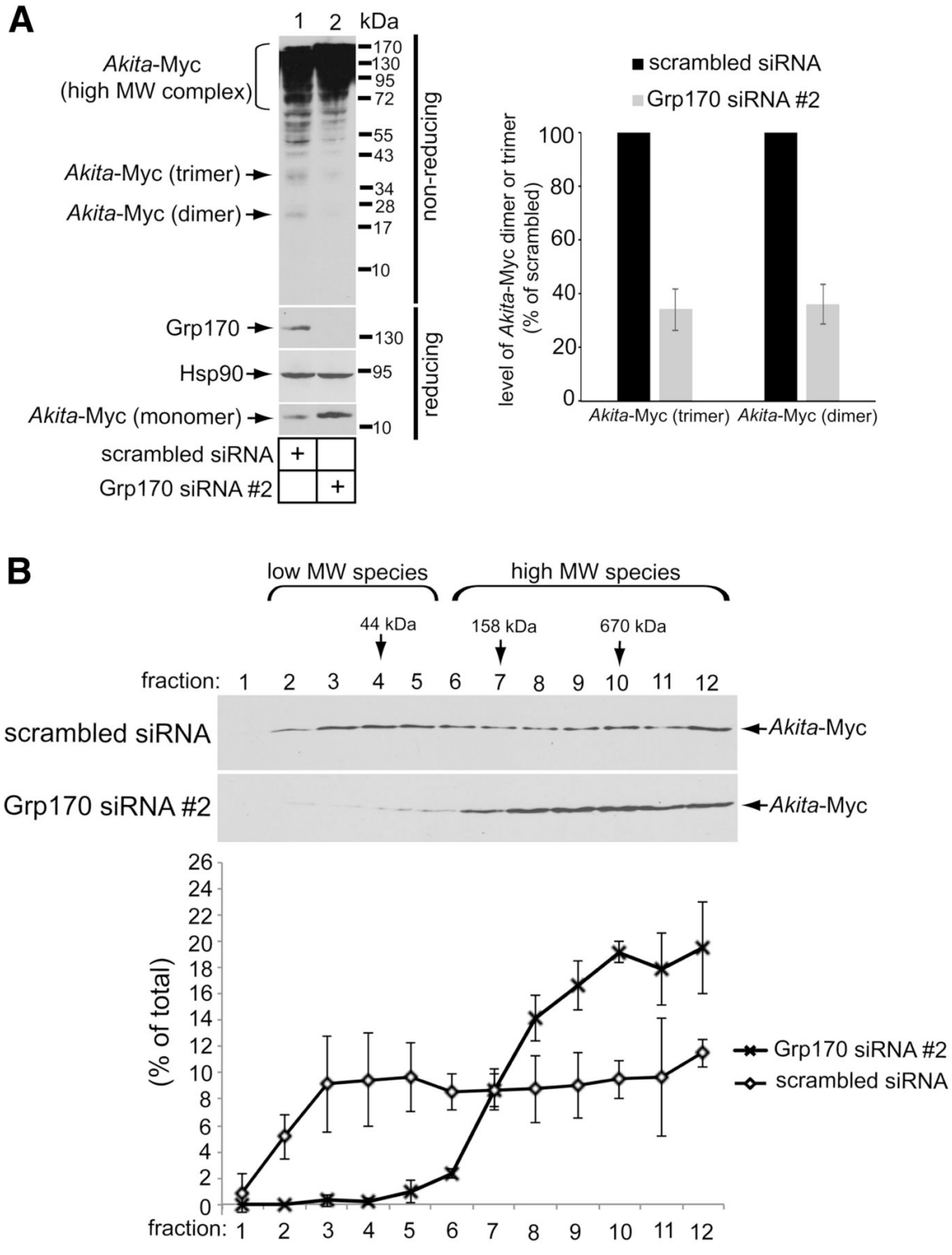

Figure 3-2. Depleting Grp170 increases the size of *Akita* oligomeric complexes. *A*: 293T cells expressing *Akita*-Myc (1 μg) were transfected with either scrambled siRNA or Grp170 siRNA #2. The resulting WCE was subjected to nonreducing and reducing

SDS-PAGE, as indicated, and immunoblotted using the indicated antibodies. The graph shows quantification of the relative amount of *Akita*-Myc dimeric and trimeric species generated from at least three independent experiments. *B*: 293T cells expressing *Akita* were transfected with either scrambled siRNA or Grp170 siRNA #2. Cells were harvested, lysed, and precleared; loaded onto a 10–50% sucrose gradient; and ultracentrifuged for 24 h. Samples were collected into 12 fractions, subjected to reducing SDS-PAGE, and immunoblotted. The lower graph shows the relative quantity of *Akita*-Myc in each fraction. Data represent the mean ± SD of at least three independent experiments.

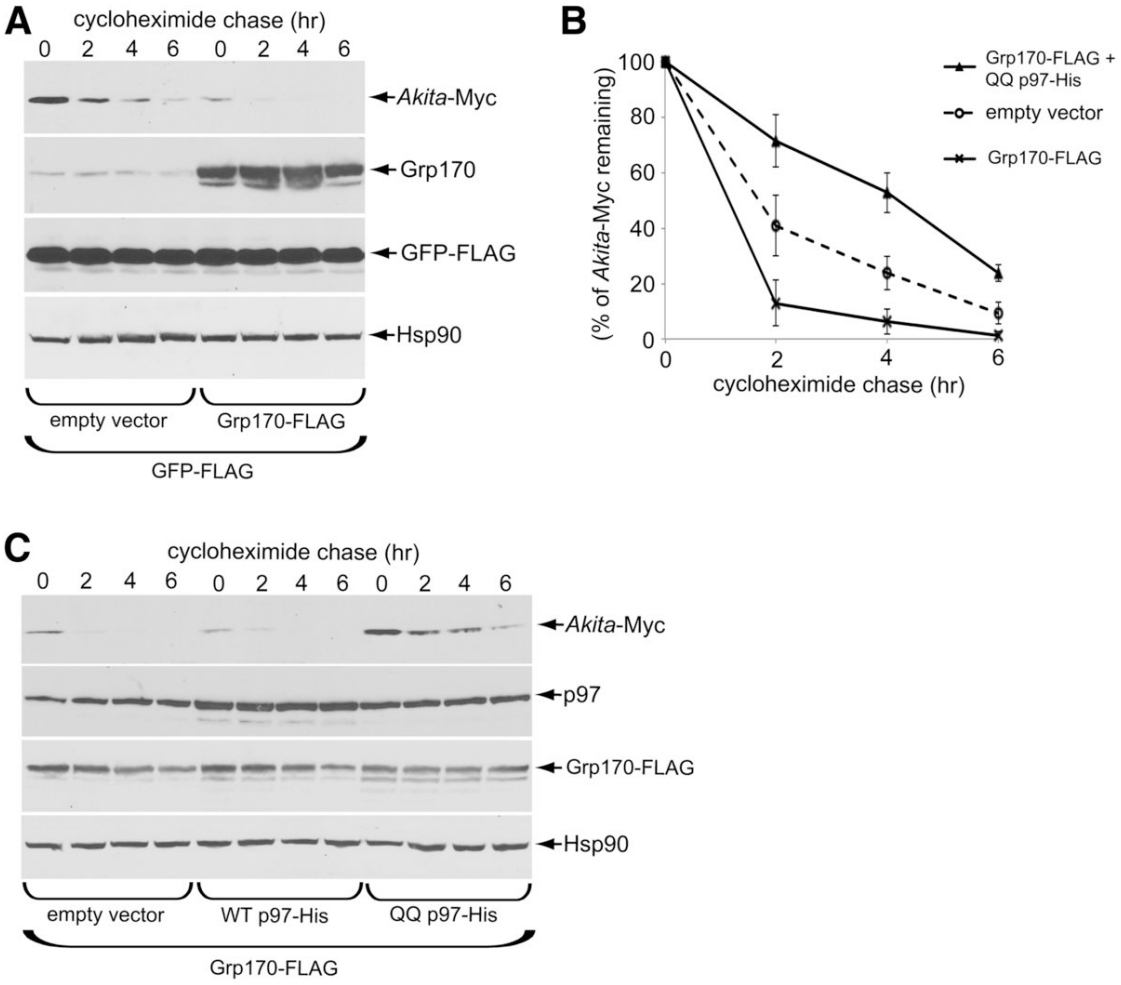
A
cycloheximide chase (hr)
0 2 4 6 0 2 4 6
Akita-Myc
Grp170
GFP-FLAG
Hsp90
empty vector
Grp170-FLAG
GFP-FLAG
B
(% of Akita-Myc remaining)
100
80
60
40
20
0
0 2 4 6
cycloheximide chase (hr)
Grp170-FLAG + QQ p97-His
empty vector
Grp170-FLAG
C
cycloheximide chase (hr)
0 2 4 6 0 2 4 6 0 2 4 6
Akita-Myc
p97
Grp170-FLAG
Hsp90
empty vector
WT p97-His
QQ p97-His
Grp170-FLAG
D
low MW species
high MW species
44 kDa
158 kDa
670 kDa
fraction: 1 2 3 4 5 6 7 8 9 10 11 12
+MG132
GFP-FLAG
Grp170-FLAG
Akita-Myc
Akita-Myc
(% of total)
22
20
18
16
14
12
10
8
6
4
2
0
fraction: 1 2 3 4 5 6 7 8 9 10 11 12
Grp170-FLAG
GFP-FLAG

Figure 3-3. Overexpression of Grp170 stimulates *Akita* degradation. *A*: 293T cells expressing *Akita*-Myc (1 μg) and GFP-FLAG (0.25 μg) were transfected with an empty vector or a Grp170-FLAG plasmid (1 μg). Cells were then treated with cycloheximide for the indicated time and harvested, and the resulting WCE was analyzed by immunoblotting using the indicated antibodies. *B*: The *Akita*-Myc band intensity in *A* and *C* was quantified with ImageJ. Data represent the mean ± SD of at least three independent experiments. *C*: As in *A*, except cells were transfected with Grp170-FLAG (1 μg) and additional empty vector, WT p97-His, or QQ p97-His construct (0.25 μg). *D*: 293T cells expressing *Akita*-Myc (1 μg) were transfected with GFP-FLAG or Grp170-FLAG plasmids (1 μg). Three hours preharvest, cells were treated with 10 μmol/L MG132. Cells were then harvested and separated on a 10–50% sucrose gradient by ultracentrifugation. The resulting fractions were separated using reducing SDS-PAGE and subjected to immunoblotting analysis. The lower graph shows relative distribution of *Akita*-Myc in each fraction. Data represent the mean ± SD of at least three independent experiments.

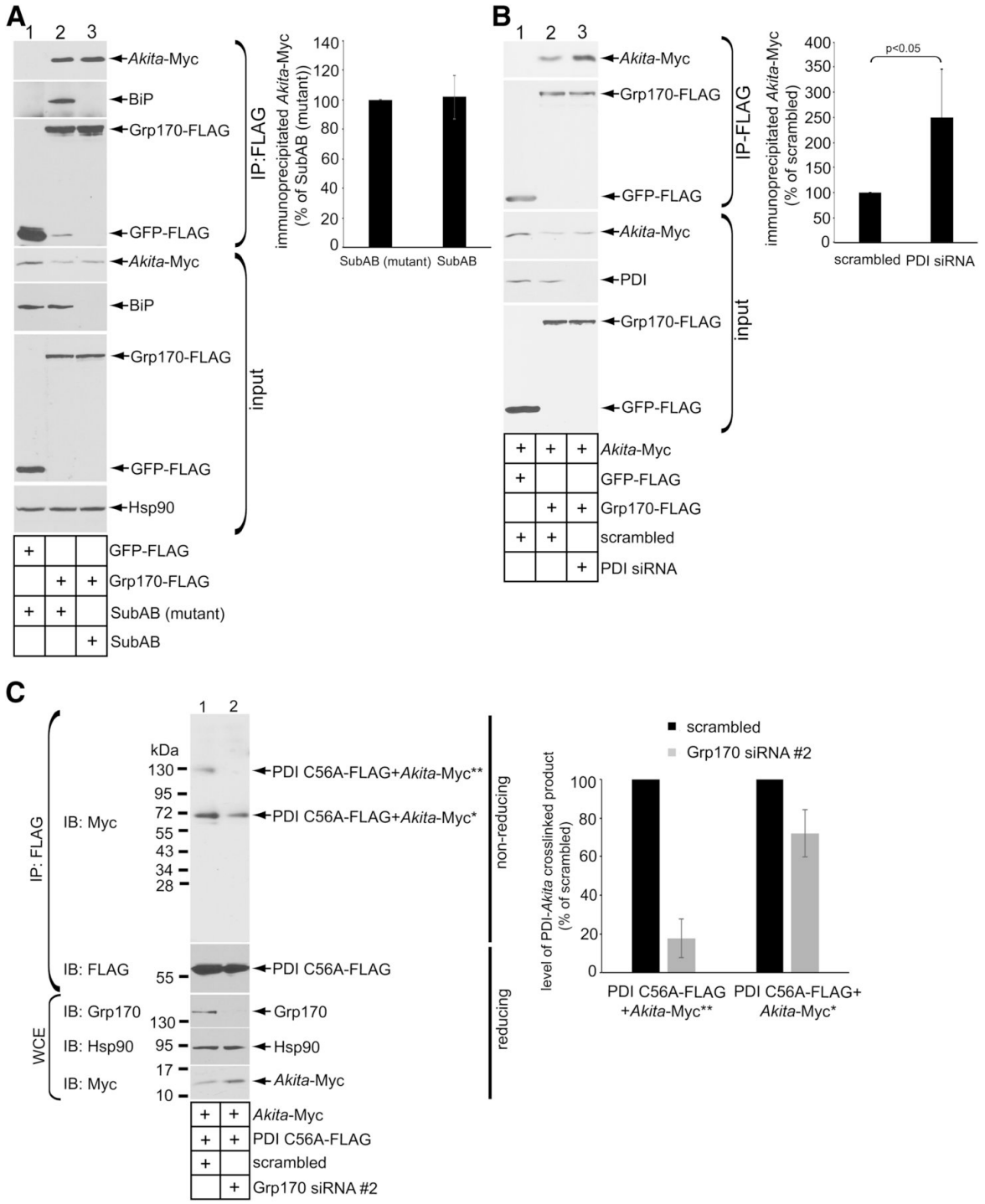

Figure 3-4. Grp170 promotes the interaction of PDI with *Akita* proinsulin. *A*: 293T cells expressing *Akita* (1 µg) were transfected with GFP-FLAG or Grp170-FLAG (1 µg), with intoxication of SubAB (0.5 µg/mL) or mutant $SubA_{A272}B$ (0.5 µg/mL) where indicated for 6 h before harvest. FLAG-tagged proteins were immunoprecipitated from the resulting WCE using FLAG antibody conjugated beads. The precipitated material

and input were subjected to reducing SDS-PAGE as indicated and immunoblotted using the appropriate antibodies. The graph represents the amount of immunoprecipitated *Akita*-Myc normalized to the level of immunoprecipitated *Akita*-Myc under the SubAB (mutant) control condition. *B*: 293T cells expressing *Akita*-Myc (1 μg) were transfected with scrambled siRNA or PDI siRNA as indicated. Cells were harvested and the resulting WCEs were subjected to IP using FLAG antibody conjugated beads. The immunoprecipitated material and input were subjected to reducing SDS-PAGE as indicated and immunoblotted using the indicated antibodies. The graph represents the immunoprecipitated *Akita*-Myc level normalized to the level of immunoprecipitated *Akita*-Myc in the scrambled control. *C*: Similar to *B*, except PDI C56A-FLAG (1 μg) was transfected into cells transfected with scrambled siRNA or Grp170 siRNA #2. The resultant WCE was incubated with FLAG antibody conjugated beads, and the precipitated material was separated on nonreducing and reducing SDS-PAGEs followed by immunoblotting with the indicated antibodies. Single and double asterisks indicate covalent adducts containing monomer or dimer of PDI C56A-FLAG + *Akita*-Myc, respectively. The graph represents the level of PDI-*Akita* crosslinked product formation normalized to the levels of these products generated under the scrambled siRNA control condition. IB, immunoblot.

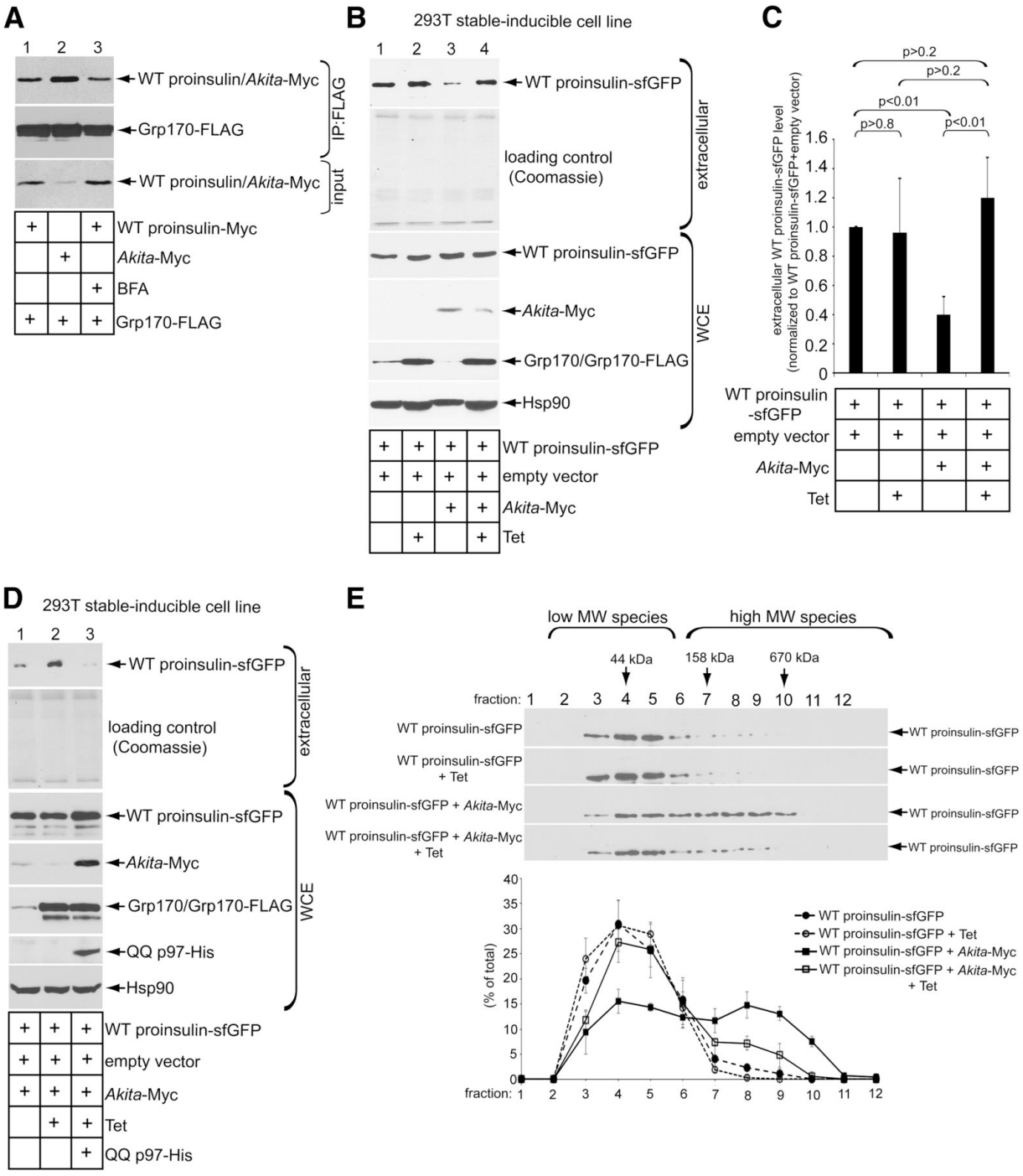

Figure 3-5. Grp170 overexpression promotes ERAD of *Akita* and ER export of coexpressed WT proinsulin. *A*: 293T cells expressing Grp170-FLAG (1 μg) were transfected with WT proinsulin-Myc or *Akita*-Myc (1 μg) and treated with EtOH or 2.5 μmol/L brefeldin A for 1 h. Cells were harvested, lysed, and subjected to IP using FLAG antibody conjugated beads. The precipitated material and input were separated on a reducing SDS-PAGE and subjected to immunoblotting with the indicated antibodies. *B*: Secretion of WT proinsulin-sfGFP assay was performed in Grp170-inducible 293T cells under indicated transfection conditions. The extracellular medium and WCE were

harvested, separated on SDS-PAGE, and subjected to immunoblotting with the indicated antibody. *C*: The WT proinsulin-sfGFP band intensity in *B* was quantified with ImageJ. Data represent the mean ± SD of at least three independent experiments. The Student *t* test was used to calculate the *P* values. *D*: As in *B*, except cells were transfected with QQ p97-His (0.25 μg) where indicated. *E*: The MW size of WT proinsulin-sfGFP in the WCE in *B* was analyzed by sucrose sedimentation centrifugation, as described in Fig. 3-2*B*. The lower graph represents the relative level of WT proinsulin-sfGFP in each fraction under the indicated experimental conditions.

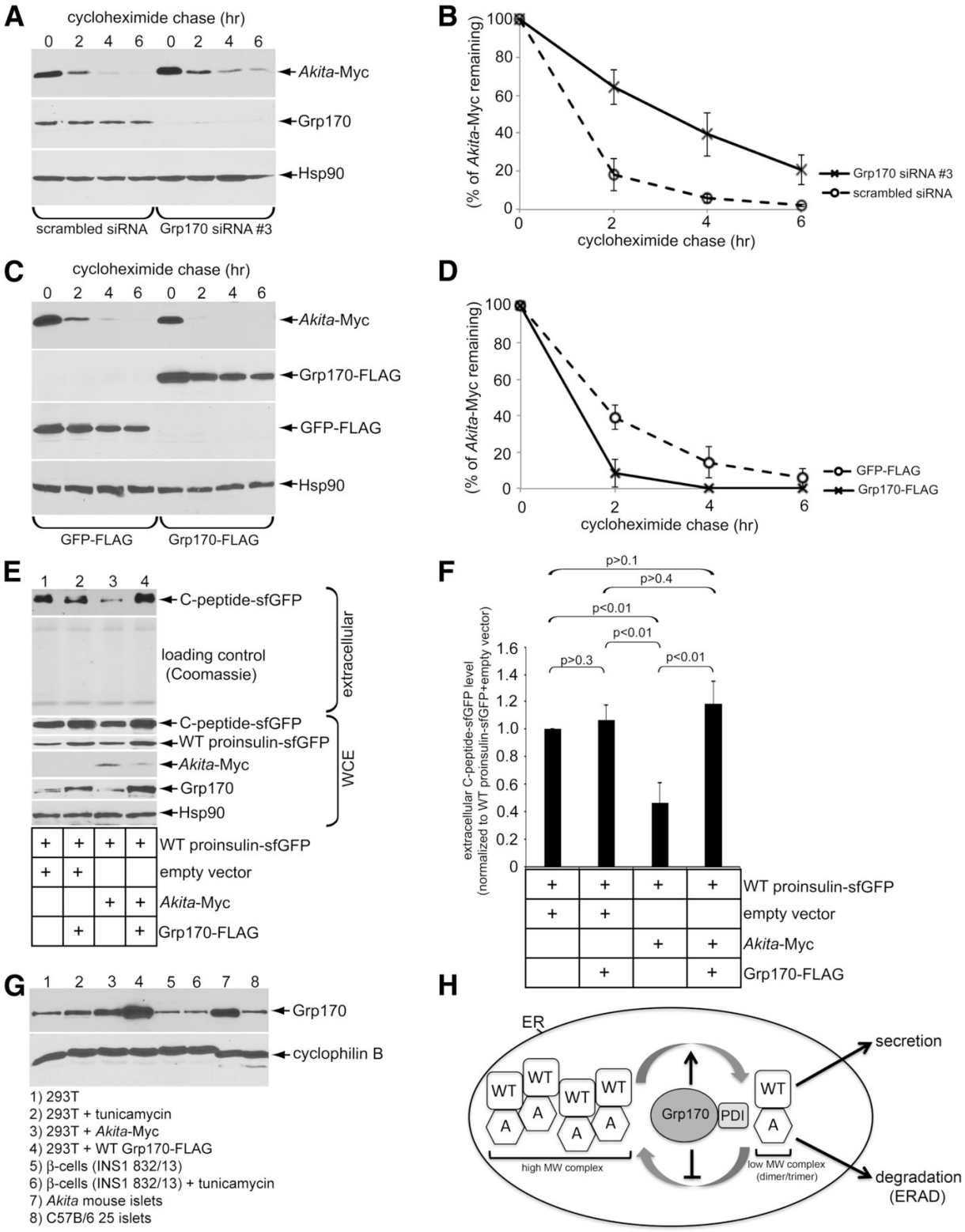

Figure 3-6. The role of Grp170 in *Akita* proinsulin degradation and WT proinsulin secretion in β-cells. *A*: β-Cells expressing *Akita*-Myc (1 µg) were transfected with

scrambled siRNA or Grp170 siRNA #3 (because Grp170 siRNA #1 or #2 did not efficiently deplete endogenous Grp170 in these cells). Cells were then treated with cycloheximide for the indicated time and harvested, and the resulting WCE was analyzed by immunoblotting using the indicated antibodies. *B*: The *Akita*-Myc band intensity in *A* was quantified using ImageJ. Data represent the mean ± SD of at least three independent experiments. *C*: β-Cells expressing *Akita*-Myc (1 μg) were transfected with GFP-FLAG or Grp170-FLAG (1 μg). Cells were then treated with cycloheximide for the indicated time and harvested, and the resulting WCE was analyzed by immunoblotting using the indicated antibodies. *D*: The *Akita*-Myc band intensity in *C* was quantified using ImageJ. Data represent the mean ± SD of at least three independent experiments. *E*: Secretion of WT proinsulin C-peptide-sfGFP assay was performed in the β-cells under the indicated transfection conditions. The extracellular medium and WCE were harvested, separated on SDS-PAGE, and subjected to immunoblotting with the indicated antibodies. *F*: The WT proinsulin C-peptide-sfGFP band intensity in *E* was quantified using ImageJ. Data represent the mean ± SD of at least three independent experiments. The Student *t* test was used to calculate the *P* values. *G*: Endogenous Grp170 protein expression across different physiological and pharmacology conditions. Treatment with 2.5 μg/mL tunicamycin was administered for 5 h. All transient transfections consisted of 1 μg of plasmid DNA for 24 h. Twenty-five *Akita* mouse islets (female) and 25 C57B/6 mouse islets (female) were harvested and lysed in 40 μL RIPA buffer with 10 mmol/L NEM plus protease inhibitors. *H*: A model depicting how Grp170 coordinates with PDI to promote ERAD of *Akita* (A) to restore WT proinsulin secretion (see Discussion for more details).

REFERENCES

Allen, J.R., Nguyen, L.X., Sargent, K.E., Lipson, K.L., Hackett, A., and Urano, F. (2004). High ER stress in beta-cells stimulates intracellular degradation of misfolded insulin. Biochem Biophys Res Commun *324*, 166-170.

Andreasson, C., Rampelt, H., Fiaux, J., Druffel-Augustin, S., and Bukau, B. (2010). The endoplasmic reticulum Grp170 acts as a nucleotide exchange factor of Hsp70 via a mechanism similar to that of the cytosolic Hsp110. J Biol Chem *285*, 12445-12453.

Behnke, J., Feige, M.J., and Hendershot, L.M. (2015). BiP and its nucleotide exchange factors Grp170 and Sil1: mechanisms of action and biological functions. J Mol Biol *427*, 1589-1608.

Behnke, J., and Hendershot, L.M. (2014). The large Hsp70 Grp170 binds to unfolded protein substrates in vivo with a regulation distinct from conventional Hsp70s. J Biol Chem *289*, 2899-2907.

Behnke, J., Mann, M.J., Scruggs, F.L., Feige, M.J., and Hendershot, L.M. (2016). Members of the Hsp70 Family Recognize Distinct Types of Sequences to Execute ER Quality Control. Mol Cell *63*, 739-752.

Gorasia, D.G., Dudek, N.L., Safavi-Hemami, H., Perez, R.A., Schittenhelm, R.B., Saunders, P.M., Wee, S., Mangum, J.E., Hubbard, M.J., and Purcell, A.W. (2016). A prominent role of PDIA6 in processing of misfolded proinsulin. Biochim Biophys Acta *1864*, 715-723.

Haataja, L., Snapp, E., Wright, J., Liu, M., Hardy, A.B., Wheeler, M.B., Markwardt, M.L., Rizzo, M., and Arvan, P. (2013). Proinsulin intermolecular interactions during secretory trafficking in pancreatic beta cells. J Biol Chem *288*, 1896-1906.

Hales, C.N. (1971). The role of insulin in the regulation of glucose metabolism. Proc Nutr Soc *30*, 282-288.

He, K., Cunningham, C.N., Manickam, N., Liu, M., Arvan, P., and Tsai, B. (2015). PDI reductase acts on Akita mutant proinsulin to initiate retrotranslocation along the Hrd1/Sel1L-p97 axis. Mol Biol Cell *26*, 3413-3423.

Inoue, T., and Tsai, B. (2015). A nucleotide exchange factor promotes endoplasmic reticulum-to-cytosol membrane penetration of the nonenveloped virus simian virus 40. J Virol *89*, 4069-4079.

Inoue, T., and Tsai, B. (2016). The Grp170 nucleotide exchange factor executes a key role during ERAD of cellular misfolded clients. Mol Biol Cell *27*, 1650-1662.

Klausner, R.D., Donaldson, J.G., and Lippincott-Schwartz, J. (1992). Brefeldin A: insights into the control of membrane traffic and organelle structure. J Cell Biol *116*, 1071-1080.

Li, X., Srinivasan, S.R., Connarn, J., Ahmad, A., Young, Z.T., Kabza, A.M., Zuiderweg, E.R., Sun, D., and Gestwicki, J.E. (2013). Analogs of the Allosteric Heat Shock Protein 70 (Hsp70) Inhibitor, MKT-077, as Anti-Cancer Agents. ACS Med Chem Lett *4*.

Liu, M., Haataja, L., Wright, J., Wickramasinghe, N.P., Hua, Q.X., Phillips, N.F., Barbetti, F., Weiss, M.A., and Arvan, P. (2010a). Mutant INS-gene induced diabetes of youth: proinsulin cysteine residues impose dominant-negative inhibition on wild-type proinsulin transport. PLoS One *5*, e13333.

Liu, M., Hodish, I., Haataja, L., Lara-Lemus, R., Rajpal, G., Wright, J., and Arvan, P. (2010b). Proinsulin misfolding and diabetes: mutant INS gene-induced diabetes of youth. Trends Endocrinol Metab *21*, 652-659.

Liu, M., Hodish, I., Rhodes, C.J., and Arvan, P. (2007). Proinsulin maturation, misfolding, and proteotoxicity. Proc Natl Acad Sci U S A *104*, 15841-15846.

Mattoo, R.U., Sharma, S.K., Priya, S., Finka, A., and Goloubinoff, P. (2013). Hsp110 is a bona fide chaperone using ATP to unfold stable misfolded polypeptides and reciprocally collaborate with Hsp70 to solubilize protein aggregates. J Biol Chem *288*, 21399-21411.

Meunier, L., Usherwood, Y.K., Chung, K.T., and Hendershot, L.M. (2002). A subset of chaperones and folding enzymes form multiprotein complexes in endoplasmic reticulum to bind nascent proteins. Mol Biol Cell *13*, 4456-4469.

Nillegoda, N.B., Kirstein, J., Szlachcic, A., Berynskyy, M., Stank, A., Stengel, F., Arnsburg, K., Gao, X., Scior, A., Aebersold, R.*, et al.* (2015). Crucial HSP70 co-chaperone complex unlocks metazoan protein disaggregation. Nature *524*, 247-251.

Ozawa, K., Miyazaki, M., Matsuhisa, M., Takano, K., Nakatani, Y., Hatazaki, M., Tamatani, T., Yamagata, K., Miyagawa, J., Kitao, Y.*, et al.* (2005). The endoplasmic reticulum chaperone improves insulin resistance in type 2 diabetes. Diabetes *54*, 657-663.

Paton, A.W., Beddoe, T., Thorpe, C.M., Whisstock, J.C., Wilce, M.C., Rossjohn, J., Talbot, U.M., and Paton, J.C. (2006). AB5 subtilase cytotoxin inactivates the endoplasmic reticulum chaperone BiP. Nature *443*, 548-552.

Paton, A.W., Srimanote, P., Talbot, U.M., Wang, H., and Paton, J.C. (2004). A new family of potent AB(5) cytotoxins produced by Shiga toxigenic Escherichia coli. J Exp Med *200*, 35-46.

Rampelt, H., Kirstein-Miles, J., Nillegoda, N.B., Chi, K., Scholz, S.R., Morimoto, R.I., and Bukau, B. (2012). Metazoan Hsp70 machines use Hsp110 to power protein disaggregation. EMBO J *31*, 4221-4235.

Ravindran, M.S., Bagchi, P., Inoue, T., and Tsai, B. (2015). A Non-enveloped Virus Hijacks Host Disaggregation Machinery to Translocate across the Endoplasmic Reticulum Membrane. PLoS Pathog *11*, e1005086.

Ruggiano, A., Foresti, O., and Carvalho, P. (2014). Quality control: ER-associated degradation: protein quality control and beyond. J Cell Biol *204*, 869-879.

Shorter, J. (2011). The mammalian disaggregase machinery: Hsp110 synergizes with Hsp70 and Hsp40 to catalyze protein disaggregation and reactivation in a cell-free system. PLoS One *6*, e26319.

Smith, M.H., Ploegh, H.L., and Weissman, J.S. (2011). Road to ruin: targeting proteins for degradation in the endoplasmic reticulum. Science *334*, 1086-1090.

Steiner, D.F., Cunningham, D., Spigelman, L., and Aten, B. (1967). Insulin biosynthesis: evidence for a precursor. Science *157*, 697-700.

Stoy, J., Edghill, E.L., Flanagan, S.E., Ye, H., Paz, V.P., Pluzhnikov, A., Below, J.E., Hayes, M.G., Cox, N.J., Lipkind, G.M.*, et al.* (2007). Insulin gene mutations as a cause of permanent neonatal diabetes. Proc Natl Acad Sci U S A *104*, 15040-15044.

Tsai, B., Ye, Y., and Rapoport, T.A. (2002). Retro-translocation of proteins from the endoplasmic reticulum into the cytosol. Nat Rev Mol Cell Biol *3*, 246-255.

Wang, J., Takeuchi, T., Tanaka, S., Kubo, S.K., Kayo, T., Lu, D., Takata, K., Koizumi, A., and Izumi, T. (1999). A mutation in the insulin 2 gene induces diabetes with severe pancreatic beta-cell dysfunction in the Mody mouse. J Clin Invest *103*, 27-37.

Weiss, M.A. (2013). Diabetes mellitus due to the toxic misfolding of proinsulin variants. FEBS Lett *587*, 1942-1950.

Williams, J.M., Inoue, T., Chen, G., and Tsai, B. (2015). The nucleotide exchange factors Grp170 and Sil1 induce cholera toxin release from BiP to enable retrotranslocation. Mol Biol Cell *26*, 2181-2189.

Ye, Y., Meyer, H.H., and Rapoport, T.A. (2001). The AAA ATPase Cdc48/p97 and its partners transport proteins from the ER into the cytosol. Nature *414*, 652-656.

Zhu, S., Larkin, D., Lu, S., Inouye, C., Haataja, L., Anjum, A., Kennedy, R., Castle, D., and Arvan, P. (2016). Monitoring C-Peptide Storage and Secretion in Islet beta-Cells In Vitro and In Vivo. Diabetes *65*, 699-709.

CHAPTER 4: Cells Deploy a Two-Pronged Strategy to Rectify Misfolded Proinsulin Aggregates

INTRODUCTION

Formation of protein aggregates is a signature of many protein misfolding diseases, including Alzheimer's disease, Parkinson's disease, Huntington's disease, and diabetes (Bates, 2003; Irvine et al., 2008; Mukherjee et al., 2015). Not surprisingly, there is intense interest in learning how to stimulate cellular mechanisms that decrease the levels of potentially toxic aggregates to combat disease. In principle, these mechanisms may be comprised of pre-emptively preventing the formation of such aggregates, as well as either disaggregation or clearance of the aggregated species once they have formed. For the development of effective therapies, it may be necessary to stimulate more than one mechanism to decrease aggregate accumulation.

Proinsulin is the precursor of insulin, a hormone secreted by pancreatic β-cells that controls blood glucose levels (Steiner et al., 1967). Biosynthesis of proinsulin is initiated when the precursor preproinsulin translocates into the endoplasmic reticulum (ER)(Chan et al., 1976). Upon translocation into the ER, the signal sequence of preproinsulin is removed to generate proinsulin, which contains the B chain, connecting C-peptide, and the A-chain. Folding of proinsulin ensues with concomitant generation of

three conserved disulfide bonds (cysteine in the 7th residue of the B chain linked to cysteine in the 7th residue of the A-chain denoted as the B7-A7 disulfide bond, plus the B19-A20 and A6-A11 disulfide bonds). Upon proper folding, proinsulin exits the ER and is transported to the Golgi, and further, to immature secretorygranules. In these granules, bioactive insulin is formed when the C-peptide is excised, with the A and B chains connected via the two interchain disulfide bonds. Exocytosis of secretory granules ultimately releases bioactive insulin to the bloodstream. In the autosomal-dominant diabetic syndrome called Mutant *INS* gene–induced Diabetes of Youth (MIDY), misfolded mutant proinsulin is thought to initiate disease (Liu et al., 2010b; Stoy et al., 2007; Weiss, 2009) with association and impaired trafficking of wild-type proinsulin (Cunningham et al., 2017; Hodish et al., 2010; Liu et al., 2010a; Liu et al., 2007). Over 30 missense mutations in the human *INS* gene have been identified; in almost all cases, MIDY proinsulin mutants cannot fold properly and consequently fail to become bioactive insulin (Arunagiri et al., 2018). Instead, they are entrapped in the ER, dominantly interfering with the folding of wild type (WT) proinsulin which also becomes impaired in its exit from the ER, decreasing WT insulin production (Liu et al., 2010a; Liu et al., 2010b). However, whether misfolding of the mutant proinsulin leads to insoluble protein aggregation of either the mutant or WT gene product, is currently unknown. What is known is that decreased circulating insulin renders patients (and animal models) susceptible to increased blood glucose that provokes further proinsulin biosynthesis (both mutant and WT), exacerbating proinsulin misfolding in the ER and resulting in enhanced ER stress with eventual β-cell failure.

The best-characterized MIDY mutant is *Akita* proinsulin (herein simply called '*Akita*'), in which cysteine in the 7th position of the A chain is mutated to tyrosine, leaving cysteine in the 7th position of the B chain unpaired (Wang et al., 1999). This lone cysteine forms non-native disulfide bonds, leading to intermolecular disulfides engaging additional *Akita* molecules, which generate high molecular weight (MW) protein complexes (Cunningham et al., 2017; Liu et al., 2007). The accumulating presence of such complexes somehow recruits WT proinsulin, preventing its ER exit and secretion, which leads to the disease (Liu et al., 2010b). The ultimate sizes of these *Akita*-containing high MW protein complexes, and the full spectrum of ER protein quality control pathways available to limit the build-up of *Akita*-containing high MW complexes, are questions of direct relevance to the pathogenesis and treatment of MIDY.

To date, we and others have demonstrated that one major ER quality control pathway called ER-associated degradation (ERAD) can dispose of soluble forms of *Akita* (Allen et al., 2004; Cunningham et al., 2017; He et al., 2015; Liu et al., 2010a). ERAD targets misfolded ER proteins for retrotranslocation to the cytosol for proteasomal destruction (Ruggiano et al., 2014; Smith et al., 2011; Tsai et al., 2002). We recently reported that the ER-resident chaperone Grp170, an atypical member of the Hsp70 ATPase family, helps to facilitate ERAD of soluble *Akita* which enhances the secretion of WT insulin (Cunningham et al., 2017). However, the mechanistic basis by which Grp170 facilitates ERAD could potentially involve the targeting of *Akita* monomers, complexes (small or large) or even massive insoluble species.

Here we demonstrate that in the ER, *Akita* forms detergent-insoluble protein aggregates that entrap WT proinsulin. Strikingly, we find that two distinct ER quality control pathways are coordinately deployed to help limit the levels of these aggregates. First, Grp170 acts to prevent the formation of detergent-insoluble *Akita* aggregates which otherwise recruit and capture WT proinsulin. Second, to the extent that detergent-insoluble aggregates form despite Grp170 action, an ER-phagy pathway that relies critically upon reticulon3 (RTN3) actively removes these species. Remarkably, clearance of aggregated *Akita* restores proper intracellular transport of WT proinsulin. These results suggest that insoluble aggregates of *Akita* with WT proinsulin help to drive the pathogenesis of MIDY, and reveal a new potential therapeutic strategy to block the disease. We also report that RTN3-dependent ER-phagy disposes of two additional, unrelated prohormone aggregates — together, these represent the first identified substrates of RTN3-mediated ER-phagy, and the data highlight a more general role of RTN3 in the disposal of pathogenic insoluble protein complexes in the ER.

STAR+METHODS

KEY RESOURCES TABLE

REAGENT or RESOURCE	SOURCE	IDENTIFIER
Antibodies		
Rabbit anti-Myc	Immunology Consultants Laboratory	Cat#RMYC-45A
Mouse anti-Myc	Laboratory of Kristen Verhey	N/A
Rabbit anti-Orp150/Grp170	Abcam	Cat# ab124884, RRID:AB_10973544
Rabbit anti-BiP	Abcam	Cat# ab21685, RRID:AB_2119834
Mouse anti-Hsp90alpha/beta (F-8)	Santa Cruz Biotechnology	Cat# sc-13119, RRID:AB_675659
Mouse anti-PDI	Abcam	Cat# ab2792, RRID:AB_303304
Mouse anti-GFP	Proteintech Group	Cat# 66002-1-Ig, RRID:AB_11182611
Rabbit anti-Hrd1	Proteintech Group	Cat# 13473-1-AP, RRID:AB_2287023
Rabbit anti-Beclin1	MBL International	Cat# PD017, RRID:AB_1278767
Rabbit anti-CCPG1	Proteintech Group	Cat# 13861-1-AP, RRID:AB_2074010
Rabbit anti-Sec62 [EPR9212]	Abcam	Cat# ab137022
Rabbit anti-RTN3	Bethyl Laboratories	Cat# A302-860A

Rabbit anti-RTN3	Boster Biological Technology	Cat# PA2256, RRID:AB_2665372
Rabbit anti-FAM134B	Proteintech Group	Cat# 21537-1-AP
Rabbit anti-RTN4	Santa Cruz Biotechnology	Cat# sc-271878, RRID:AB_10709573
Rabbit anti-FLAG	Millipore Sigma	Cat# F7425, RRID:AB_439687
Mouse anti-FLAG	Millipore Sigma	Cat# F3165, RRID:AB_259529
Goat anti-Rabbit IgG (H+L) Highly Cross-Adsorbed Secondary Antibody, Alexa Fluor 594	Thermo Fisher Scientific	Cat# A-11037, RRID:AB_2534095
Goat anti-Mouse IgG (H+L) Highly Cross-Adsorbed Secondary Antibody, Alexa Fluor 488	Thermo Fisher Scientific	Cat# A-11029, RRID:AB_2534088
Chemicals, Peptides, and Recombinant Proteins		
Phenylmethylsulfonyl fluoride (PMSF)	Acros Organics	Cat# AC215740010; Cas: 329-98-6
N-ethylmaleimide (NEM)	Millipore Sigma	Cat# E3876; Cas: 128-53-0
Dithiobis-succinimidyl-propionate (DSP) Crosslinker	Thermo Fisher Scientific	Cat# 22585; Cas: 57757-57-0
Cycloheximide	VWR	Cat# 94271; Cas 66-81-9
MG132	Cayman Chemicals	Cat# 10012628; Cas: 133407-82-6
DL-Dithiothreitol	Millipore Sigma	Cat# D0632; Cas: 3483-12-3

BSA	Millipore Sigma	Cat# A6003; Cas: 9048-46-8
Grp170-FLAG	(Inoue and Tsai, 2015); This Paper	N/A
G41L Grp170-FLAG	(Inoue and Tsai, 2015); This Paper	N/A
BiP-FLAG	This Paper	N/A
Ponceau-S	Fisher Scientific	Cat# BP103-10; Cas: 6226-79-5
Bafilomycin A1	Millipore Sigma	Cat# 508409 CAS: 88899-55-2
Polyethylenimine	Fisher Scientific	Cat# AC178571000; Cas: 9002-98-6; 7732-18-5
Prolong Gold Antifade Mountant with DAPI	Thermo Fisher Scientific	Cat# P36931
Experimental Models: Cell Lines		
Human: HEK 293T	ATCC	Cat# CRL-3216, RRID:CVCL_0063
Rat: INS1 832/13	Laboratory of Christopher Newgard	RRID:CVCL_7226
Oligonucleotides		
siGrp170: GCUCAAUAAGGCCAAGUUUdTdT	Millipore Sigma	N/A
siHrd1: GGAGACUGCCACUACAGUUGUdTdT	Millipore Sigma	N/A
Human siBeclin1: GGUCUAAGACGUCCAACAAdTdT	Millipore Sigma	N/A
Rat siBeclin1: GGAAGGGACAAGAGGUAAAUUdTdT	Millipore Sigma	N/A
siCCPG1: UUCCAUGUACCAGCUUAGUUAdTdT	Millipore Sigma	N/A
siSec62: GAAGGAUGAGAAAUCUGAAUUdTdT	Millipore Sigma	N/A
siRTN3: UCAGUGUCAUCAGUGUGGUUUCUUAdTdT	Millipore Sigma	N/A
siFAM134B: CAAAGATGACAGTGAATTAdTdT	Millipore Sigma	N/A

siRTN4: GUUCAGAAGUACAGUAAUUdTdT	Millipore Sigma	N/A
Recombinant DNA		
pTarget-hProCpepMyc	(Liu et al., 2010a)	N/A
pTarget-hProC(A7)Y-CpepMyc	(Liu et al., 2010a)	N/A
pTarget-hProCpepSfGFP	(Haataja et al., 2013)	N/A
pTarget-hProC(A7)Y-CpepSfGFP	(Haataja et al., 2013)	N/A
pcDNA3.1-FLAG-RTN3L	(Grumati et al., 2017); Laboratory of Ivan Dikic	N/A
pcDNA3.1-FLAG-RTN3LΔ6LIRs	(Grumati et al., 2017); Laboratory of Ivan Dikic	N/A
pAc-GFPC1-Sec61beta	Laboratory of Tom Rapoport	RRID:Addgene_15108
pAc-GFPC1-Rtn3c	Laboratory of Tom Rapoport	N/A
pAc-GFPC1-Rtn4a	Laboratory of Tom Rapoport	N/A
pAc-GFPC1-Rtn4HD	Laboratory of Tom Rapoport	N/A
pcDNA3.1-Grp170-FLAG	(Inoue and Tsai, 2015); this paper	N/A
pcDNA3.1-G41L Grp170-FLAG	(Inoue and Tsai, 2015); this paper	N/A
pcDNA3.1-FLAG-BiP	This paper	N/A
pcDNA3.1-C28F POMC-FLAG	(Kim et al., 2018) Laboratory of Ling Qi	N/A
pRc/RSV-G57S Pro-AVP-FLAG	(Shi et al., 2017) Laboratory of Ling Qi	N/A

CONTACT FOR REAGENT AND RESOURCE SHARING

Further information and requests for resources and reagents should be directed to and will be fulfilled by the Lead Contacts, Peter Arvan (parvan@med.umich.edu) and Billy Tsai (btsai@med.umich.edu).

EXPERIMENTAL MODEL AND SUBJECT DETAILS

HEK 293T were cultured in Dulbecco's modified Eagle's medium (DMEM), supplemented with 10% fetal bovine serum in an incubator at 37°C and 5% CO_2. Rat insulinoma INS1 832/13 cells were cultured in Roswell Park Memorial Institute medium (RPMI) 1640, supplemented with 10% fetal bovine serum, 10 mM HEPES (pH 7.5), 1 mM Sodium Pyruvate, and 50 μM β-mercaptoethanol.

METHOD DETAILS

Plasmid Transfection, Cycloheximide Chase, Immunoprecipitation, and Immunoblotting

Cells were seeded 1 day prior to transfection with 0.01-4 μg of plasmid DNA using polyethylenimine (PEI) or Lipofectamine 2000 (Invitrogen). 48 or 24 h post transfection, cells were harvested without treatment, treated with MG132 (10 μM) for 3 h, or treated with cycloheximide and chased for 0, 2, 4, and 6 h. Cells were harvested in PBS supplemented with 10 mM *N*-ethylmaleimide (NEM). For crosslinking immunoprecipitation experiments, cells crosslinked with DSP (per manufacturer's protocol) were lysed in 500 μL of 1% Triton X-100 in HN buffer (50 mM HEPES pH 7.5, 150 mM NaCl) containing 10 mM NEM and 1 mM PMSF. Cells were then incubated on ice for 10 min and centrifuged. The resulting whole cell extract was incubated with M2-FLAG conjugated beads (Thermo Fisher) at 4°C for 2 h. Beads were washed with lysis buffer supplemented with NEM and PMSF, and boiled in SDS sample buffer with 100 mM dithiothreitol (DTT). For immunoblot analysis, cells were lysed and immunoblotted

as previously described (Cunningham et al., 2017). Briefly, cells were lysed in 100 µL RIPA buffer supplemented with NEM and PMSF, incubated on ice for 10 min and centrifuged. The resulting extract was subjected to reducing SDS-PAGE with 100 mM DTT, transferred to nitrocellulose, and incubated with primary and secondary antibodies prior to exposure using ECL.

Small interfering RNA knockdown

Small interfering RNA (siRNA) was transfected into cells using RNAiMAX (Invitrogen), and cells were chased or harvested 48 h after treatment.

Detergent-insolubility Assay

Cells were lysed in 100 µL of RIPA supplemented with 10 mM NEM and 1 mM PMSF, and incubated on ice for 10 min and centrifuged. The extracted material represents the soluble fraction, while material the pellet (which was extracted by 2% SDS sample buffer) represents the insoluble fraction. Soluble and insoluble samples were subjected to SDS-PAGE and immunoblotting as described above.

Sucrose Gradient Fractionation Assay

This assay was previously described (Cunningham et al., 2017). Briefly, cells were lysed in RIPA buffer to generate a whole cell extract. The extract is cleared using an ultracentrifuge at 50,000 rpm for 20 min. The resulting cleared extract is layered on top

of a 10-50% or 30-70% discontinuous sucrose gradient and centrifuged on a Beckman SW50.1 rotor at 29,000 rpm for 24 h at 4°C. After centrifugation, 12 50 µL fractions were collected, and analyzed by SDS-PAGE followed by immunoblotting.

Immunoprecipitation using Pooled Sucrose Fractions

Fractions were pooled as follows: fractions 1-4, 5-8, and 9-12. 50% sucrose and HN buffer were added to the three pools to normalize the sucrose concentration. The pooled samples were incubated with anti-Myc antibody (1:200) at 4°C for 24 h, followed by 2 h of incubation with A/G-agarose beads (Pierce) at 4°C. The precipitated material was subjected to SDS-PAGE followed by immunoblotting.

***In vitro* Aggregation Assay**

HEK 293T cells transfected with *Akita*-Myc were semipermeabilized in 300 µL of HCN buffer (50 mM HEPES pH 7.5, 150 mM NaCl, 2 mM $CaCl_2$), supplemented with 0.01% digitonin, 10 mM NEM and 1 mM PMSF. Cells were incubated on ice for 10 min, and centrifuged at 16,100 rpm for 10 min. This generates a supernatant fraction that contains cytosolic proteins, and a pellet fraction that contains membranes including the ER; *Akita*-Myc in the pellet fraction was subsequently solubilized by RIPA buffer containing 10 mM NEM and 1 mM PMSF. Purification of recombinant Grp170-FLAG, BiP-FLAG, and G41L Grp170-FLAG were prepared as previously described (Inoue et al., MBoC 2016). Recombinant FLAG-tagged proteins were stored at -80°C in 0.1% Triton X-100 in HN buffer. During the reaction, each tube contains a membrane extract

harboring soluble *Akita*-Myc, 100 μM ATP, 10 mM $MgCl_2$, 1 mM KCl, and either 0.3 mg/mL of BSA or the indicated purified protein (Grp170-FLAG, G41L Grp170-FLAG, or BiP-FLAG). Each tube was then incubated in a thermomixer (800 rpm) at 37°C for the indicated time: 10, 5, 3, 1, or 0 min. After incubation, the sample was centrifuged at 16,100 g for 10 min to generate a supernatant fraction that contains soluble *Akita*-Myc and a pellet fraction that harbors aggregated *Akita*-Myc. Aggregated *Akita*-Myc was resuspended in a SDS sample buffer. Samples containing soluble or aggregated *Akita*-Myc were subjected to reducing SDS-PAGE followed by immunoblotting.

XBP1 Splicing Assay

HEK 293T cells transfected with plasmids encoding *Akita*-Myc or an empty vector (pcDNA3.1) were co-transfected with either scrambled or RTN3 siRNA. XBP1 splicing assay was performed as described in (Uemura et al., 2009).

Immunofluorescence Staining and Imaging

INS1 832/13 cells were fixed with 4% PFA for 20 minutes, permeabilized with 0.2% Triton X-100/TBS/3% BSA for 20 minutes, and blocked with 0.2% Tween-20/TBS/3% BSA for one hour at room temperature. Primary antibodies were diluted in 0.2% Tween-20/TBS/3% BSA and incubated overnight at 4°C. Secondary antibodies were also diluted in 0.2% Tween-20/TBS/3% BSA and incubated at room temperature for one hour. Cells were mounted with Prolong Gold anti-fade reagent with DAPI. Microscopy was performed using a Zeiss LSM 800 confocal laser scanning microscope with a Plan-

Apochromat 40x/1.4 oil differential interference contrast (DIC) M27 objective. Images were processed in Zen 2.3 software. 3D reconstruction was performed on Zen 2.3 software powered by Arivis.

Proinsulin Secretion Assay

Proinsulin secretion assay was previously described (Cunningham et al., 2017), with few modifications indicated below. Briefly, HEK 293T cells were transfected with a plasmid encoding WT proinsulin-sfGFP. 8 h post transfection, the medium was replaced with 500 µL of fresh medium and incubated for 16 h. Medium, the whole cell extract, and the insoluble samples were collected and subjected to SDS-PAGE and analyzed by immunoblotting.

Quantification and Statistical Analysis

Details on statistical analyses can be found in each figure legend. Each experiment shown was replicated at least n=3 times. Additionally, western blot quantification was performed using NIH ImageJ v1.52i with significance $p<0.05$.

RESULTS

Depletion of Grp170 promotes formation of detergent-insoluble *Akita* proinsulin

We previously used sucrose gradient sedimentation analysis to analyze the oligomeric state of *Akita* (Cunningham et al., 2017). In this experiment, HEK 293T cells transiently expressing *Akita*-Myc (in which Myc is inserted within the C-peptide domain) were lysed in RIPA buffer (containing 1.0% Triton X-100 and 0.1% SDS) before sedimentation on a 10%-50% discontinuous sucrose gradient. After centrifugation, fractions were collected and subjected to reducing SDS-PAGE and immunoblotting using an antibody against Myc. As previously reported, *Akita*-Myc was found in all fractions (Cunningham et al., 2017). In this report, we have defined fractions 1-4 as low MW *Akita* species, fractions 5-8 as the mid MW species, and fractions 9-12 as high MW species (Fig. 4-1A).

Although Grp170 was previously shown to bind to *Akita* and to promote its ERAD-dependent degradation (Cunningham et al., 2017), it is unclear which size *Akita* complexes this chaperone preferentially interacts with. In a discontinuous sucrose gradient, the bulk of cellular Grp170 in the steady state resides in the middle of the gradient (Fig. 4-1B, first set of panels, “input”). *Akita* in the low, mid, and high MW species were then immunoprecipitated (with anti-Myc) and subjected to SDS-PAGE followed by immunoblotting with an antibody against Grp170 (Fig. 4-1B, first set of panels) or the ER-resident chaperone BiP (second set of panels). Strikingly, Grp170 was specifically co-precipitated with *Akita* from the high MW species (Fig. 4-1B, lane 3) whereas pull-down of *Akita* from the mid MW species co-precipitated BiP (Fig. 4-1B,

second set of panels, lane 5). These findings demonstrate that Grp170 preferentially engages the high MW *Akita* complexes.

What might be the functional significance of Grp170 binding selectively to high MW *Akita* complexes? One possibility is that this binding prevents *Akita* from extending even further to form insoluble protein complexes. To determine if Grp170 prevents higher order *Akita* aggregation, we assessed the extent to which *Akita* can be extracted into the soluble phase in RIPA buffer — the molecules resistant to extraction are referred to as insoluble aggregates — but can be re-solubilized under stronger detergent conditions (1%-2% SDS). Using this method, we found that in cells expressing *Akita*-Myc and transfected with a control siRNA, *Akita* was extracted into the soluble fraction with a negligible pool of insoluble molecules (Fig. 4-1C, first panel, compare lane 1 to 5). By contrast, upon knockdown of Grp170 [siRNA #1, (Cunningham et al., 2017)], the level of *Akita*-Myc in the insoluble fraction increased significantly (Fig. 4-1C, first panel, compare lane 6 to 5; quantified in right graph). Grp170 knockdown also modestly increased the *Akita* level in the soluble fraction (Fig. 4-1C, first panel, compare lane 2 to 1). Appearance of *Akita* in the insoluble phase is not due to non-specific partitioning because neither Grp170 nor cytosolic Hsp90 appeared in this fraction under any condition (Fig. 4-1C, second and third panels). Hence, the observation that depleting Grp170 increased the level of aggregated *Akita* suggests that Grp170 functions to prevent *Akita* aggregation.

To probe the size of *Akita* complexes in the soluble and insoluble fraction (re-solubilized in SDS), we layered these fractions from Grp170-depleted cells over a heavier 30%-70% discontinuous sucrose gradient. Whereas soluble *Akita* migrated to the lighter fractions (2-6) as expected, insoluble *Akita* was found only in the densest fraction (12) (Fig. 4-1D, compare first to second panels). However, when *Akita* from the insoluble fraction was pretreated with the reducing agent dithiothreitol (DTT), it now migrated to lighter fractions (2-3) (Fig. 4-1D, third panel), indicating that insoluble *Akita* consists of a massive disulfide-bonded protein complex.

Given the large size of insoluble *Akita*, we asked to what extent proteasomal activity might play a role in clearing or preventing these insoluble aggregates in control cells (transfected only with a scrambled siRNA). However, our findings demonstrate that in control cells, treatment with the proteasome inhibitor MG132 increased the *Akita* level in the insoluble fraction to a lesser extent than in cells with Grp170 knockdown (Fig. 4-1C, first panel, compare lane 7 to 5; quantified in the right graph). Similarly, in cells transfected with Grp170 siRNA, the level of insoluble *Akita* was not enhanced by MG132 (Fig. 4-1C, first panel, compare lane 8 to 6; quantified in the right graph). These findings raise the possibility that a proteasome-independent pathway is used to remove aggregated *Akita* (see below).

Grp170 prevents formation of aggregated *Akita in vitro*

Our cell-based results demonstrate that Grp170 prevents the accumulation of insoluble *Akita* aggregates. In parallel, we developed a system to directly test whether *Akita*-Myc released from an ER-containing fraction is predisposed to form aggregates *in vitro*. This simple assay is based on the idea that *Akita*-Myc aggregates can be pelleted by centrifugation (Fig. 4-2A, top). If so, addition of Grp170 could then be tested for its ability to prevent *Akita*-Myc aggregation (Fig. 4-2A, bottom).

To isolate soluble *Akita*-Myc, HEK 293T cells expressing *Akita*-Myc were first treated with a low digitonin concentration (0.01%) and centrifuged to generate a supernatant that harbors cytosolic proteins (cytosol fraction) and a pellet that contains the membrane fraction including the ER. When the cytosol and membrane fractions were subjected to SDS-PAGE, cytosolic Hsp90 was found predominantly in the cytosol fraction whereas the ER-resident PDI was present only in the membrane fraction (containing ER, Fig. 4-2B). Importantly, *Akita*-Myc partitioned only in the membrane fraction (Fig. 4-2B, third panel) and the soluble pool of proteins from this fraction were released with RIPA buffer. In parallel, we immunopurified FLAG-tagged WT Grp170 (Grp170-FLAG), BiP (BiP-FLAG), and an ATPase-defective Grp170 (G41L Grp170-FLAG) from HEK 293T cells (Fig. 4-2C).

Remarkably, when soluble *Akita*-Myc was mixed with a control protein (bovine serum albumin, BSA) and incubated for various times, *Akita*-Myc rapidly became insoluble as detected by centrifugation: it was depleted from the soluble fraction within 10 min while

increasing in the pellet (Fig. 4-2D upper panel; *Akita*-Myc in the pellet is quantified in the right graph). In contrast, when soluble WT proinsulin-Myc was incubated with BSA and processed similarly, it remained mostly soluble (Fig. 4-2D. fifth panel; quantified in the right graph). Strikingly, when purified Grp170-FLAG (but not the ATPase-deficient G41L Grp170-FLAG) was added, *Akita*-Myc solubility was preserved (Fig. 4-2D, compare second to first and third panels; quantified in the right graph). Incubation of soluble *Akita*-Myc with an equal amount of BiP-FLAG also prevented insolubility of *Akita*, but was less efficient than Grp170-FLAG (Fig. 4-2D, compare fourth to second panel; quantified in the right graph). Together, these findings support the cell-based results (Fig. 4-1), demonstrating that mutant *Akita* proinsulin has a high propensity to aggregate, and that Grp170 uses an energy-driven reaction (blocked by the G41L mutation) to maintain *Akita* solubility.

Grp170 prevents WT proinsulin from entering detergent-insoluble aggregates

Because *Akita* is thought to dominantly interfere with the proper folding of WT proinsulin (Liu et al., 2007), insoluble *Akita* may recruit WT proinsulin entry into these insoluble aggregates. If so, we reasoned that Grp170's ability to prevent formation of insoluble *Akita* aggregates might also prevent the aggregation of WT proinsulin. To test this, cells expressing superfolder GFP-tagged WT proinsulin (in which sfGFP is inserted in the C-peptide domain) were transfected with scrambled or Grp170 siRNA, along with either a control empty vector or *Akita*-Myc. Indeed, expression of *Akita*-Myc stimulated WT proinsulin-sfGFP to enter into the detergent-insoluble fraction (Fig. 4-3A, first panel, compare lane 7 to 5; quantified in the right graph), supporting the notion that *Akita*

promotes aggregation of WT proinsulin. Knockdown of Grp170 increased the level of WT proinsulin-sfGFP in the detergent-insoluble fraction, and this was essentially additive with the insoluble WT proinsulin promoted by the presence of *Akita* (Fig. 4-3A, first panel, lanes 6-8; quantified in the right graph). Importantly, similar results were found when the experiments were repeated in the more physiologically-relevant rat pancreatic β-cell line (INS1 832/13) (Fig. 4-3B). Together, these data indicate that Grp170 prevents aggregation of WT proinsulin recruited by aggregated *Akita*. Intriguingly, the finding that Grp170 prevents aggregation of WT proinsulin in the absence of *Akita* suggests that Grp170 may also serve a protective role against misfolding of WT proinsulin.

We used the aforementioned *in vitro* system (Fig. 4-2) to further examine this finding. WT proinsulin-Myc was expressed in HEK 293T cells and solubilized from an ER-enriched fraction, using the same method noted above for *Akita*-Myc. When soluble WT proinsulin-Myc was incubated with BSA and the sample processed as before, a low level of WT proinsulin-Myc in the pellet fraction was detected (Fig. 4-3C, first panel; quantified in the bottom graph); presumably, this fraction represents the extent of aggregation of WT proinsulin. However, if soluble WT proinsulin-Myc was co-isolated from cells co-expressing sfGFP-tagged *Akita* (*Akita*-sfGFP, in which sfGFP is appended within the C-peptide region), incubation (with BSA) now resulted in increased insolubility of WT proinsulin-Myc (Fig. 4-3C, second panel; quantified in the bottom graph), consistent with the idea that *Akita* promotes the aggregation of WT proinsulin. Strikingly, if purified Grp170-FLAG was added, the aggregation of WT proinsulin was blocked (Fig.

4-3C, third panel; quantified in the bottom graph), supporting the idea that Grp170 prevents WT proinsulin from recruitment into aggregates promoted by *Akita* proinsulin.

Beclin1-dependent autophagy disposes of aggregated *Akita*

Because additional mechanisms beyond Grp170 activity are likely to limit the accumulation of *Akita* aggregates (Fig. 4-1C), we sought to better understand the disposal pathways that participate in the clearance of these insoluble species. Two major ER quality control pathways are 1) ERAD and 2) ER-phagy, a degradative pathway that relies on elements of the macro-autophagy machinery in which subdomains of the ER are delivered to the lysosome for destruction (Bernales et al., 2006; Bernales et al., 2007). With this in mind, we compared the extent to which the key ERAD component Hrd1 (Bays et al., 2001; Bordallo et al., 1998; Hampton et al., 1996) or a critical regulator of macro-autophagy Beclin1 (Cao and Klionsky, 2007; Kang et al., 2011) play roles in the clearance of *Akita* aggregates. Remarkably, our results demonstrated that knockdown of Beclin1 but not Hrd1 robustly increased the level of *Akita*-Myc in the detergent-insoluble fraction (Fig. 4-4A, top panel, compare lane 8 to 6; quantified in the right graph). In fact, Beclin1 knockdown caused insoluble Akita-Myc to increase to a level higher than that observed with Grp170 knockdown (Fig. 4-4A, top panel, compare lane 8 to 7; quantified in the right graph). Not surprisingly, sucrose sedimentation analysis (using a 30%-70% gradient) revealed that the accumulation of aggregated *Akita*-Myc after Beclin1 knockdown represents a massive protein complex, which is significantly larger than *Akita*-Myc in the soluble fraction (Fig. 4-4B). These

results strongly suggest that macro-autophagy is used to dispose of insoluble *Akita*, rather than ERAD (Fig. 4-1C).

We next assessed the degradation rate of *Akita*-Myc in the insoluble and soluble fractions under different knockdown conditions. Whereas *Akita*-Myc in the insoluble fraction was rapidly degraded when Grp170 was depleted, its degradation was more stabilized in Beclin1-depleted cells (Fig. 4-4C, top panel, compare lanes 7-9 to 10-12; quantified in the top right graph; degradation of insoluble *Akita*-Myc in Hrd1-depleted cells was not further analyzed due to the low level of the mutant proinsulin protein at the initial time point). These findings, demonstrating that loss of Beclin1 significantly impairs the clearance of aggregated *Akita*, reinforce the idea that Beclin1-dependent autophagy is critical for degrading insoluble *Akita* aggregates. In contrast, degradation of *Akita*-Myc in the soluble fraction is impaired by depletion of either Hrd1, Grp170, or Beclin1 (Fig. 4-4C, third panel, compare lanes 4-6, 7-9, and 10-12 to 1-3; quantified in the right bottom graph), indicating that all three gene products participate in the turnover of soluble *Akita*. By preventing *Akita* from aggregation, Grp170 retains mutant proinsulin in the soluble phase, enabling it to undergo Hrd1-mediated ERAD (He et al., 2015). However, the apparent role of Beclin1 in controlling the fate of soluble *Akita* might be indirect, i.e., buildup of *Akita* in the insoluble fraction in Beclin1-deficient cells could promote back-up into the soluble fraction.

RTN3-dependent ER-phagy promotes degradation of *Akita* aggregates

Because Beclin1-mediated macro-autophagy is critical for removing detergent-insoluble *Akita* aggregates from the ER, we asked if specific ER-phagy receptors participate in this pathway. Strikingly, similar to knockdown of Beclin1, we found that depletion of RTN3 [but not other ER-phagy receptors including CCPG1, Sec62, or FAM134B (Fumagalli et al., 2016; Grumati et al., 2017; Khaminets et al., 2015; Smith et al., 2018)] increased the level of *Akita*-Myc in the detergent-insoluble fraction (Fig. 4-5A, first panel, compare lane 10 to 7). RTN3 exists as a long (3A) form that contains an N-terminal extension protruding into the cytosol, and a short (3C) form lacking this extension; the antibody used in this experiment does not recognize RTN3C. [Although knockdown of CCPG1 and FAM134B moderately decreased the *Akita*-Myc level in the soluble fraction (Fig. 4-5A, first panel, compare lanes 2 and 5 to 1), this effect was likely due to enhanced autophagic degradation of soluble *Akita* that could be inhibited by the autophagy inhibitor bafilomycin A1 (Fig. 4-S1, top panel, compare lane 4 to 3 and lane 10 to 9)]. Together, our analyses suggest that RTN3 exerts an important function in clearance of aggregated *Akita* from the ER.

In the RTN3-depleted state, the level of *Akita*-Myc in the soluble fraction also accumulated (Fig. 4-5A, first panel, compare lane 4 to 1), supporting that a build-up of *Akita*-Myc in the insoluble fraction may lead to back-up of *Akita*-Myc in the soluble fraction. To test if this condition triggers ER stress, we examined XBP1 splicing. In control cells, *Akita*-Myc expression moderately increased XBP1 splicing (Fig. 4-5B, top panel, compare lane 2 to 1), consistent with a previous report (Nozaki et al., 2004), whereas knockdown of RTN3 induced a robust increase in ER stress response, and this

effect was dependent upon expression of the misfolded substrate protein, *Akita*-Myc (Fig. 4-5B, top panel, compare lanes 4 to 3). These results indicate that accumulation of *Akita*-Myc due to impairment of ER-phagy induces marked ER stress.

We next evaluated if RTN4 might also facilitate degradation of aggregated *Akita*. In contrast to knockdown of RTN3, depletion of the long (4A) and short (4B) forms of RTN4 did not result in accumulation of *Akita* in the detergent-insoluble fraction (Fig. 4-5C, first panel, compare lane 8 to 6; quantified in the bottom graph), although this did modestly enhance the effect of depleting RTN3 (Fig. 4-5C, first panel, compare lane 9 to 7; quantified in the bottom graph). Thus, RTN3 appears to play a primary and specific role in removing *Akita* aggregates during ER-phagy, whereas the role of RTN4 appears to be secondary. This role may even be dependent on RTN3 because our binding analysis demonstrated that RTN3A-FLAG interacts with endogenous RTN4A and RTN4B (Fig. 4-5D).

We then tested whether accumulation of aggregated *Akita* in the detergent-insoluble fraction that results when RTN3 is knocked down can be blocked when GFP-tagged RTN3C (RTN3C-GFP, which is resistant to the RTN3 siRNA) is exogenously expressed. Indeed, when compared to expression of the control ER membrane protein Sec61-GFP, expressing RTN3C-GFP robustly decreased the level of *Akita* aggregates (Fig. 4-5E. first panel, compare lanes 5 to 4). These findings verify the integrity of the RTN3 siRNA, unambiguously demonstrating that accumulation of aggregated *Akita*

triggered by siRNA-mediated RTN3 knockdown is not caused by unintended off-target effects. These data also suggest that the N-terminal cytosolic extension of RTN3 is dispensable in clearing aggregated *Akita*. Interestingly, overexpressing RTN4A-GFP also blocked the accumulation of aggregated *Akita* upon RTN3 knockdown (Fig. 4-5E, first panel, compare lane 6 to 4), suggesting that in the absence of RTN3, exogenously expressed RTN4 can replace RTN3 activity.

The accumulation of aggregated *Akita*-Myc due to knockdown of Grp170 (instead of RTN3) could similarly be decreased by overexpression of RTN4HD-GFP, RTN4A-GFP, RTN3C-GFP, RTN3A-FLAG, or RTN3AΔLIR-FLAG (Fig. 4-5F, first panel, compare lanes 2-6 to 1). RTN4HD-GFP is a mutant GFP-tagged RTN4 construct lacking its N-terminal cytosolic domain (aa 1-960) (Shibata et al., 2008), while RTN3AΔLIR-FLAG is a mutant FLAG-tagged RTN3A construct missing the six LC3-interacting regions (LIR) located in its N-terminal cytosolic domain (Grumati et al., 2017). Importantly, intact Beclin1 is required for any of these overexpressed proteins to efficiently decrease the accumulation of aggregated *Akita* due to knockdown of Grp170 (Fig. 4-5F, first panel, compare lanes 8-12 to 2-6), suggesting that macro-autophagy is essential during RTN-dependent clearance of aggregated *Akita*. RTN3 also clears aggregated *Akita* in the pancreatic INS1 832/13 β-cell line because insoluble *Akita*-Myc in these cells is largely eliminated by expressing either RTN3C-GFP or RTN3A-FLAG (Fig. 4-5G, top panel, compare lane 5 and 6 to 4). These results demonstrate that in the physiologically-relevant β cells, RTN3 is deployed to remove insoluble proinsulin aggregates.

In these β–cells, confocal image analyses revealed that siRNA-mediated knockdown of Beclin1 led to the formation of RTN3 puncta (Fig. 4-S2A; the percent of β–cells containing at least one puncta is quantified in Fig. 4-S2B). Importantly, while RTN3 does not appear to colocalize with *Akita*-Myc in control cells, these RTN3 puncta generated in the Beclin1-depleted cells do colocalize with *Akita*-Myc (Fig. 4-S2A; the percent of RTN3 puncta colocalizing with *Akita*-Myc is quantified in Fig. 4-S2C). These RTN3 puncta, which can be further visualized by 3D-reconstruction (Fig. 4-S3), may represent structures that actively recruit aggregated *Akita*-Myc in order to initiate disposal of *Akita*-Myc via the ER-phagy pathway. Our findings strongly support the idea that RTN3 acts as an ER-phagy receptor that couples the removal of an aggregated ER client to Beclin1-dependent macro-autophagy.

RTN3-mediated ER-phagy clears other mutant pro-hormone aggregates

Does RTN3-dependent removal of insoluble protein aggregates operate more generally? To address this, we asked if RTN3 exerts any role during protein quality control of other mutant prohormones, such as the C28F mutation found in the precursor of the pituitary hormone proopiomelanocortin (C28F POMC), and the G57S mutation found in the precursor of pro-arginine-vasopressin (G57S Pro-AVP). Indeed, similar to *Akita*, knockdown of RTN3 (but not FAM134B) in HEK 293T cells increased the level of detergent-insoluble C28F POMC-FLAG (Fig. 4-6A, first panel, compare lane 6 to 5 and 8; quantified in graph below); this accumulation was reversed when RTN3C-GFP was

expressed (Fig. 4-6A, first panel, compare lane 7 to 6; quantified in graph below). A comparable result was observed for G57S Pro-AVP-FLAG: while depletion of RTN3 (but not FAM134B) enhanced the level of aggregated G57S Pro-AVP-FLAG (Fig. 4-6B, first panel, compare lane 6 to 5 and 8; quantified in graph below), expression of RTN3C-GFP decreased the accumulation of aggregates (Fig. 4-6B, first panel, compare lane 7 to 6; quantified in graph below). Thus, RTN3 functions broadly as an ER-phagy receptor to remove mutant prohormone aggregates.

Enhanced clearance of *Akita* aggregates partially rescues WT proinsulin secretion

Finally, we evaluated the functional consequence of RTN3-dependent clearance of pro-hormone aggregates. In the case of *Akita*, our findings revealed that aggregation of *Akita* provokes aggregation of WT proinsulin (Fig. 4-3), which presumably prevents WT proinsulin from exiting the ER. Indeed, in HEK 293T cells transfected with WT proinsulin-sfGFP and an empty vector, co-expression of *Akita*-Myc (along with the control Sec61-GFP) decreased the level of WT proinsulin-sfGFP in the media (Fig. 4-7A, first panel, compare lane 2 to 1; quantified in the bottom graph). However, overexpressing increasing amounts of RTN3A-FLAG partially restored WT proinsulin-sfGFP secretion (Fig. 4-7A, first panel, compare lanes 3 and 4 to 2; quantified in the bottom graph). Moreover, when RTN3C-GFP, RTN4A-GFP, or RTN4HD-GFP was overexpressed (instead of RTN3A-FLAG) under the same experimental set-up as in Figure 7A, similar results were found (Fig. 4-7B-D, first panel, compare lane 4 to 2; quantified in the bottom graph). These findings demonstrate that clearance of *Akita*

aggregates by overexpressing RTN3 (or RTN4) can in some measure restore the WT proinsulin export that is needed for insulin production.

DISCUSSION

Two ER quality control strategies work together to limit accumulation of misfolded proinsulin aggregates

Formation of protein aggregates is a signature feature of many human conformational diseases. Hence, identifying cellular mechanisms that minimize the accumulation of these aggregates will likely provide therapeutic approaches to alleviate such diseases. In the diabetic syndrome called MIDY, misfolding of mutant proinsulin (e.g., *Akita*) is thought to initiate disease progression (Liu et al., 2010b) by entrapping WT proinsulin in the ER, thereby preventing production of mature insulin (Liu et al., 2010b; Liu et al., 2007). In this manuscript, we found that in the ER, *Akita* forms detergent-insoluble aggregates that recruit WT proinsulin to also enter into these insoluble complexes (Fig. 4-7E). Importantly, our studies reveal that cells can deploy two distinct ER-dependent quality control mechanisms to minimize the buildup of aggregated *Akita*. First, the ER-resident Grp170 acts to prevent aggregation of *Akita* (Fig. 4-7E). Second, RTN3-dependent ER-phagy removes any aggregates that are formed despite the activity of Grp170 (Fig. 4-7E). Enhancing the clearance of aggregated *Akita* restores WT proinsulin export, suggesting that the *Akita* aggregates exert an important role during pathogenesis of MIDY.

Grp170 prevents *Akita* aggregation

Using a cell-based strategy, we found that Grp170 prevents *Akita* from entering into a detergent-insoluble fraction characteristic of aggregated proteins. An *in vitro*

reconstitution approach further revealed that purified Grp170 (but not the ATPase-defective G41L Grp170) retains *Akita* in the soluble fraction, suggesting that Grp170 uses an energy-dependent chaperone activity to impede *Akita* aggregation. Because Grp170 is an established nucleotide-exchange factor (NEF) of BiP (Weitzmann et al., 2006) and because G41L Grp170 displays attenuated NEF activity (Inoue and Tsai, 2015), Grp170 might in principle operate in concert with BiP to prevent aggregation of *Akita*. However, this seems unlikely because depletion of BiP in cells did not lead to accumulation of *Akita* in the detergent-insoluble fraction (data not shown), and purified BiP did not inhibit the aggregation of soluble *Akita* as efficiently as Grp170.

How then might Grp170 prevent *Akita* from aggregation? The complexes contained in detergent-insoluble *Akita* were found to be much larger than those in the soluble fraction, suggesting that soluble *Akita* progressively enlarges from the low, mid, to high MW species to eventually become detergent-insoluble aggregates. We also showed that Grp170 associates selectively with the high MW soluble species, suggesting that Grp170 is targeted to these species, interfering with further *Akita* extension into higher-order aggregates. Indeed, a previous study reported that Grp170 (in contrast to BiP) preferentially interacts with aggregation-prone amino acid sequences in a client (Behnke et al., 2016). This raises the possibility that when *Akita* multimerizes into the high MW species, it adopts a physical conformation in which aggregation surfaces are preferentially displayed, thereby recruiting Grp170. The idea that Grp170 prevents aggregation of *Akita* is also in agreement with previous studies suggesting that this

chaperone can block aggregation of the model substrate luciferase under an artificial heat treatment condition (Park et al., 2003).

We previously reported that Grp170 uses its chaperone activity to facilitate ERAD-dependent degradation of soluble *Akita* (Cunningham et al., 2017). We believe that by shifting the substrate from higher to lower MW species, *Akita* becomes more competent to undergo ERAD. Based on our new results, we hypothesize that the high MW species of *Akita* is a dynamic protein complex that continually experiences extension and shrinking – by blocking the extension of high MW *Akita*, Grp170 in turn favors the generation of the low MW species, which can be disposed of by ERAD to the extent that its accumulation does not exceed the capacity of the ERAD pathway.

In MIDY, pancreatic β-cells harbor one WT and one mutant copy of the *INS* gene. In this setting, we found that aggregated *Akita* proinsulin recruits the aggregation of WT proinsulin. These findings were observed in HEK 293T cells and a pancreatic β-cell line, highlighting their physiological significance. Because aggregated WT proinsulin cannot exit the ER required for its subsequent processing, the formation of combined mutant-WT aggregates represents a critical reaction that impairs insulin production, which is central to the pathogenesis of MIDY. Whether other MIDY mutations also cause their encoded protein products to form insoluble aggregates is presently unknown. Importantly, Grp170 suppresses aggregation of WT proinsulin recruited by *Akita*. This may reflect the ability of Grp170 to block aggregation of *Akita*, which in turn prevents

WT proinsulin from aggregating. However, our cell-based studies also found that Grp170 suppresses aggregation of WT proinsulin even in the absence of *Akita*, suggesting that WT proinsulin itself might have some predisposition to misfold and aggregate independent of any dominant interfering effect of mutant proinsulin. In such a circumstance, WT proinsulin would directly benefit from the action of Grp170. Thus, prevention of WT proinsulin aggregation in MIDY is likely through the activity of Grp170 on both mutant and WT proinsulin.

RTN3-dependent ER-phagy pathway clears *Akita* aggregates

In addition to the action of Grp170, we postulate that cells deploy additional mechanisms to minimize the accumulation of aggregated prohormones. This would provide cells with a clear advantage in maintaining proper proteostasis, as dysfunction in any one pathway can be compensated by the other. Indeed, our results identify RTN3-dependent ER-phagy as an ER protein quality control pathway that removes aggregated *Akita*. The best evidence in support of this idea is that depletion of RTN3 results in accumulation of detergent-insoluble *Akita*, indicating that RTN3 promotes clearance of *Akita* aggregates. Additionally, under this depleted condition, expression of the short isoform of RTN3 (called RTN3C) is sufficient to eliminate insoluble *Akita* proinsulin. Because this short isoform lacks the N-terminal cytosolic domain that harbors LC3-interacting regions (LIR) typically used to recruit core autophagy components, this result raises intriguing questions about how RTN3 is functionally linked to the macro-autophagy pathway during clearance of aggregated *Akita*. We envision two possibilities. First, RTN3C may oligomerize with other ER membrane

proteins that harbor LIRs and in this way, RTN3C is indirectly connected to the autophagy pathway. For instance, because RTN3 oligomerizes with RTN4, which plays a secondary role in clearance of aggregated *Akita* and has primary amino acid sequences in its cytosolic domain that resemble LIRs, RTN3C may partner with RTN4 to eliminate aggregated *Akita* via autophagy. Second, RTN3 might use an LIR-independent but Beclin1-dependent macro-autophagy pathway to remove aggregated *Akita*. Distinguishing these two possibilities clearly will require further investigation.

In this context, we note a previous report demonstrating that full-length RTN3, via its LIR domains, functions as an ER-phagy receptor in the turnover of tubular ER during starvation (Grumati et al., 2017). Whether RTN3 in this process operates in the same manner as during the removal of specific ER aggregated client proteins remains unclear. By image analyses, we found that RTN3 forms puncta when the macro-autophagy machinery is disabled; importantly, under this condition, the RTN3 puncta colocalize with *Akita*. One possible interpretation of this finding is that aggregated *Akita* is actively recruited into RTN3-containing puncta from which disposal of *Akita* is initiated via the ER-phagy pathway.

Regardless of the precise mechanism, reticulon-driven clearance of *Akita* aggregates results in improved ER export of WT proinsulin. Because *Akita* aggregates recruit WT proinsulin, removal of aggregated *Akita* would enable WT proinsulin to remain in the soluble phase so that it can proceed via anterograde intracellular transport, an essential

step in the production of mature insulin. These observations suggest that enhancing the activity of RTN3-mediated autophagy might offer a new therapeutic strategy to ameliorate MIDY. Moreover, given that a low level of WT proinsulin itself also aggregates, this strategy might have therapeutic value to combat the pathogenesis of other forms of diabetes.

Beyond mutant proinsulin, our findings that RTN3 eliminates misfolded POMC and pro-AVP aggregates suggest that this ER-phagy receptor serves other protein clients and may function in a general mechanism to dispose of prohomone aggregates. Elucidating the structural features that enable these prohormone aggregates to exploit the function of RTN3 requires future investigations. Regardless, these data raise the possibility that therapeutic approaches targeting this ER-phagy receptor might have broader implications for a number of distinct human conformational diseases.

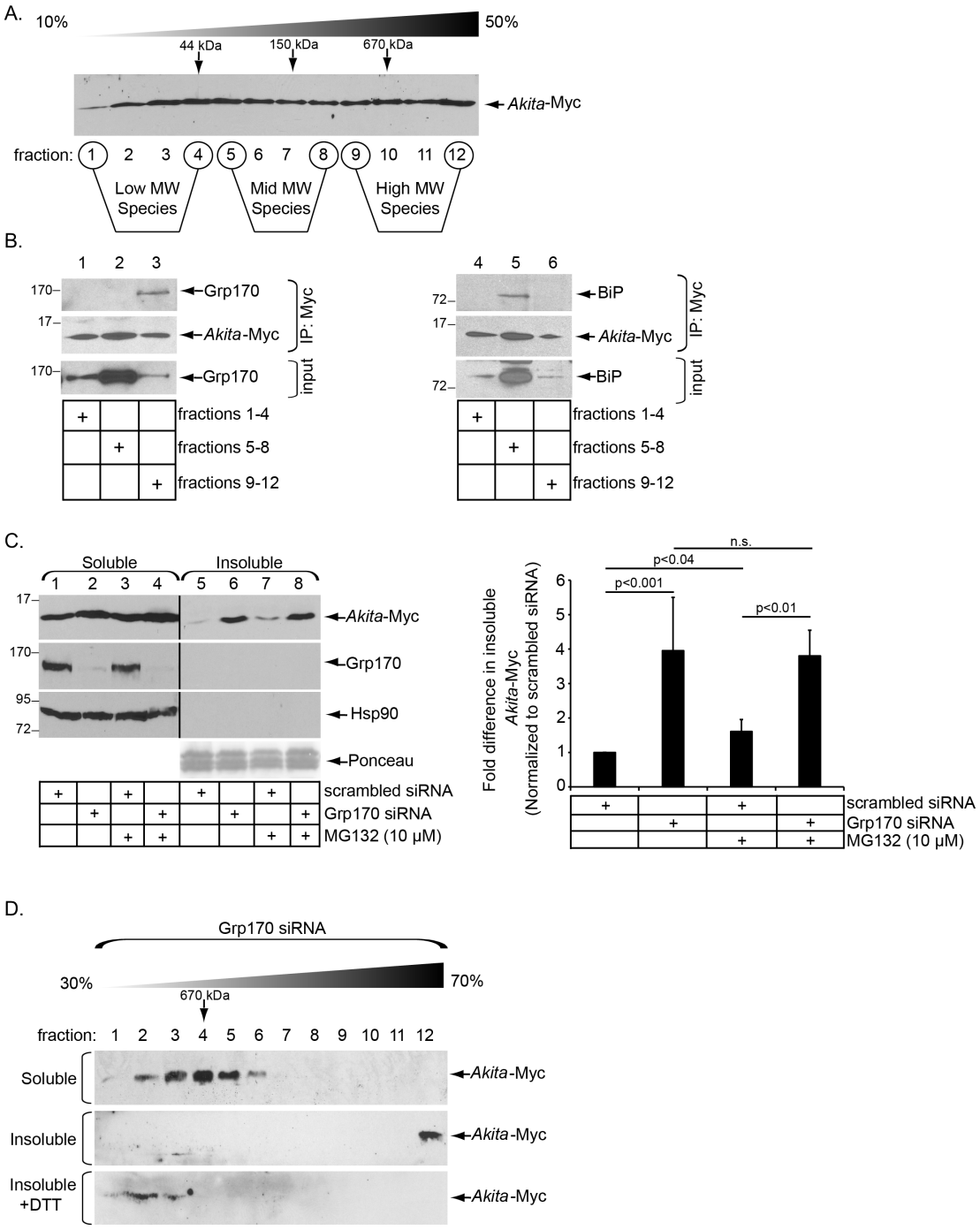

Figure 4-1. Depletion of Grp170 promotes formation of detergent-insoluble *Akita*. A. A whole cell extract derived from HEK 293T cells transfected with *Akita*-Myc was layered over a discontinuous 10-50% sucrose gradient. The sample was centrifuged, and each fraction (fractions 1-12) was subjected to SDS-PAGE followed by immunoblotting with an Myc antibody to detect *Akita*-Myc. *Akita*-Myc in fractions 1-4 is referred to as the low MW species, fractions 5-8 as the mid MW species, and fractions

9-12 as the high MW species. B. Fractions 1-4, 5-8, and 9-12 were pooled, and *Akita*-Myc from the pooled fractions were immunoprecipitated. The precipitated material was subjected to SDS-PAGE followed by immunoblotting with the indicated antibodies. C. Cells expressing *Akita*-Myc and transfected with either a scrambled (control) or Grp170 siRNA were treated with or without MG132, and lysed with a RIPA buffer. After centrifugation, the supernatant represents the soluble fraction and the pellet represents the insoluble fraction; material the insoluble fraction was resuspended in a sample buffer containing 2% SDS. Both the soluble and insoluble fractions were subjected to SDS-PAGE followed by immunoblotting with the indicated antibodies. The protein levels revealed by Ponceau staining of the insoluble fraction serve as the loading control. The intensity of the *Akita*-Myc band was quantified with ImageJ (NIH). The right graph depicts the insoluble *Akita*-Myc level normalized to the level of insoluble *Akita*-Myc present in the scrambled control. Data represent the mean ± SD of at least three independent experiments; *p*-values are generated from student's T-test. The black line indicates that an intervening lane from the same blot has been excised. D. The soluble (first panel) and insoluble (second panel) fractions derived from Grp170-depleted cells expressing *Akita*-Myc were layered over a 30-70% discontinuous sucrose gradient and centrifuged as in A. Each fraction was collected, subjected to SDS-PAGE, and immunoblotted with an antibody against Myc. The insoluble fraction was also treated with DTT prior to sucrose gradient analysis (third panel).

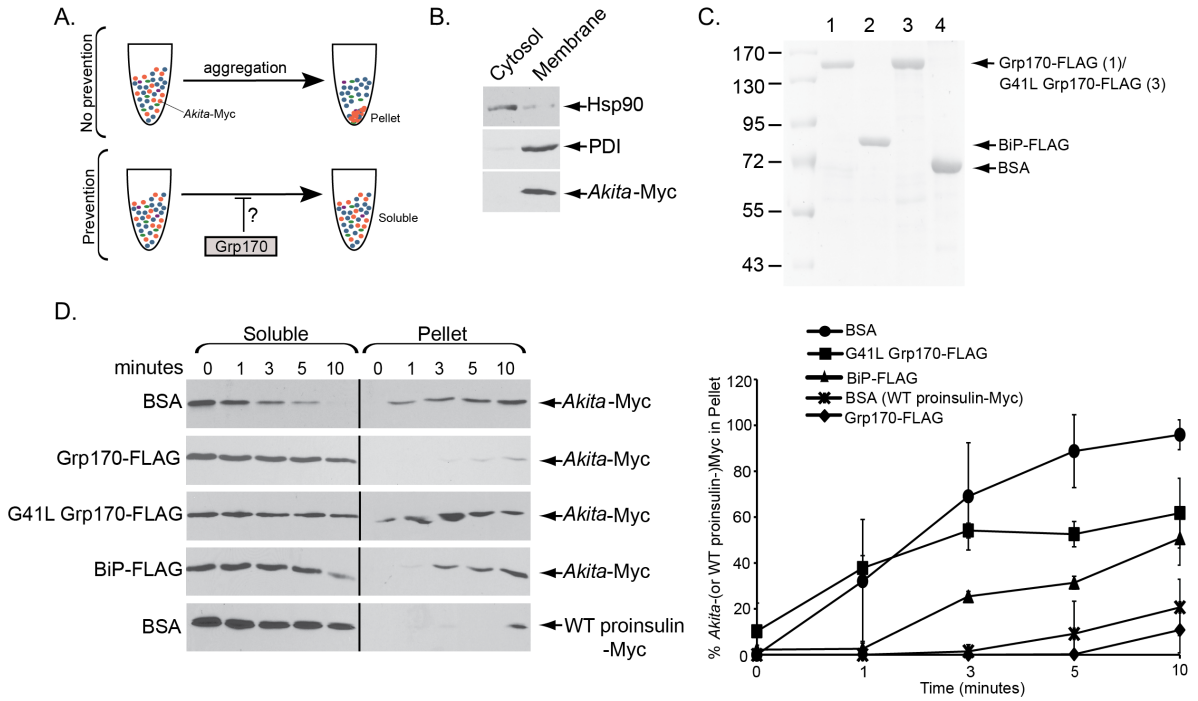

Figure 4-2. Grp170 prevents formation of aggregated *Akita in vitro*. A. Schematic of the *in vitro* aggregation assay. (top) When *Akita*-Myc present in a membrane extract aggregates, it forms a pellet after centrifugation. (bottom) However, if the membrane extract containing *Akita*-Myc was incubated with purified Grp170, aggregation is prevented. Thus *Akita*-Myc remains in the soluble phase even after centrifugation. B. To generate *Akita*-Myc in the membrane extract, HEK 293T cells expressing *Akita*-Myc were treated with digitonin and centrifuged to generate two fractions. The supernatant fraction contains cytosol proteins (cytosol) and the pellet fraction harbors membranes including the ER (membrane); as *Akita*-Myc resides in the ER, it is expected to be in the membrane fraction. Both the cytosol and membrane extracts were subjected to SDS-PAGE followed by immunoblotting with the indicated antibodies. C. Coomassie gel of purified FLAG-tagged Grp170 (lane 1), BiP (lane 2), G41L Grp170 (lane 3), as well as the control protein BSA (lane 4). D. (1^{st} – 4^{th} panels) A membrane fraction containing *Akita*-Myc was incubated with the indicated purified protein for the indicated time. The samples were centrifuged, and the supernatant material separated from the pellet; the pellet material was resuspended in a sample buffer containing 2% SDS. Both the supernatant and pellet material were analyzed by SDS-PAGE followed by immunoblotting with an antibody against Myc. (5^{th} panel) A membrane extract containing WT proinsulin-Myc was incubated with BSA, and processed as above. The right graph represents the percentage of *Akita* (or WT proinsulin)-Myc in the pellet fraction compared to the total *Akita*-Myc signal at each time point from both the soluble and pellet fractions. Data represented the mean ± SD of at least three independent experiments. The black line indicates that an intervening lane from the same blot has been excised.

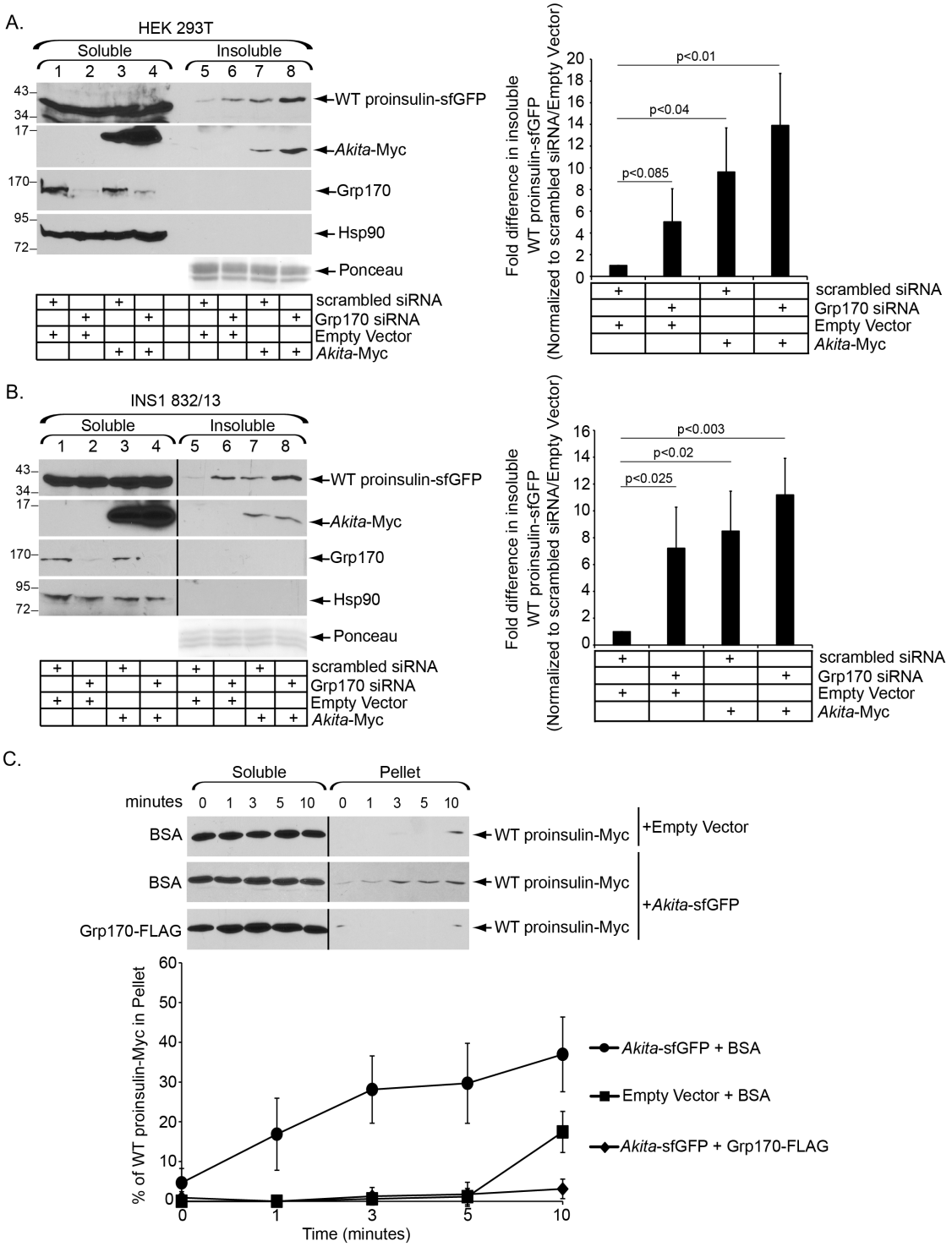

Figure 4-3. Grp170 prevents WT proinsulin from entering detergent-insoluble aggregates. A. HEK 293T cells expressing WT proinsulin-sfGFP were transfected with scrambled or Grp170 siRNA along with either *Akita*-Myc, or an empty vector. Cells were processed to generate the soluble and insoluble fractions as in 4-1C. The right graph depicts the insoluble WT proinsulin-sfGFP level normalized to the level of insoluble WT

proinsulin-sfGFP present in the scrambled/empty vector control. Data represent the mean ± SD of at least three independent experiments; *p*-values are generated from student's T-test. B. As in *A*, except data were generated from rat INS1 832/13 cells. The black line indicates that an intervening lane from the same blot has been excised. C. *In vitro* aggregation of WT proinsulin-Myc. A membrane extract derived from cells transfected with either WT proinsulin-Myc and an empty vector, or WT proinsulin-Myc and *Akita*-sfGFP were incubated with either BSA or Grp170-FLAG. Samples were processed as in 4-2D. The bottom graph represents the percentage of WT proinsulin-Myc in the pellet fraction as compared to the total WT proinsulin-Myc signal at each time point from both the soluble and pellet fractions. Data represents ± SD of at least three independent experiments. The black line indicates that an intervening lane from the same blot has been excised.

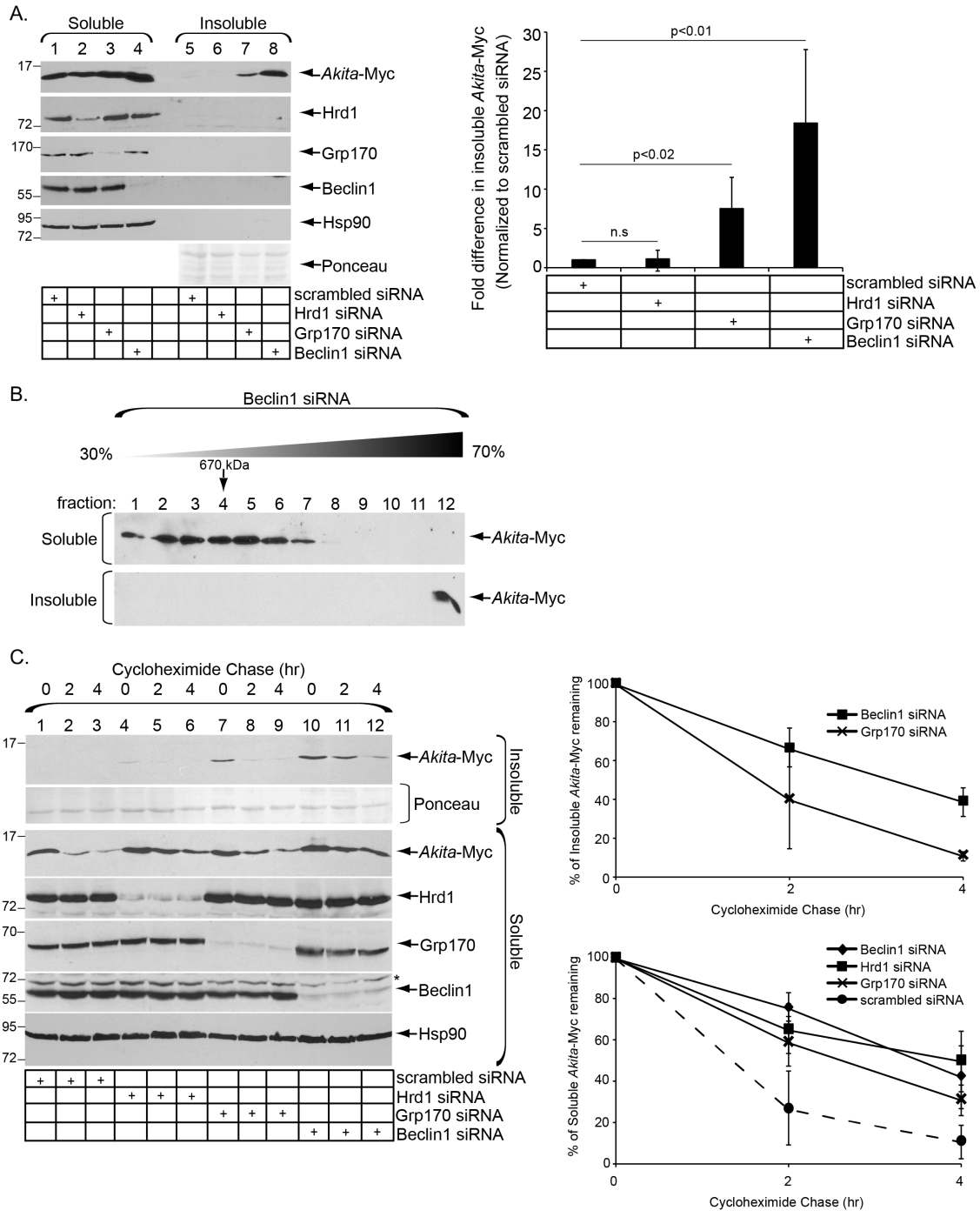

Figure 4-4. Beclin1-dependent autophagy disposes aggregated *Akita*. A. HEK 293T cells were transfected with *Akita*-Myc and either scrambled, Hrd1, Grp170, or Beclin1 siRNA. Soluble and insoluble fractions were generated and processed as in 4-1C. The right graph represents insoluble *Akita*-Myc level normalized to the level of insoluble *Akita*-Myc in the scrambled control. Data represent the mean ± SD of at least three independent experiments; *p*-values from student's T-test. B. As in 4-1D, except

the soluble (first panel) and insoluble (second panel) fractions were derived from Beclin1-depleted cells. C. HEK 293T cells expressing *Akita*-Myc and transfected with indicated siRNAs were treated with cycloheximide for 0, 2, 4 h. Soluble and insoluble fractions were generated as in 4-1C. Samples were subjected to SDS-PAGE and immunoblotted with the indicated antibodies. The top right graph represents the percentage of insoluble *Akita*-Myc remaining, and the bottom right graph represents the percentage of soluble *Akita*-Myc remaining. Data represents mean ±SD of at least three independent experiments.

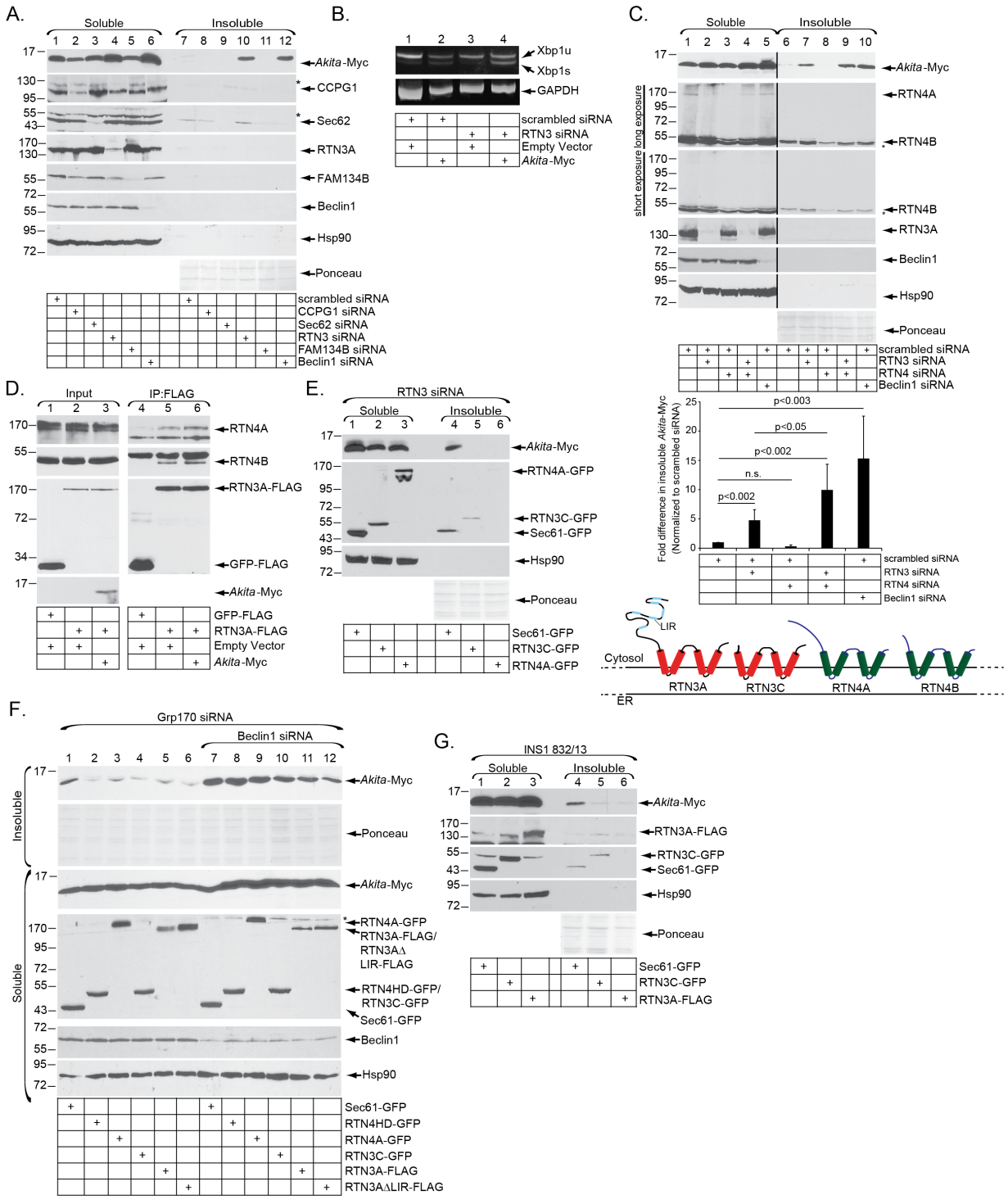

Figure 4-5. RTN3-dependent ER-phagy promotes degradation of *Akita* aggregates. A. siRNA screen of known ER-phagy receptors. HEK 293T cells expressing *Akita*-Myc were transfected with the indicated siRNAs. Soluble and insoluble fractions were generated and processed as in 4-1C. B. HEK 293T cells transfected with an empty vector or an *Akita*-Myc plasmid were co-transfected with either scrambled or RTN3

siRNA. RNA was extracted, reverse transcribed to cDNA, and the cDNA amplified using PCR. C. Cells transfected with the indicated siRNA(s) were processed as in A. The bottom graph represents insoluble *Akita*-Myc level normalized to the level of insoluble *Akita*-Myc in the scrambled control. Data represent the mean ± SD of at least three independent experiments; *p*-values from student's T-test. The schematic depicts the topology of RTN3A, RTN3C, RTN4A, RTN4B. RTN3A contains 6 LIR domains not present in RTN3C. The black line indicates that an intervening lane from the same blot has been excised. D. HEK 293T cells transfected with the indicated construct were chemically crosslinked with DSP. The resulting cell extract was subjected to FLAG-immunoprecipitation, with the immunoprecipitated material analyzed by SDS-PAGE and immunoblotting. E. RTN3-depleted cells expressing *Akita*-Myc were transfected with Sec61-GFP, RTN3C-GFP, or RTN4A-GFP. Soluble and insoluble fractions were generated and processed as in 4-1C. The bottom graph represents the percentage of insoluble *Akita*-Myc normalized to the level of the Sec61-GFP condition. Data represent the mean ± SD of at least three independent experiments; *p*-values from student's T-test. F. Cells expressing *Akita*-Myc that were depleted of either Grp170 alone or Grp170 and Beclin1 were transfected with the indicated constructs. The soluble and insoluble fractions were generated and processed as in 4-1C. G. The rat pancreatic β cell line (INS1 832/13) was transfected with the indicated constructs. The soluble and insoluble fractions were generated and processed as in 4-1C.

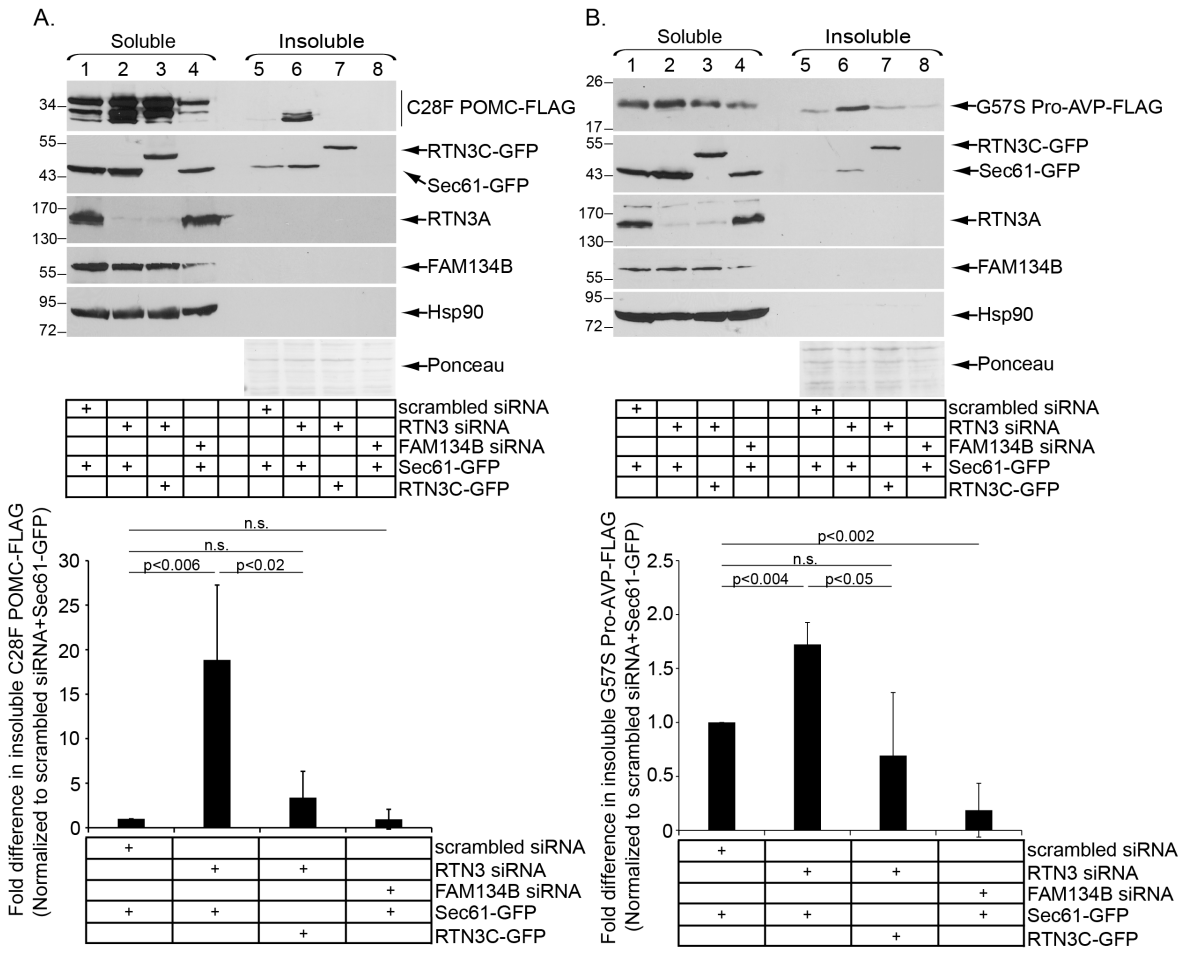

Figure 4-6. RTN3-mediated ER-phagy clears mutant prohormone aggregates. A. HEK 293T cells expressing C28F POMC-FLAG were co-transfected with scrambled, RTN3, or FAM134B siRNA, along with either Sec61-GFP or RTN3C-GFP. Soluble and insoluble fractions were generated as in 4-1C. The bottom graph represents insoluble C28F POMC-FLAG level normalized to the level of insoluble C28F POMC-FLAG in the scrambled control + Sec61-GFP. Data represent the mean ± SD of at least three independent experiments; *p*-values generated from student's T-test. B. as in A, except cells were transfected with G57S Pro-AVP-FLAG. The bottom graph represents insoluble G57S Pro-AVP-FLAG level normalized to the level of insoluble G57S Pro-AVP-FLAG in the scrambled control + Sec61-GFP.

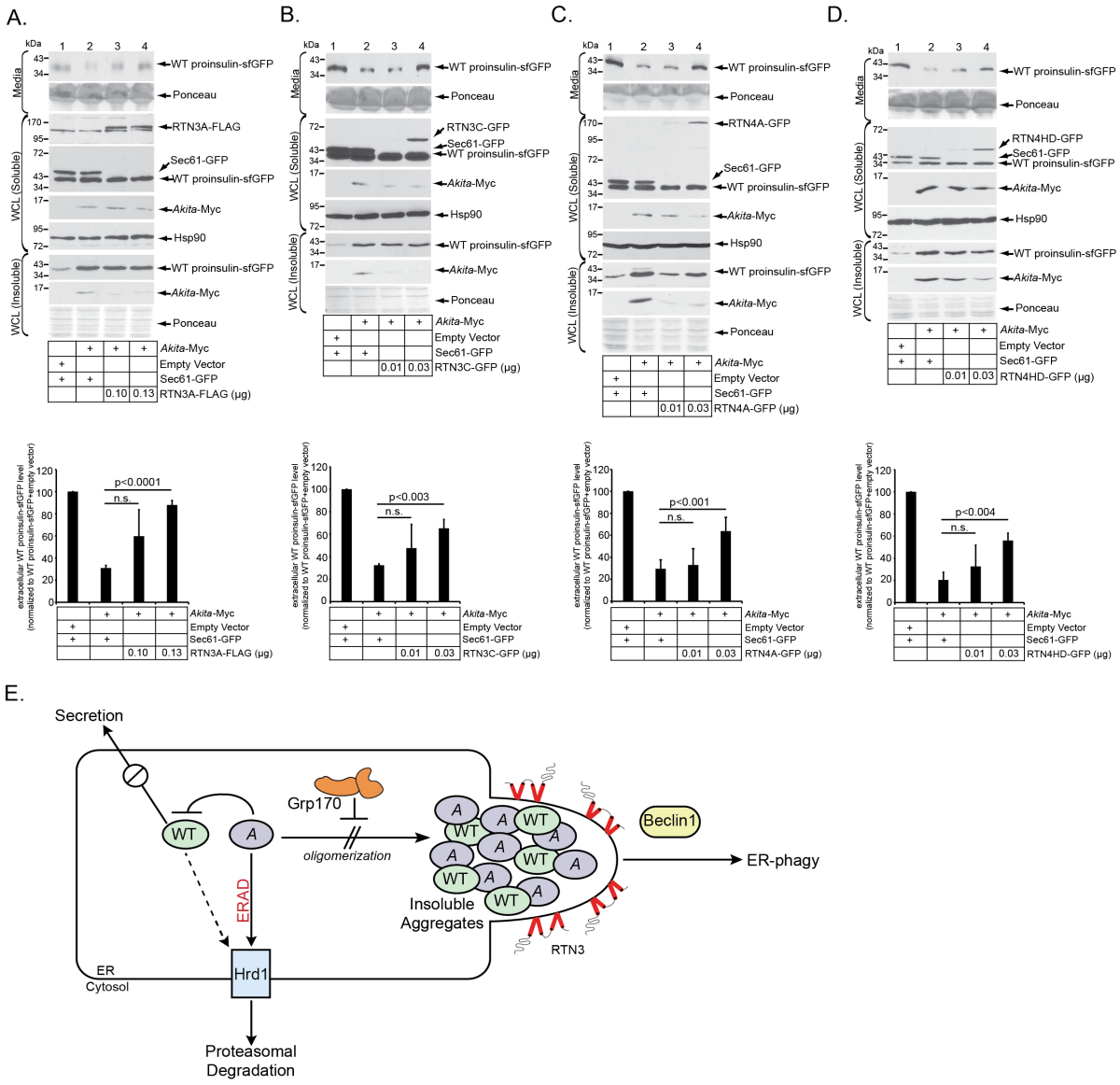

Figure 4-7. Enhanced clearance of *Akita* aggregates partially rescues WT proinsulin secretion. A. HEK 293T cells expressing WT proinsulin-sfGFP were transfected with the indicated construct. Media and cells were harvested. Cells were lysed and the samples subjected to SDS-PAGE followed by immunoblotting with the indicated antibodies. The bottom graph represents WT proinsulin-sfGFP level in the media normalized to the empty vector/Sec61-GFP condition (lane 1). Data represent the mean ± SD of at least three independent experiments; *p*-values from student's T-test. B. As in *A*, except RTN3C-GFP was used. C. As in *A*, except RTN4A-GFP was used. D. As in *A*, except RTN4HD-GFP was used. E. Model depicting the coordinated deployment of a two-pronged approach to minimize the level of *Akita* aggregates. The MIDY disease results when a mutant proinsulin molecule such as *Akita* misfolds, forming detergent-insoluble aggregates. These aggregates sequester WT proinsulin in the ER, thereby preventing its proper exit from the ER, maturation and secretion,

leading to disease. To rectify this, Grp170 actively prevents formation aggregated *Akita*. If aggregated *Akita* forms despite the activity of Grp170, RTN3-mediated ER-phagy is able to efficiently remove the aggregates through a Beclin1-dependent macro-autophagy mechanism.

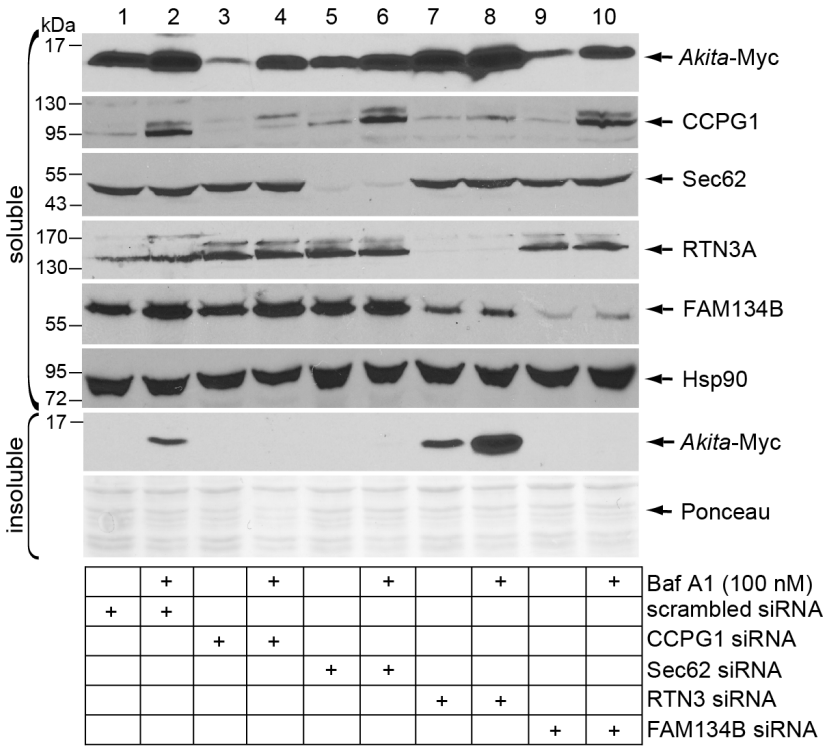

Figure 4-S1. Bafilomycin A1 treatment restores the decrease in soluble *Akita*-Myc level in CCPG1- or FAM134B-depleted cells. As in Figure 4-5A, except cells were treated with 100 nM of bafilomycin A1 (Baf A1) for 12 h.

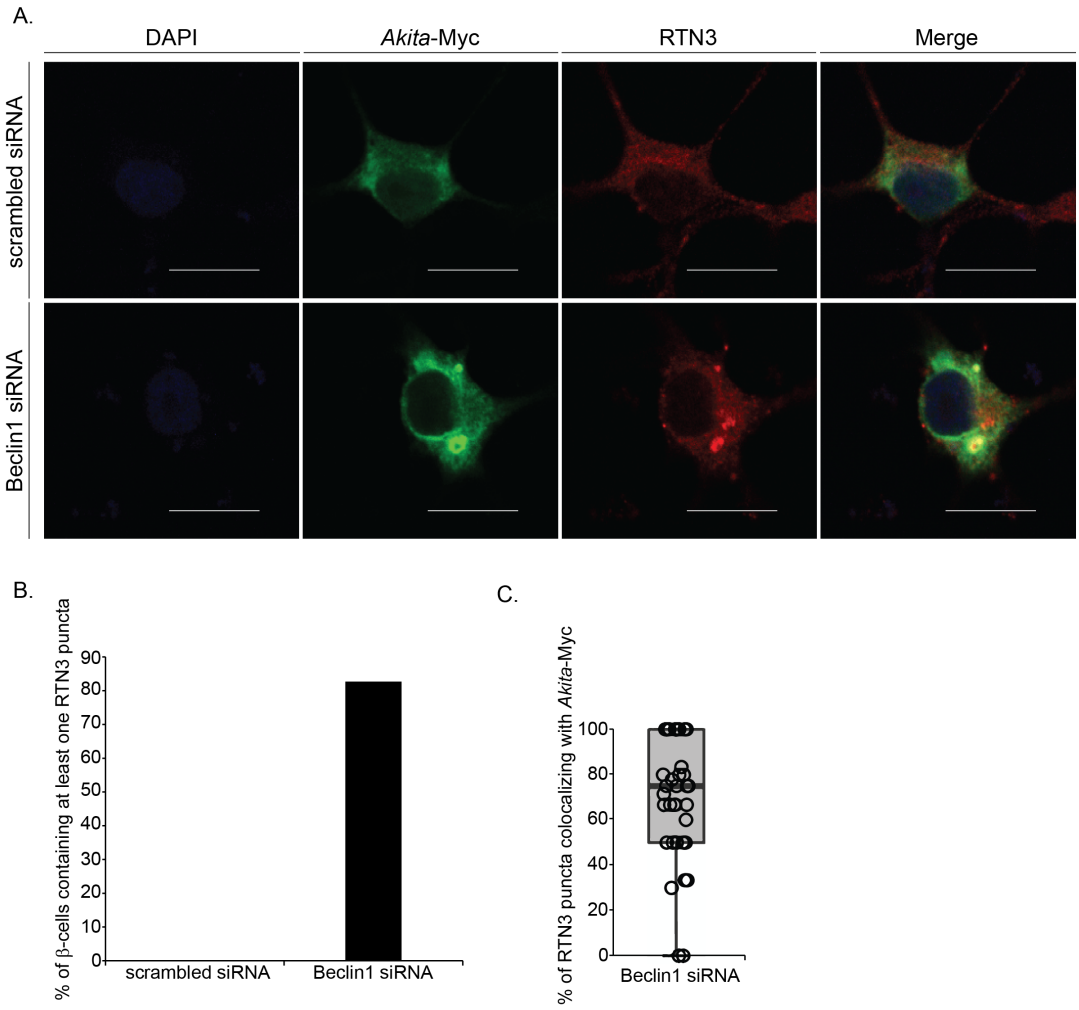

Figure 4-S2. RTN3 puncta form in Beclin1-depleted β-cells which colocalize with *Akita*-Myc. A. INS1 832/13 cells transfected with the indicated siRNAs for 48 h and *Akita*-Myc for 24 h were fixed, permeabilized, and stained for the indicated antibodies. Images were taken on a Zeiss LSM 800 confocal microscope. Scale bars are 20 μm. B. Quantification of the percentage of cells in A containing at least one RTN3 puncta. The number within the parenthesis indicates the number of cells analyzed in each condition. C. Quantification of the percentage of RTN3 puncta in Beclin1-depleted cells in A colocalizing with *Akita*-Myc. The number within the parenthesis indicates the number of cells analyzed. Colocalization was determined by analyzing all Z-stacks taken of each cell.

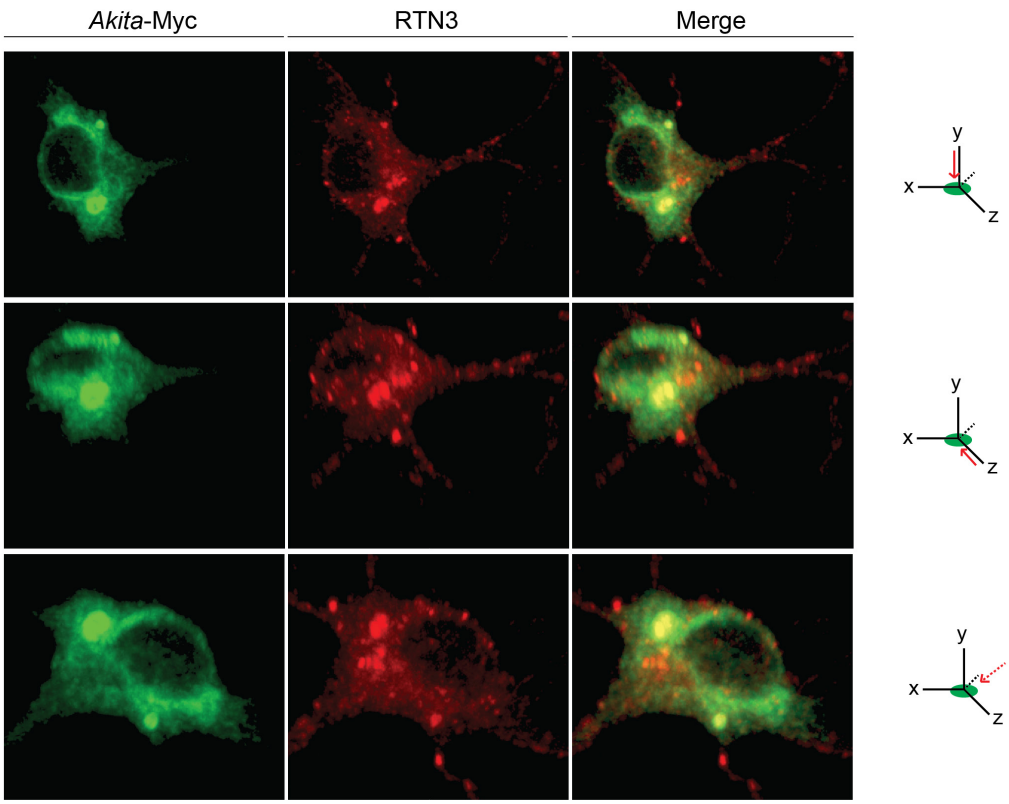

Figure 4-S3. 3D reconstruction of RTN3 puncta in Beclin1-depleted β-cell which colocalize with *Akita*-Myc. 3D reconstruction of Beclin1-depleted cell in Fig. 4-S2A using the Zen software powered by Arivis. Red arrows on the x,y,z axes indicate the angle of observation.

REFERENCES

Allen, J.R., Nguyen, L.X., Sargent, K.E., Lipson, K.L., Hackett, A., and Urano, F. (2004). High ER stress in beta-cells stimulates intracellular degradation of misfolded insulin. Biochem Biophys Res Commun *324*, 166-170.

Arunagiri, A., Haataja, L., Cunningham, C.N., Shrestha, N., Tsai, B., Qi, L., Liu, M., and Arvan, P. (2018). Misfolded proinsulin in the endoplasmic reticulum during development of beta cell failure in diabetes. Ann N Y Acad Sci *1418*, 5-19.

Bates, G. (2003). Huntingtin aggregation and toxicity in Huntington's disease. Lancet *361*, 1642-1644.

Bays, N.W., Gardner, R.G., Seelig, L.P., Joazeiro, C.A., and Hampton, R.Y. (2001). Hrd1p/Der3p is a membrane-anchored ubiquitin ligase required for ER-associated degradation. Nat Cell Biol *3*, 24-29.

Behnke, J., Mann, M.J., Scruggs, F.L., Feige, M.J., and Hendershot, L.M. (2016). Members of the Hsp70 Family Recognize Distinct Types of Sequences to Execute ER Quality Control. Mol Cell *63*, 739-752.

Bernales, S., McDonald, K.L., and Walter, P. (2006). Autophagy counterbalances endoplasmic reticulum expansion during the unfolded protein response. PLoS Biol *4*, e423.

Bernales, S., Schuck, S., and Walter, P. (2007). ER-phagy: selective autophagy of the endoplasmic reticulum. Autophagy *3*, 285-287.

Bordallo, J., Plemper, R.K., Finger, A., and Wolf, D.H. (1998). Der3p/Hrd1p is required for endoplasmic reticulum-associated degradation of misfolded lumenal and integral membrane proteins. Mol Biol Cell *9*, 209-222.

Cao, Y., and Klionsky, D.J. (2007). Physiological functions of Atg6/Beclin 1: a unique autophagy-related protein. Cell Res *17*, 839-849.

Chan, S.J., Keim, P., and Steiner, D.F. (1976). Cell-free synthesis of rat preproinsulins: characterization and partial amino acid sequence determination. Proc Natl Acad Sci U S A *73*, 1964-1968.

Cunningham, C.N., He, K., Arunagiri, A., Paton, A.W., Paton, J.C., Arvan, P., and Tsai, B. (2017). Chaperone-Driven Degradation of a Misfolded Proinsulin Mutant in Parallel With Restoration of Wild-Type Insulin Secretion. Diabetes *66*, 741-753.

Fumagalli, F., Noack, J., Bergmann, T.J., Cebollero, E., Pisoni, G.B., Fasana, E., Fregno, I., Galli, C., Loi, M., Solda, T.*, et al.* (2016). Translocon component Sec62 acts in endoplasmic reticulum turnover during stress recovery. Nat Cell Biol *18*, 1173-1184.

Grumati, P., Morozzi, G., Holper, S., Mari, M., Harwardt, M.I., Yan, R., Muller, S., Reggiori, F., Heilemann, M., and Dikic, I. (2017). Full length RTN3 regulates turnover of tubular endoplasmic reticulum via selective autophagy. Elife *6*.

Haataja, L., Snapp, E., Wright, J., Liu, M., Hardy, A.B., Wheeler, M.B., Markwardt, M.L., Rizzo, M., and Arvan, P. (2013). Proinsulin intermolecular interactions during secretory trafficking in pancreatic beta cells. J Biol Chem *288*, 1896-1906.

Hampton, R.Y., Gardner, R.G., and Rine, J. (1996). Role of 26S proteasome and HRD genes in the degradation of 3-hydroxy-3-methylglutaryl-CoA reductase, an integral endoplasmic reticulum membrane protein. Mol Biol Cell *7*, 2029-2044.

He, K., Cunningham, C.N., Manickam, N., Liu, M., Arvan, P., and Tsai, B. (2015). PDI reductase acts on Akita mutant proinsulin to initiate retrotranslocation along the Hrd1/Sel1L-p97 axis. Mol Biol Cell *26*, 3413-3423.

Hodish, I., Liu, M., Rajpal, G., Larkin, D., Holz, R.W., Adams, A., Liu, L., and Arvan, P. (2010). Misfolded proinsulin affects bystander proinsulin in neonatal diabetes. J Biol Chem *285*, 685-694.

Inoue, T., and Tsai, B. (2015). A nucleotide exchange factor promotes endoplasmic reticulum-to-cytosol membrane penetration of the nonenveloped virus simian virus 40. J Virol *89*, 4069-4079.

Irvine, G.B., El-Agnaf, O.M., Shankar, G.M., and Walsh, D.M. (2008). Protein aggregation in the brain: the molecular basis for Alzheimer's and Parkinson's diseases. Mol Med *14*, 451-464.

Kang, R., Zeh, H.J., Lotze, M.T., and Tang, D. (2011). The Beclin 1 network regulates autophagy and apoptosis. Cell Death Differ *18*, 571-580.

Khaminets, A., Heinrich, T., Mari, M., Grumati, P., Huebner, A.K., Akutsu, M., Liebmann, L., Stolz, A., Nietzsche, S., Koch, N.*, et al.* (2015). Regulation of endoplasmic reticulum turnover by selective autophagy. Nature *522*, 354-358.

Kim, G.H., Shi, G., Somlo, D.R., Haataja, L., Song, S., Long, Q., Nillni, E.A., Low, M.J., Arvan, P., Myers, M.G., Jr.*, et al.* (2018). Hypothalamic ER-associated degradation regulates POMC maturation, feeding, and age-associated obesity. J Clin Invest *128*, 1125-1140.

Liu, M., Haataja, L., Wright, J., Wickramasinghe, N.P., Hua, Q.X., Phillips, N.F., Barbetti, F., Weiss, M.A., and Arvan, P. (2010a). Mutant INS-gene induced diabetes of youth: proinsulin cysteine residues impose dominant-negative inhibition on wild-type proinsulin transport. PLoS One *5*, e13333.

Liu, M., Hodish, I., Haataja, L., Lara-Lemus, R., Rajpal, G., Wright, J., and Arvan, P. (2010b). Proinsulin misfolding and diabetes: mutant INS gene-induced diabetes of youth. Trends Endocrinol Metab *21*, 652-659.

Liu, M., Hodish, I., Rhodes, C.J., and Arvan, P. (2007). Proinsulin maturation, misfolding, and proteotoxicity. Proc Natl Acad Sci U S A *104*, 15841-15846.

Mukherjee, A., Morales-Scheihing, D., Butler, P.C., and Soto, C. (2015). Type 2 diabetes as a protein misfolding disease. Trends Mol Med *21*, 439-449.

Nozaki, J., Kubota, H., Yoshida, H., Naitoh, M., Goji, J., Yoshinaga, T., Mori, K., Koizumi, A., and Nagata, K. (2004). The endoplasmic reticulum stress response is stimulated through the continuous activation of transcription factors ATF6 and XBP1 in Ins2+/Akita pancreatic beta cells. Genes Cells *9*, 261-270.

Park, J., Easton, D.P., Chen, X., MacDonald, I.J., Wang, X.Y., and Subjeck, J.R. (2003). The chaperoning properties of mouse grp170, a member of the third family of hsp70 related proteins. Biochemistry *42*, 14893-14902.

Ruggiano, A., Foresti, O., and Carvalho, P. (2014). Quality control: ER-associated degradation: protein quality control and beyond. J Cell Biol *204*, 869-879.

Shi, G., Somlo, D.R.M., Kim, G.H., Prescianotto-Baschong, C., Sun, S., Beuret, N., Long, Q., Rutishauser, J., Arvan, P., Spiess, M.*, et al.* (2017). ER-associated degradation is required for vasopressin prohormone processing and systemic water homeostasis. J Clin Invest *127*, 3897-3912.

Shibata, Y., Voss, C., Rist, J.M., Hu, J., Rapoport, T.A., Prinz, W.A., and Voeltz, G.K. (2008). The reticulon and DP1/Yop1p proteins form immobile oligomers in the tubular endoplasmic reticulum. J Biol Chem *283*, 18892-18904.

Smith, M.D., Harley, M.E., Kemp, A.J., Wills, J., Lee, M., Arends, M., von Kriegsheim, A., Behrends, C., and Wilkinson, S. (2018). CCPG1 Is a Non-canonical Autophagy Cargo Receptor Essential for ER-Phagy and Pancreatic ER Proteostasis. Dev Cell *44*, 217-232 e211.

Smith, M.H., Ploegh, H.L., and Weissman, J.S. (2011). Road to ruin: targeting proteins for degradation in the endoplasmic reticulum. Science *334*, 1086-1090.

Steiner, D.F., Cunningham, D., Spigelman, L., and Aten, B. (1967). Insulin biosynthesis: evidence for a precursor. Science *157*, 697-700.

Stoy, J., Edghill, E.L., Flanagan, S.E., Ye, H., Paz, V.P., Pluzhnikov, A., Below, J.E., Hayes, M.G., Cox, N.J., Lipkind, G.M.*, et al.* (2007). Insulin gene mutations as a cause of permanent neonatal diabetes. Proc Natl Acad Sci U S A *104*, 15040-15044.

Tsai, B., Ye, Y., and Rapoport, T.A. (2002). Retro-translocation of proteins from the endoplasmic reticulum into the cytosol. Nat Rev Mol Cell Biol *3*, 246-255.

Uemura, A., Oku, M., Mori, K., and Yoshida, H. (2009). Unconventional splicing of XBP1 mRNA occurs in the cytoplasm during the mammalian unfolded protein response. J Cell Sci *122*, 2877-2886.

Wang, J., Takeuchi, T., Tanaka, S., Kubo, S.K., Kayo, T., Lu, D., Takata, K., Koizumi, A., and Izumi, T. (1999). A mutation in the insulin 2 gene induces diabetes with severe pancreatic beta-cell dysfunction in the Mody mouse. J Clin Invest *103*, 27-37.

Weiss, M.A. (2009). Proinsulin and the genetics of diabetes mellitus. J Biol Chem *284*, 19159-19163.

Weitzmann, A., Volkmer, J., and Zimmermann, R. (2006). The nucleotide exchange factor activity of Grp170 may explain the non-lethal phenotype of loss of Sil1 function in man and mouse. FEBS Lett *580*, 5237-5240.

CHAPTER 5: Conclusion

This thesis elucidates how cells deploy concerted ER protein quality control pathways to dispose *Akita* mutant proinsulin. In Chapter 2, we identified cellular components that target *Akita* mutant proinsulin along the ERAD pathway for degradation. Specifically, we find that the ER luminal oxidoreductase PDI reduces *Akita* high MW complexes, generating smaller oligomeric species that are competent to undergo ERAD through the Hrd1-Sel1L-p97 axis. In Chapter 3, we begin to clarify a role for Grp170, an atypical ER-resident Hsp70, in ERAD-dependent clearance of *Akita*. A major finding in this chapter is that Grp170 overexpression stimulates *Akita* degradation which enables efficient WT insulin secretion – this provides a rational therapeutic strategy to alleviate the MIDY disease. In Chapter 4, our mechanistic studies reveal that Grp170 acts to prevent formation of *Akita* insoluble aggregates, while the ER membrane protein RTN3 disposes these aggregates via ER-phagy. Importantly, RTN3-mediated ER-phagy also degrades other prohormone aggregates. These data uncover the first series of substrates degraded by RTN3-dependent ER-phagy.

ERAD is responsible for degrading a variety of misfolded ER substrates, including the *Akita* mutant proinsulin. In the ER lumen, *Akita* first encounters PDI and Grp170. PDI is the canonical member of the PDI family. Each of the twenty family members, excluding ERp29, contains a Cys-X-X-Cys motif (where X is any amino acid) that is responsible

for isomerization, reduction, and oxidation reactions (Benham, 2012; Ellgaard and Ruddock, 2005). An outstanding question is how each of these enzymes display selectivity for their substrates. For instance, in the case of *Akita*, PDI (but not p5 or ERdj5) binds to and catalytically reduces the disulfide bonds present in *Akita* high MW oligomers, producing smaller *Akita* species competent to undergo ERAD (Chapter 2, Figure 2-4). Whether PDI can reduce disulfide bonds of other MIDY mutant proinsulins is unknown, and requires additional experimentations. Although PDIa5 can bind to *Akita* (Gorasia et al., 2016 BBA), there is no evidence that it reduces the disulfide bonds of *Akita* high MW oligomers. Thus, structural features enabling a functional interaction between PDI and *Akita* remain unclear to date. It is interesting to note that while PDI is also required for proAVP degradation through ERAD (Shi et al., 2017), the role of other PDI family members in this pathway remains unknown.

In Chapter 3, our analysis identified Grp170, an atypical Hsp70, as a luminal chaperone that acts in concert with PDI to facilitate *Akita* degradation via the ERAD pathway. Mechanistically, Grp170 either promoted the disaggregation of high MW *Akita* aggregates, or prevented the formation of these aggregates. This question was resolved in Chapter 4, in which we used cell-based and a partially purified reconstituted system to unambiguously demonstrate that Grp170 functions to prevent formation of high MW *Akita* aggregates. This is consistent with a seminal study showing that Grp170 uniquely recognizes amino acid sequences that are prone to aggregation (Behnke et al., 2016). The idea that Grp170 can prevent protein aggregate formation is not without precedent, as this chaperone had been shown to prevent heat-induced aggregation of

the luciferase artificial substrate (Park et al., 2003). Our findings establish *Akita* as the first endogenous substrate that is prevented from aggregation by Grp170. Beyond MIDY, Grp170 has also been shown to maintain cellular homeostasis in models of type 2 diabetes (Ozawa et al., 2005); whether Grp170's ability to prevent protein aggregation is responsible for this phenotype is unclear and deserves further attention. Because Grp170 expression is high in purkinje neurons whose destruction due to protein aggregation can lead to neurodegenerative diseases (Kitao et al., 2004), Grp170 may serve a protective role in this context.

Although our data demonstrated Grp170's ability to prevent protein aggregation, whether it can drive disaggregation of preformed protein aggregates remains an open question. Grp170 is homologous to cytosolic Hsp110, which is responsible for various chaperone-mediated client triage reactions in the cytosol. Interestingly, Hsp110 is also a key component of a recently discovered cytosolic disaggregation complex (Nillegoda et al., 2015). In this complex, Hsp110, along with Hsp70 and Hsp40 J proteins, functions to disaggregate different model clients such as luciferase and α-synuclein fibrils *in vitro*. Thus, if a homologous ER-resident disaggregation machinery exists, Grp170 is likely a component of this complex. Other members of this putative disaggregation machinery are likely BiP (homologous to Hsp70), and ERdj3 and ERdj4 (ER-resident J proteins).

The coordinated action of PDI and Grp170 on *Akita* ultimately generates a soluble, low MW species poised to undergo retrotranslocation across the ER membrane to reach the cytosol. In Chapter 2, we demonstrated that the soluble *Akita* species are degraded via

the canonical ER membrane-bound E3 ubiquitin ligase Hrd1. Another transmembrane E3 ubiquitin ligase that executes a critical role in ERAD is called GP78. Although the role of this E3 ubiquitin ligase in facilitating *Akita* degradation remains to be tested, neuroserpin polymers that accumulate in the ER were shown to be degraded in a GP78-dependent mechanism (Ying et al., 2011).

One of the major unanswered questions in ERAD is how the actual process of retrotranslocation – in which a misfolded ER substrate crosses a proteinaceous channel embedded in the ER membrane to reach the cytosol – is accomplished. Strong biochemical evidence depicts a model in which Hrd1 serves as the protein-conducting channel (Baldridge and Rapoport, 2016; Schoebel et al., 2017). In this model, the transmembrane helices 3-8 (TM3-8) of Hrd1 form a pore through which misfolded substrates can be funneled (Schoebel et al., 2017). By cryo-EM structural analysis, this pore is envisioned to be regulated by the TM1 helix of a partner Hrd1 molecule, forming a functional dimer. Although GP78, RNF145 and RNF139 (two additional membrane-bound E3 ligases implicated in ERAD) have sequence similarities to Hrd1, it is unclear whether any of these proteins form pores comparable to Hrd1. Further, how any of the E3 ubiquitin ligases select specific misfolded substrates to guide them across the ER membrane and into the cytosol remains equally enigmatic.

Acting in parallel to ERAD, we found that ER-phagy also disposes *Akita*. Specifically, the aggregated form of *Akita* is degraded by a RTN3-mediated ER-phagy pathway (Chapter 4, Figure 4-5-7). This pathway is also responsible for degradation of two

additional prohormone aggregates. Collectively, these results identified a first series of substrates for RTN3-mediated ER-phagy. ER-phagy is a relatively new field of research, with the initial identification of Atg39 and Atg40 in yeast and FAM134B in mammalian cells as ER-phagy receptors (Khaminets et al., 2015; Mochida et al., 2015). After these discoveries, Sec62, RTN3, and CCPG1 were shown to be additional ER-phagy receptors (Fumagalli et al., 2016; Grumati et al., 2017; Smith et al., 2018). Indeed, many new questions have emerged based on these findings.

A key question is the identity of the endogenous substrates for ER-phagy, as well as how the substrates are recognized by the individual ER-phagy receptors. Prior to our work, several ER-phagy substrates were identified, including procollagen, mutant NPC1, and alpha-1-antitrypsin Z variant polymers for the FAM134 receptor (Forrester et al., 2019; Fregno et al., 2018; Schultz et al., 2018), and trypsinogen, amylase, and CBPA for the CCPG1 receptor (Smith et al., 2018). Our results identified *Akita*, C28F POMC, and G57S Pro-AVP aggregates as substrates for RTN3-mediated ER-phagy. Because the RTN3-mediated substrates identified in this thesis are all prohormone aggregates, these findings raise the possibility that mutant prohormone aggregates may generally exploit RTN3 as their ER-phagy receptor.

RTN3 and FAM134B are ER membrane proteins that do not fully traverse both leaflets of the ER lipid bilayer but instead only insert into the cytosolic leaflet of this membrane (Fregno and Molinari, 2018). As a result, they do not extend into the ER lumen. This is in contrast to RTN4/NOGO, which is thought to traverse the entire ER membrane

(Schwab, 2010). The topology of RTN3 and FAM134B raises an interesting conundrum: if these receptors are not exposed to the ER lumen, how do they capture the luminally-localized aggregates? One resolution to this problem can be seen in the case of the substrate procollagen. Procollagen is an ER luminal substrate of FAM134B-mediated ER-phagy. Strikingly, procollagen binds to calnexin, an ER transmembrane protein with a large luminal domain that typically engages misfolded soluble glycoproteins (Williams, 2006); importantly, calnexin itself associates with FAM134B (Fregno et al., 2018). Thus calnexin acts as the direct cargo-binding receptor, linking procollagen to FAM134B for ER-phagy. It is worth noting that FAM134B is localized to ER sheets (a subdomain within the complex ER network), while RTN3 is found in the ER-tubule rich subdomain of the ER.

What mechanism might enable RTN3 to engage the aggregated substrate? Reticulons are ER membrane morphogenic proteins that induce membrane curvature to ER tubules. These tubules are approximately 60-100 nanometers in diameter (Voeltz et al., 2002), which limits the physical space needed to accommodate the large ER luminal aggregates. We envision two distinct mechanisms by which RTN3 captures its luminal substrate. In one mechanism, RTN3 complexes with a transmembrane protein containing a luminal domain, which in turn directly binds to the substrate; this would be reminiscent of the mechanism by which FAM134B interacts with its substrate. Perhaps an unbiased biochemical IP-mass spectrometry approach to identify RTN3 membrane-binding partners is a reasonable strategy to test this mechanism.

In a second mechanism, we envision that a large aggregate might mechanically induce stress to the inner leaflet of the ER due to its large size. The tension exerted on the membrane recruits RTN3 to this site, resulting in ER-phagy of the surrounding ER tubule and as a consequence, removal of any luminal constituents in this ER subdomain. To test this second mechanism, an inducible oligomerization system (i.e. chemically-induced dimerization strategy such as the FRB-FKBP system) could be used to artificially generate an aggregated model substrate in the ER lumen via oligomerization of the substrate (DeRose et al., 2013). As this artificial aggregated substrate is unlikely to have a cognate receptor in the ER, its ability to use RTN3-mediated ER-phagy would suggest a mechanical stress-induced mechanism operates to “activate” the RTN3 pathway.

In principle, CCPG1 and potentially Sec62 do not require an additional cargo receptor to recruit a luminal substrate because these two ER-phagy receptors contain ER luminal domains. CCPG1 has a 518 amino acid luminal tail, which could directly engage the aggregated substrate. Sec62 has a small luminal domain containing only 16 amino acids between two transmembrane domains, so its requirement for substrate identification and engagement could be limited without a cargo receptor.

In conclusion, my thesis revealed that cells deploy coordinated ER protein quality control mechanisms to dispose the MIDY mutant proinsulin *Akita*. We believe these insights should lay the foundation for many future studies that will illuminate various

aspects of ER protein quality control, protein misfolding dynamics, and homeostatic mechanisms underlying the MIDY disease.

REFERENCES

Baldridge, R.D., and Rapoport, T.A. (2016). Autoubiquitination of the Hrd1 Ligase Triggers Protein Retrotranslocation in ERAD. Cell *166*, 394-407.

Behnke, J., Mann, M.J., Scruggs, F.L., Feige, M.J., and Hendershot, L.M. (2016). Members of the Hsp70 Family Recognize Distinct Types of Sequences to Execute ER Quality Control. Mol Cell *63*, 739-752.

Benham, A.M. (2012). The protein disulfide isomerase family: key players in health and disease. Antioxid Redox Signal *16*, 781-789.

DeRose, R., Miyamoto, T., and Inoue, T. (2013). Manipulating signaling at will: chemically-inducible dimerization (CID) techniques resolve problems in cell biology. Pflugers Arch *465*, 409-417.

Ellgaard, L., and Ruddock, L.W. (2005). The human protein disulphide isomerase family: substrate interactions and functional properties. EMBO Rep *6*, 28-32.

Forrester, A., De Leonibus, C., Grumati, P., Fasana, E., Piemontese, M., Staiano, L., Fregno, I., Raimondi, A., Marazza, A., Bruno, G.*, et al.* (2019). A selective ER-phagy exerts procollagen quality control via a Calnexin-FAM134B complex. EMBO J *38*.

Fregno, I., Fasana, E., Bergmann, T.J., Raimondi, A., Loi, M., Solda, T., Galli, C., D'Antuono, R., Morone, D., Danieli, A.*, et al.* (2018). ER-to-lysosome-associated degradation of proteasome-resistant ATZ polymers occurs via receptor-mediated vesicular transport. EMBO J *37*.

Fregno, I., and Molinari, M. (2018). Endoplasmic reticulum turnover: ER-phagy and other flavors in selective and non-selective ER clearance. F1000Res *7*, 454.

Fumagalli, F., Noack, J., Bergmann, T.J., Cebollero, E., Pisoni, G.B., Fasana, E., Fregno, I., Galli, C., Loi, M., Solda, T.*, et al.* (2016). Translocon component Sec62 acts in endoplasmic reticulum turnover during stress recovery. Nat Cell Biol *18*, 1173-1184.

Grumati, P., Morozzi, G., Holper, S., Mari, M., Harwardt, M.I., Yan, R., Muller, S., Reggiori, F., Heilemann, M., and Dikic, I. (2017). Full length RTN3 regulates turnover of tubular endoplasmic reticulum via selective autophagy. Elife *6*.

Khaminets, A., Heinrich, T., Mari, M., Grumati, P., Huebner, A.K., Akutsu, M., Liebmann, L., Stolz, A., Nietzsche, S., Koch, N.*, et al.* (2015). Regulation of endoplasmic reticulum turnover by selective autophagy. Nature *522*, 354-358.

Kitao, Y., Hashimoto, K., Matsuyama, T., Iso, H., Tamatani, T., Hori, O., Stern, D.M., Kano, M., Ozawa, K., and Ogawa, S. (2004). ORP150/HSP12A regulates Purkinje cell

survival: a role for endoplasmic reticulum stress in cerebellar development. J Neurosci *24*, 1486-1496.

Mochida, K., Oikawa, Y., Kimura, Y., Kirisako, H., Hirano, H., Ohsumi, Y., and Nakatogawa, H. (2015). Receptor-mediated selective autophagy degrades the endoplasmic reticulum and the nucleus. Nature *522*, 359-362.

Nillegoda, N.B., Kirstein, J., Szlachcic, A., Berynskyy, M., Stank, A., Stengel, F., Arnsburg, K., Gao, X., Scior, A., Aebersold, R.*, et al.* (2015). Crucial HSP70 co-chaperone complex unlocks metazoan protein disaggregation. Nature *524*, 247-251.

Ozawa, K., Miyazaki, M., Matsuhisa, M., Takano, K., Nakatani, Y., Hatazaki, M., Tamatani, T., Yamagata, K., Miyagawa, J., Kitao, Y.*, et al.* (2005). The endoplasmic reticulum chaperone improves insulin resistance in type 2 diabetes. Diabetes *54*, 657-663.

Park, J., Easton, D.P., Chen, X., MacDonald, I.J., Wang, X.Y., and Subjeck, J.R. (2003). The chaperoning properties of mouse grp170, a member of the third family of hsp70 related proteins. Biochemistry *42*, 14893-14902.

Schoebel, S., Mi, W., Stein, A., Ovchinnikov, S., Pavlovicz, R., DiMaio, F., Baker, D., Chambers, M.G., Su, H., Li, D.*, et al.* (2017). Cryo-EM structure of the protein-conducting ERAD channel Hrd1 in complex with Hrd3. Nature *548*, 352-355.

Schultz, M.L., Krus, K.L., Kaushik, S., Dang, D., Chopra, R., Qi, L., Shakkottai, V.G., Cuervo, A.M., and Lieberman, A.P. (2018). Coordinate regulation of mutant NPC1 degradation by selective ER autophagy and MARCH6-dependent ERAD. Nat Commun *9*, 3671.

Schwab, M.E. (2010). Functions of Nogo proteins and their receptors in the nervous system. Nat Rev Neurosci *11*, 799-811.

Shi, G., Somlo, D.R.M., Kim, G.H., Prescianotto-Baschong, C., Sun, S., Beuret, N., Long, Q., Rutishauser, J., Arvan, P., Spiess, M.*, et al.* (2017). ER-associated degradation is required for vasopressin prohormone processing and systemic water homeostasis. J Clin Invest *127*, 3897-3912.

Smith, M.D., Harley, M.E., Kemp, A.J., Wills, J., Lee, M., Arends, M., von Kriegsheim, A., Behrends, C., and Wilkinson, S. (2018). CCPG1 Is a Non-canonical Autophagy Cargo Receptor Essential for ER-Phagy and Pancreatic ER Proteostasis. Dev Cell *44*, 217-232 e211.

Voeltz, G.K., Rolls, M.M., and Rapoport, T.A. (2002). Structural organization of the endoplasmic reticulum. EMBO Rep *3*, 944-950.

Williams, D.B. (2006). Beyond lectins: the calnexin/calreticulin chaperone system of the endoplasmic reticulum. J Cell Sci *119*, 615-623.

Ying, Z., Wang, H., Fan, H., and Wang, G. (2011). The endoplasmic reticulum (ER)-associated degradation system regulates aggregation and degradation of mutant neuroserpin. J Biol Chem *286*, 20835-20844.